Multiple data sources and integrated hydrological modelling for groundwater assessment in the Central Kalahari Basin

Moiteela Lekula

PhD Graduation committee:

Chairman/Secretary

Prof.dr.ir. A. Veldkamp	University of Twente

Supervisor

Dr.ir. M.W. Lubczynski	University of Twente

Co-Supervisor

Prof.dr.ing. W. Verhoef	University of Twente
Prof.dr. E. Shemang	Botswana Int. Univ. of Science and Technology (BIUST)

Members

Prof.dr. Z. Su	University of Twente
Prof.dr. V.G. Jetten	University of Twente
Prof.dr. F.J. Samper Cavete	University of La Coruna
Prof.dr. M. Leblanc	University of Avignon
Prof.dr. P.K. Kenabatho	University of Botswana

ITC dissertation number 333
ITC, P.O. Box 217, 7500 AE Enschede, The Netherlands

ISBN 978-90-365-4639-3
DOI 10.3990/1.9789036546393

Cover designed by Benno Masselink
Printed by ITC Printing Department

UNIVERSITY OF TWENTE.

FACULTY OF GEO-INFORMATION SCIENCE AND EARTH OBSERVATION

MULTIPLE DATA SOURCES AND INTEGRATED HYDROLOGICAL MODELING FOR GROUNDWATER ASSESSMENT IN THE CENTRAL KALAHARI BASIN

DISSERTATION

to obtain
the degree of doctor at the University of Twente,
on the authority of the Rector Magnificus,
prof. dr. T.T.M. Palstra,
on account of the decision of the graduation committee,
to be publicly defended
on Wednesday 17 October 2018 at 14:45 hrs

by

Moiteela Lekula

born on 7 November 1975

in Francistown, Botswana

This thesis has been approved by:

Dr.ir. M.W. Lubczynski, Supervisor

Prof.dr. W. Verhoef, Co-supervisor

Prof.dr. E. M. Shemang, Co-supervisor

Acknowledgements

Let me take this opportunity to extend my gratitude to all the people that directly and/or indirectly supported my PhD research. Firstly I would like to thank Botswana International University of Science and Technology (BIUST) for offering me scholarship and the then Ministry of Minerals Energy and Water resources (Now Ministry of Mineral Resources, Green Technology and Energy Security) for granting me study leave to pursue my PhD. I would like to extend my gratitude to Dr. Ir. Maciek Lubczynski for his patience and guidance from initial discussion through my PhD tour, especially technical and scientific assistance on my manuscripts. To Prof. Wouter Verhoef, for his active and timely support in my PhD. My PhD could not be successful without the fieldwork support. My sincere gratitude to Prof. Elisha M. Shemang (BIUST) for going an extra mile in providing necessary field equipment and transport logistics of top technical and scientific assistance on my manuscripts. Mr. Phemelo "Picture" Makoba for his efforts during the fieldwork campaigns, especially during equipment setup and data downloads. You are a star Picture and God will bless you more. Mr. Ofentse Gabaitse and Ms Tshiamo Motlhetlhi, Ghanzi DWA, for extending their helping hands during the fieldwork. BIUST drivers who made sure that I access my study area with ease. Addition data was also vital for the successful completion of my PhD. Special thanks goes to the Department of Meteorological Services, Botswana, which provided the rain gauge data used in this study. Dr. Nicolas Novella from National Oceanic and Atmospheric Administration (NOAA) is highly acknowledged for proving information on RFE processing. The developers and managers of the free online databases of the satellite-based rainfall products used in this study, are also acknowledged. Special thanks also goes to the Department of Water Affairs in Botswana, Botswana Geoscience Institution, Debswana Diamond Mining Company, especially Mr. Banda Maswabi, Mr. Tefo Rahube, Mr. Ceasor Sebina and Mr. Obone Mabote, and Directorate of Water Resources Management in Namibia, for providing the geological and hydrogeological data, which made this study possible. Dr Richard G Niswonger and Dr Richard B Winston from USGS are highly acknowledged for the interactive discussion about the UZF1 package during the groundwater flow model development.

Additionally, I am thankful to all my PhD colleagues at ITC, who we interacted a lot especially in the WPW sessions. To Cesar Cisneros Vaca, Peiqi Yang, Tebogo Sox Masaka, Webster Gumindoga, Donald Rwasoka, Sammy Njuki, Marc Manyifika, Margaret Kimani, Chandra Ghimire, Tina Butt-Castro and Anke De Koning, you made my stay in water resources comfortable and I will miss you. All ITC hotel staff members are acknowledged for making it may second home. I would like to also extend my sincere gratitude to the many people that I have not mentioned by name whose contribution was fundamental in the

success of my PhD. Finally, I would like to thank my wife Keitimetse Maopere Lekula for taking care of my daughter Katlego and my son Letshwao Larona during the tough times through my PhD trajectory.

Table of Contents

List of figures

List of tables

List of symbols and abbreviations

1-D	one-dimension
2-D	two-dimension
3-D	three-dimension
BGI	Botswana Geoscience Institute
BF	bias factor
BRGM	Bureau de Recherches Géologiques et Minières
CC	pearson's product-moment correlation coefficient
CKB	Central Kalahari Basin
CMORPH	Climate Prediction Center (CPC) Morphing Technique
Cond	conductance
CSD	computational separation distance
CSI	critical success index
CV	coefficient of variation
DDMC	Debswana Diamond Mining Company
DEM	digital elevation model
DMS	Department of Meteorological Services
DRN	drain
DWA	Department of Water Affairs
DWRM	Directorate of Water Resources Management
EA	Ecca Aquifer
EXF_{gw}	groundwater exfiltration
ET_g	groundwater evapotranspiration
ET_{ss}	subsurface evapotranspiration
ET_{uz}	unsaturated zone evapotranspiration

EXTDP	evapotranspiration extinction depth
EXTWC	evapotranspiration extinction water content
FAR	false alarm ratio
FB	false bias
FBS	frequency bias
FEWSNET RFE	Famine Early Warning Systems Network Rainfall Estimate
Ga	giga annum
GA	Ghanzi Aquifer
GHB	general head boundary
GIS	geographical information system
GLM	generalised linear models
GMS	Groundwater Modelling System
GTS	global telecommunication stations
H_{obs}	observed heads
H_{sim}	simulated heads
HB	hit bias
HCM	hydrogeological conceptual model
HFB	horizontal flow barrier
HU	hydrostratigraphic unit
I	interception
IHM	integrated hydrological model
IKA	Inter-Karoo Aquitard
K	hydraulic conductivity
K_h	horizontal hydraulic conductivity
K_v	vertical hydraulic conductivity

$K(\theta)$	unsaturated hydraulic conductivity
KKB	Kalahari Karoo Basin
KSU	Kalahari Sand Unit
LA	Lebung Aquifer
LULC	Land Use land Cover
MAE	mean absolute error
MAR	mean annual rainfall
MB	miss bias
ME	mean error
MOD-UZF	MODFLOW-NWT model with active UZF1 Package
P	precipitation
P_e	effective precipitation
PERSIANN	Precipitation Estimates from Remotely Sensed Information Using Artificial Neural Networks
PET	potential evapotranspiration
POD	probability of detection
q_{ABS}	lateral groundwater inflow into the modelled area across the DRN boundary
q_{DRN}	groundwater abstraction
q_{GHB}	lateral groundwater inflow into the modelled area across the GHB boundary
q_{in}	lateral groundwater inflow
q_{out}	lateral groundwater outflow
R_g	gross recharge

R_n	net recharge
RMSE	root mean square error
RS	remote sensing
S_s	specific storage
S_y	specific yield
SBA	Stormberg Basalt Aquitard
SMEC	Snowy Mountains Engineering Corporation
SRE	satellite-based rainfall estimate
SRTM	shuttle Radar topography mission
T	transmissivity
TB_c	total bias
TRMM	Tropical Rainfall Measuring Mission
TVSF	time variable space fixed bias correction scheme
UPW	upstream weighting package
USGS	United States Geological Survey
UZF1	unsaturated-zone flow package
ε	Brooks and Corey exponent
ΔS	total storage change
ΔS_{uz}	storage change in unsaturated zone
ΔS_g	storage change in the saturated zone
Θ_i	soil initial water content
Θ_r	soil residual water content
Θ_s	soil saturated water content

Chapter 1 : General introduction

1.1 Background

Groundwater resources in arid and semi-arid regions is often the only, but vulnerable, source of potable water, therefore its reliable evaluation and management is critically important. Such evaluation and management is nowadays typically done through integrated hydrological models (IHM), which are considered an optimal tool for that purpose. The IHMs are based on mathematical equations integrated into algorithms and computer codes (Anderson et al., 2015; Domenico & Schwartz, 1998; Francés et al., 2015), allowing to study dynamics of surface-groundwater interactions and to predict dynamic responses of aquifers in reaction to groundwater abstraction, climatic and/or land use changes etc. The reliability of IHMs, is however constrained by development of realistic hydrogeological conceptual models (HCMs) (Lekula et al., 2018a) and by availability and quality of model input data (Meijerink et al., 2007).

HCMs summarise hydrogeological knowledge of a site to be modelled and provide a framework for IHM development. HCMs are typically reconstructed from surface and subsurface data to help hydrogeologists to understand the hydrogeological system behaviour and to support quantitative modelling (Frances et al., 2014). They usually schematize a hydrogeological system of layers into hydrostratigraphic units and associate boundary conditions, hydrogeological properties, driving forces, state variables, flow directions and preliminary water budgets (Anderson et al., 2015). Different methods to setup HCMs exist, involving analysis and integration of relevant geological and hydrogeological data, for example using database tool such as geographical information system (GIS) (Anderson et al., 2015; Trabelsi et al., 2013) or modelling environments such as Groundwater Modelling System (Environmental Modeling Research Laboratory, 1999), although there is no standard widely accepted methodology in that respect (Brassington & Younger, 2010). To manage subsurface data, in this study, 3-D geological modelling software tool, sort of subsurface GIS, was used. It has the advantage of synthesizing digitally all available data types, leading to a good understanding and realistic presentation of a geological settings for HCM (Hassen et al., 2016). The use of 3-D geological modelling for development of the HCM of the complex, multi-layered aquifer system of the Central Kalahari Basin (CKB) is described in Chapter 3.

In arid and semi-arid regions of Developing Countries, such as the CKB of this study, ground-based monitoring data are scarce. Such data scarcity, particularly rainfall data scarcity, hampers development of any water management model, including IHMs (Brunner et al., 2007; Kenabatho et al.,

2017; Leblanc et al., 2007). An alternative source of data is remote sensing (RS) method. For the past decade, the RS has played an increasing role in providing spatio-temporal information for water resources evaluation and management (Coelho et al., 2017). RS applications in surface hydrology, including surface water modelling, are already well known and include: digital elevation derivatives, land cover and land use, spatio-temporal rainfall and evapotranspiration evaluations (Schmugge et al., 2002). However, the RS contributions to groundwater hydrology and groundwater resources evaluation are less known.

The standard RS applications in groundwater hydrology involve assessment of: groundwater recharge (e.g., Awan et al., 2013; Brunner et al., 2004; Coelho et al., 2017; Jasrotia et al., 2007; Khalaf & Donoghue, 2012), surface-groundwater interaction (e.g., Bauer et al., 2006; Leblanc et al., 2007; Sarma & Xu, 2017), groundwater storage (resources) evaluation and change (e.g. Henry et al., 2011; Rodell et al., 2007; Rodell & Famiglietti, 2002; Taniguchi et al., 2011; Yeh et al., 2006). With recent advancement of IHMs, coupling surface with groundwater processes, the RS contributions to IHMs are rapidly increasing, mainly because of continuously increasing amount of downloadable RS products, such as for example rainfall or potential evapotranspiration, the two, typical driving forces of IHMs.

Rainfall is the most important driving force of IHMs. In arid and semi-arid regions, rainfall is known to be highly spatio-temporally variable (Bhalotra, 1987; Kenabatho et al., 2017; Lekula et al., 2018b). To analyse its variability over large areas such as the CKB, it would require lots of rain gauges equipped with loggers. As typically such networks are unavailable, the RS method can be considered as alternative. The RS method provides a pretty good temporal and reasonable spatial rainfall data coverage (Lekula et al., 2018b). There are various, web-based, RS rainfall products, although because different products perform differently in rainfall detection at different parts of the world, they first need to be evaluated and compared to select the optimal one (considering its spatial and temporal resolution as well as the accuracy) to be used as an input of an IHM of a given investigated area (Kenabatho et al., 2017; Lekula et al., 2018b). Besides, as RS-rainfall products are known to exhibit inaccuracies (in the form of systematic and random errors), they need to be investigated and analysed by comparing the RS-rainfall to ground measurements and correcting them where possible, before being used in hydrological models (Habib et al., 2014; Lekula et al., 2018b; Nicholson et al., 2003). These reasons and the IHM input data demand, prompted a detailed, RS-based investigation of spatio-temporal rainfall variability in the CKB (Chapter 4), in order to select optimal RS-rainfall product to be used in the IHM of the CKB.

Another IHM driving force detectable by RS is potential evapotranspiration (*PET*). The *PET* is much less spatio-temporally variable than rainfall (Zhu &

Ringler, 2012), so it does not require as high spatial resolution (Post et al., 2012; Xiaoyang et al., 2015) as the rainfall does. In this study, after validation with ground-based data, the *PET* was directly downloaded from Unites States Geological Survey Famine Early Warning System Network data portal https://earlywarning.usgs.gov/fews/datadownloads, without any specific data processing, therefore it is not addressed in a separate chapter, but only partially in chapters 3 and 5.

The RS method, can also provide various ancillary data as input of IHMs. In the CKB study, the following ancillary data facilitated the setup of the IHM: digital elevation model needed to define the topographic surface, soil data, land use and land cover data needed for the parameterisation of the unsaturated zone. The ancillary data and its integration in IHMs, are addressed in chapters 3 and 5.

The design and solution of the IHM of the CKB, i.e. the main topic of this thesis, is addressed in the Chapter 5. That task was challenging mainly because of: i) structural and hydrogeological complexity of the CKB; ii) very thick unsaturated zone; iii) large spatio-temporal variability of surface and subsurface water fluxes; iv) advanced method of integration of multiple data sources (combination of ground-based and RS-based data) in the design of the conceptual and numerical, integrated hydrological model, meant to be used for definition of sustainable management of transboundary groundwater resources of the CKB.

1.2 Research problem and objectives

Data scarcity, particularly in arid to semi-arid Developing Countries, has always been hampering development of numerical models, so also IHMs, widely applied nowadays for groundwater management. Advancement in IHMs made spatio-temporally variable RS data an alternative to scarce, ground-based data sets. Integration of the RS-data, together with other available data sets, is thus vital in water resources management in arid and semi-arid regions, hence, also for the CKB, hosting the most productive and exploitable transboundary Karoo System Aquifer in Botswana and Namibia. As such, the CKB, became an interesting study area to assess, considering its hydrogeological characteristics and importance of groundwater resources.

The main objective of this PhD research was to assess groundwater resources in the CKB using multiple data sources and integrated hydrological modelling. In order to achieve the main objective, the following specific objectives were formulated:

1) To develop the hydrogeological conceptual model of the CKB to convert it into numerical, integrated hydrological model (chapter 3).

2) To select optimal for the CKB, daily satellite-based rainfall, to use it as input of the numerical integrated hydrological model (chapter 4).
3) To present coupling of various RS products with long term in-situ monitoring data, as input of a regional scale, distributed, numerical IHM of the CKB and characterize its spatio-temporal flux dynamics, including 13 year, daily water balance estimate. (chapter 5).

1.3 Thesis outline

The PhD structure and its relation to the objectives are shown in Figure 1-1.

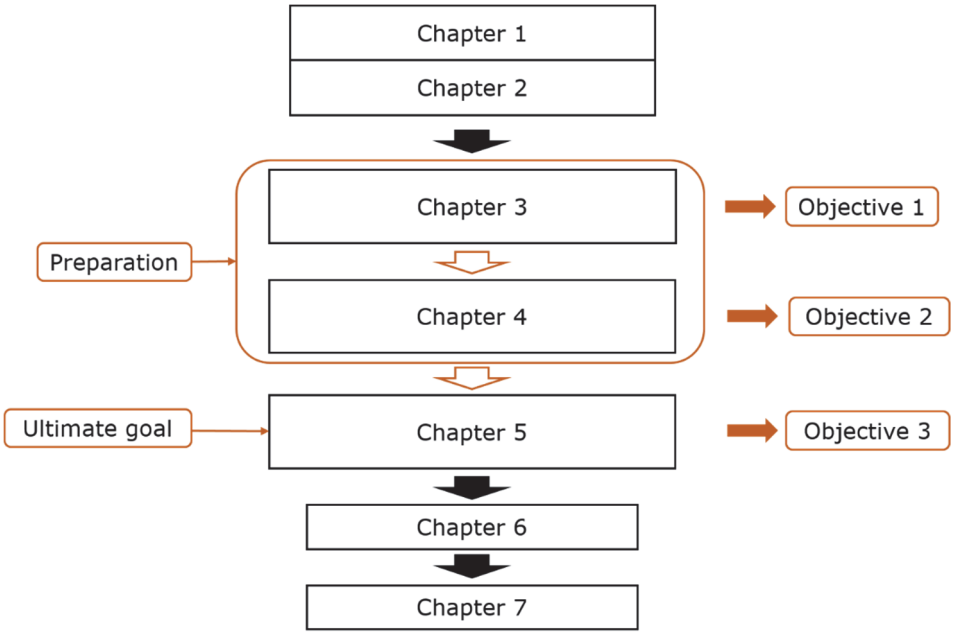

Figure 1-1: Flowchart of the research and thesis structure.

Chapter 1: Provides a general introduction and objectives of the PhD work.
Chapter 2: Introduces the study area including detailed information on its general geology and hydrogeology.
Chapter 3: Presents process of developing a regional, hydrogeological conceptual model (HCM) of a complex multi-layered aquifer system of the Central Kalahari Basin, as a basis for development of its numerical model (IHM).
Chapter 4: Presents validation of daily, satellite-based, RS-rainfall within the CKB study area, presentation of spatio-temporal rainfall variability in the CKB.
Chapter 5: Presents the, numerical, distributed, transient, integrated hydrological model (IHM) of the CKB including adaptation of

the multiple data sources, water balance and variability of surface/subsurface water fluxes.

Chapter 6: Presents the synthesis of the thesis.

Chapter 7: Presents the recommendations of this PhD study.

Chapter 2 : Description of study area

2.1 Study area

The Central Kalahari Basin (CKB) study area (Figure 2-1), occupies central Botswana (~181,000 km^2) and small part (~14,000 km^2) of Eastern Namibia, extending from 20.50^o S to 24.90^o S and from 18.70^o E to 26.75^o E. It is a large-scale hydrogeological basin, which formerly was a catchment of the fossil Okwa and Mmone River systems (de Vries, 1984). Majority of the CKB is pretty flat, having a topographic gradient of < 0.001 (Figure 2-1), with surficial accumulation of eolian sand, known as Kalahari Sand. About 90% of the CKB is occupied by Kalahari Desert, characterized by semi-arid to arid climate, because of its position under the descending limb of the Hadley cell circulation (Batisani & Yarnal, 2010). Most of the rainfall in the CKB is from convection processes such as instability showers to thunderstorms, several orders of magnitude smaller than the synoptic systems, like the Inter-Tropical Convergence Zone, which control the air-masses supplying the moisture (Bhalotra, 1987). Rainfall in the region is highly spatially and temporally variable (Lekula et al., 2018b; Obakeng et al., 2007), with highly localized rainfall showers (Bhalotra, 1987).

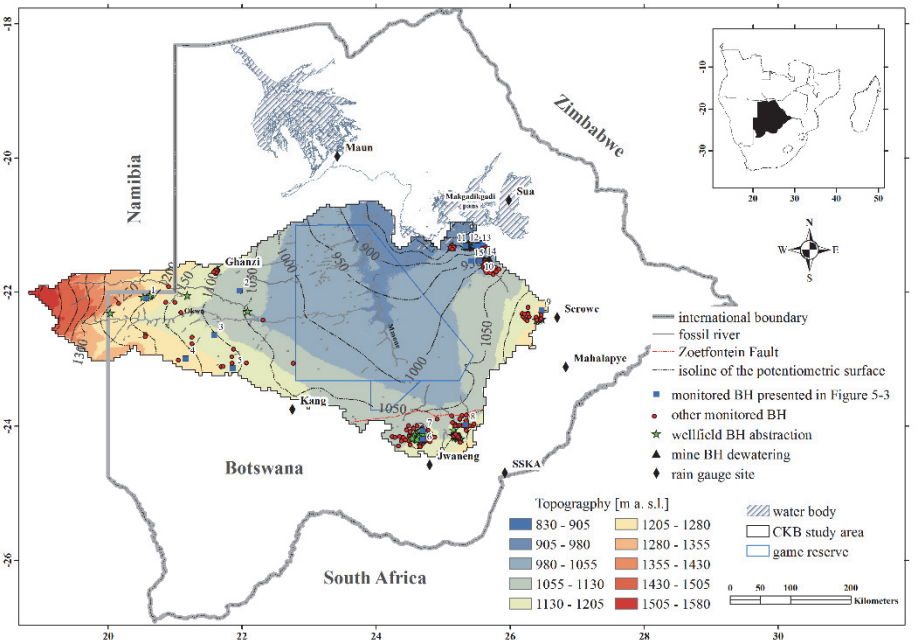

Figure 2-1: Base map of the Central Kalahari Basin including topography and simulated potentiometric surface on 31 December 2006; BH stands for borehole.

Almost all rainfall occurs during the summer, i.e., from September to April. The average annual rainfall ranges from 380 mm yr^{-1} in the southwestern to 530

mm yr^{-1} in the north-eastern parts of the CKB (Lekula et al., 2018b). The annual *PET* is much higher than annual rainfall in the CKB, being characterised by a high temporal but low spatial variability (Obakeng et al., 2007). The annual *PET* ranges between 1350 and 1450 mm (Choudhury, 1997). The majority of the study area, is covered by savannah grassland, sparse shrubs and acacia trees, which increase density towards the east. The CKB is sparsely inhabited by people, mainly at the fringes, with the interior part occupied by Central Kalahari Game Reserve.

2.1.1 General geology

Approximately two thirds of the CKB area, i.e. ~128,000 km^2, is occupied by the Kalahari Karoo Basin (KKB) rocks while the remaining ~67,000 km^2, by Pre-Karoo rocks (Figure 2-2 and Figure 2-3).

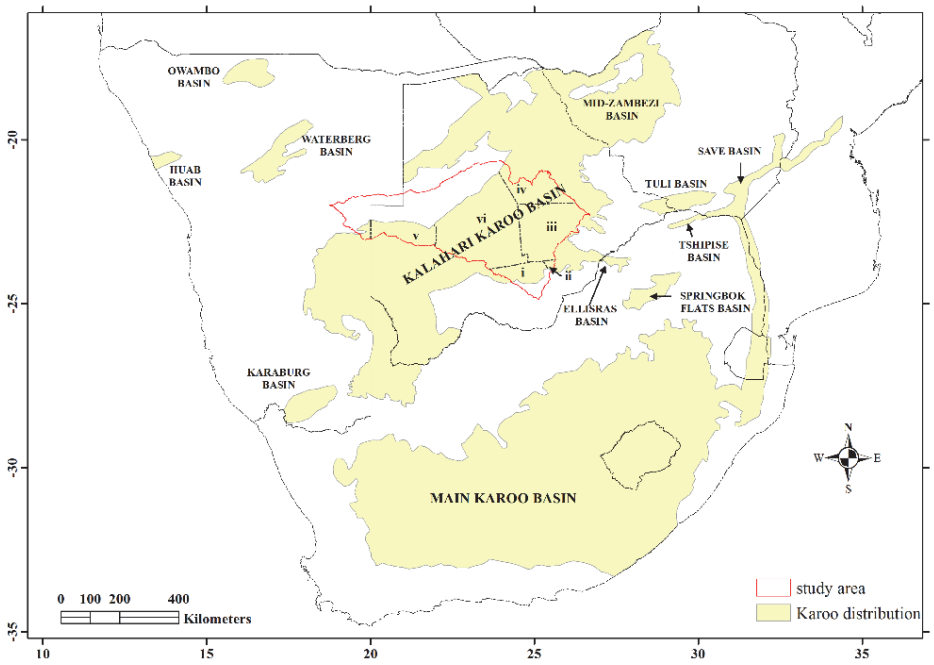

Figure 2-2: Distribution of Karoo Basins in Southern Africa after Johnson et al. (1996). The Roman numerals denote the following CKB Kalahari Karoo Sub-Basins: i) Kweneng; ii) Mmamabula; iii) South-East Central Kalahari; iv) Northern-Belt Central Kalahari; v) Western-Central Kalahari; vi) South-Western Botswana.

The KKB is a sedimentary basin type structure (Catuneanu et al., 2005; Johnson et al., 1996), with areal extent of 4.5 million km^2. It extends over most of Southern African countries (Figure 2-2) and is filled with a succession of sedimentary and volcanic rocks (Table 2-1), with a maximum vertical thickness of about 12 km (Johnson et al., 1996).

2.1.1.1 Pre-Karoo Groups

There are three Pre-Karoo rock Groups of Proterozoic age (Carney et al., 1994; Key & Ayres, 2000) (Figure 2-3) on top of Archaean Basement: i) Ghanzi Group (weakly metamorphosed purple-red, arkosic sandstones, siltstones, mudstones and rhythmites) in the north-western part of the study area; ii) Waterberg Group (reddish siliciclastic sedimentary rocks, mostly quartzitic sandstones and conglomerates) in the southern tip; iii) Transvaal Super Group (interbedded reddish, grey and purple quartzites, carbonaceous siltstones and shales, cherts, limestones, ironstones and volcanics). There are also Archaean age rocks in the CKB (Carney et al., 1994; Key & Ayres, 2000) (Table 2-1): i) Gaborone Granite; ii) Kanye Formation composed of felsites; and iii) Okwa Complex composed of porphyritic felsite, granitic gneiss, microgranite and metadolerite.

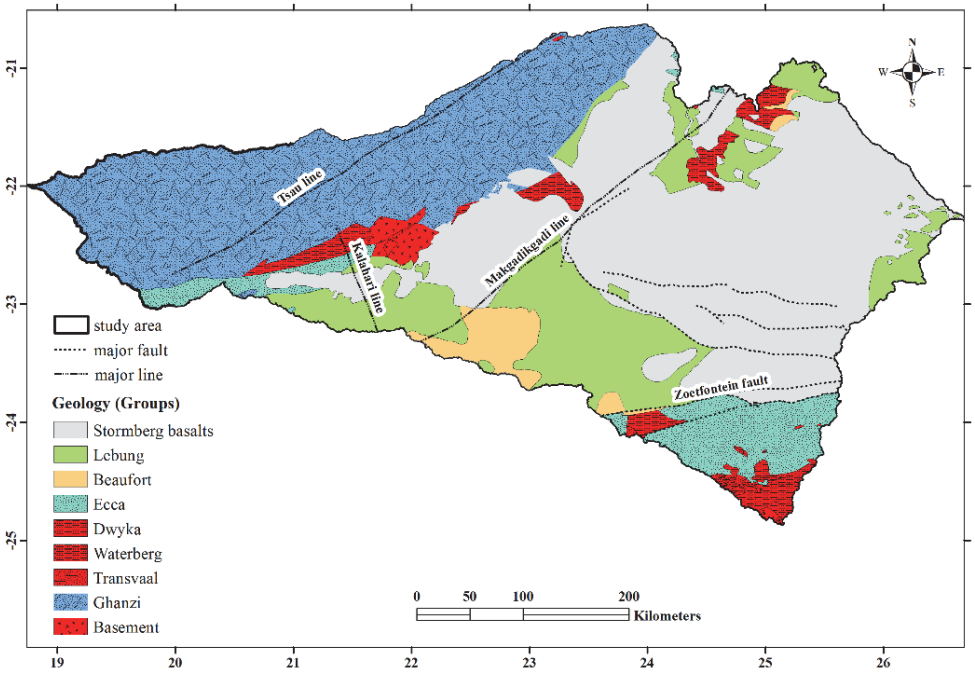

Figure 2-3: The Pre-Kalahari Group geology of the Central Kalahari Basin, modified after Key and Ayres (2000) and Carney et al. (1994).

2.1.1.2 Karoo Supergroup

The Karoo Supergroup Formation, in which the CKB groundwater resources occur, has been sub-divided by Smith (1984) into the Lower Karoo (Dwyka, Ecca and Beaufort Groups) and Upper Karoo (Lebung and Stormberg Groups), based on a regional unconformity (Table 2-1). Only the Karoo Groups that are

present in the CKB and have hydrogeological importance, are described. As such, the Dwyka Group, composed of diamictite, very thinly laminated siltstone (varvite) and sandstone, is not considered.

Ecca Group

The Ecca Group is divided into different formations in different Sub-Basins (Table 2-1). Generally this group consists of inter-layered sandstone, siltstone, mudstone with carbonaceous mudstones and coal seams (Smith, 1984). Thicknesses of different units corresponding to different formations vary spatially, so it is difficult to define their boundaries, particularly that most of the boreholes drilled in the area did not reach the bottom of the Ecca Group. The Ecca Group represents the principal aquifer in the South-Western Botswana and Kweneng Sub-Basins (Smith, 1984) (Figure 2-2 and 2-3).

Beaufort Group

The Beaufort Group follows conformably from the Ecca Group and is characterised by a largely argillaceous, non-carbonaceous and multi-coloured (yellow, brown, green, greenish grey, purple, cream, white and light grey) sequence of mudstones and subordinate siltstones, with minor fine to coarse grained sandstone intercalations (Smith, 1984). The Beaufort Group subcrops under the Kalahari Sand in the southern CKB (Figure 2-3).

Lebung Group

The Lebung Group lies uncomformably on the Beaufort Group. It is composed of sandstone and mudstone formations, which have local names in different Karoo Sub-Basins (Table 2-1, Figure 2-2 and 2-3). In the Lebung Group, there is a downward progression from medium to fine grained, well sorted, reddish to white, massive but fractured sandstones, to an argillaceous reddish brown mudstones and siltstones (Smith, 1984). The Ntane and Nakalatlou Sandstone Formations (Table 2-1) are the principal aquifers, with the former covering the majority of the CKB (Smith, 1984).

Table 2-1: Stratigraphy and hydrostratigraphy of Karoo Supergroup in the CKB, modified after Smith (1984) to include Pre-Karoo and Kalahari Rocks; the colours correspond to hydrostratigraphic units and a dash-line defines a regional unconformity

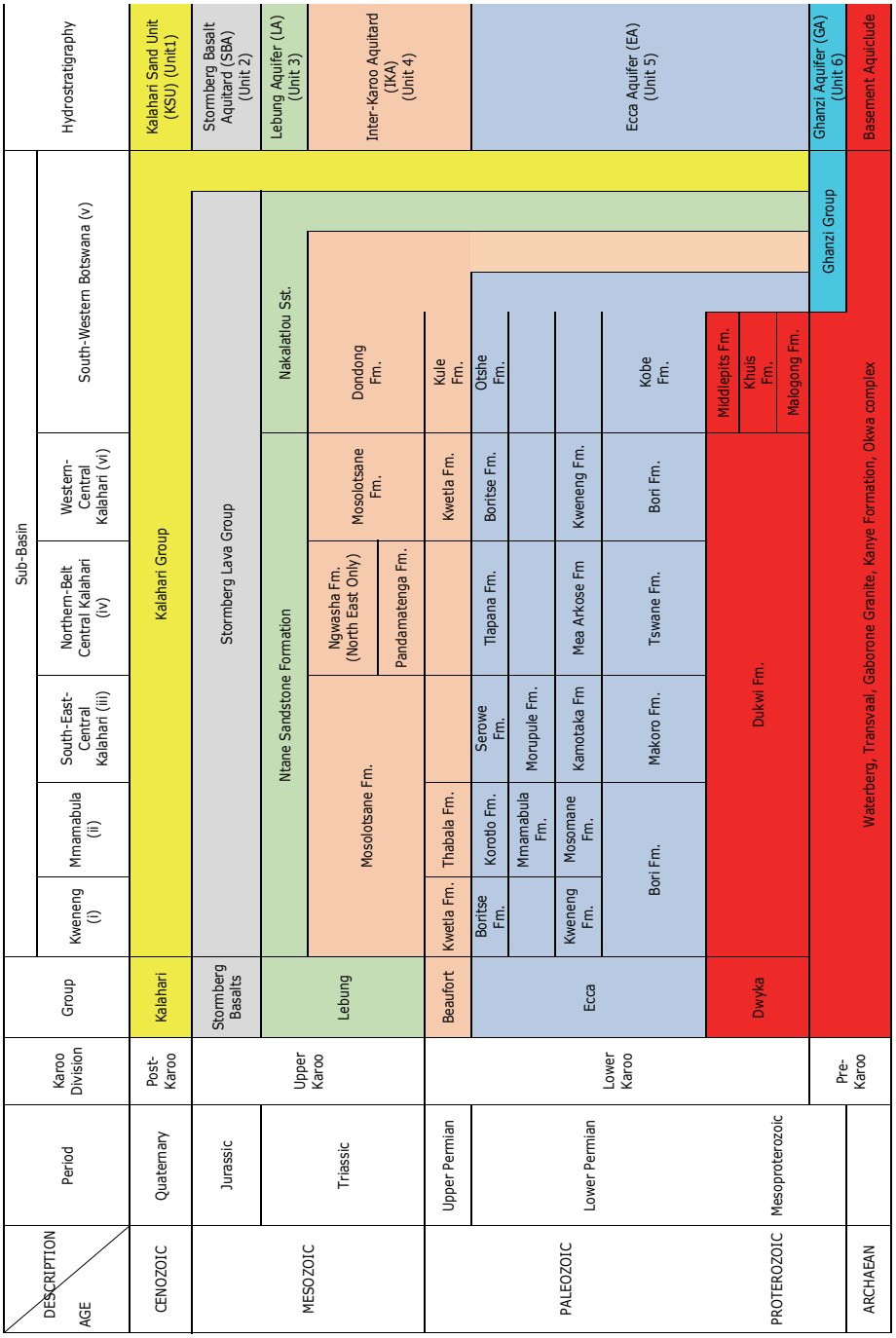

Stormberg Basalt Group

This group forms the uppermost, volcanic unit of the Karoo Super Group (Table 2-1), which has spatially limited extent (Figure 2-3). It consists of an extensive, and locally thick (>100 m) sequence of tholeiitic flood basalts. That basalt is characterised by weathered green to reddish purple, amygdaloidal lava flows, dark grey when fresh and locally fractured (Smith, 1984)..

2.1.1.3 Post Karoo Group (Kalahari Sand)

Post-Karoo (Table 2-1), superficial deposits of the Kalahari Group (commonly termed 'Kalahari Beds' or 'Kalahari Sands'), cover the whole study area and have variable thickness ranging from about 6 to more than 200 m. This group comprises a discordant and highly variable sequence of loose to poorly consolidated sand, silcrete and calcrete intercalations of variable proportions, subordinate to minor ferricrete, silcretized/calcretized sandstones and mudstones (Smith, 1984). The generally large Kalahari Sand thickness, limits recharge in the CKB (Mazor, 1982).

2.1.2 Structural geology

The principal structural elements in the CKB have been defined using aeromagnetic, seismic and gravity data interpretation (Haddon, 2005; Hutchins & Reeves, 1980). The major structural features in the CKB are: the N-S trending Kalahari Line, the NE-SW trending Makgadikgadi Line, the NE-SW trending Tsau Line and the E-W trending Zoetfontein Fault (Carney et al., 1994) (Figure 2-3). The Makgadikgadi and Kalahari Lines are major thrust faults, which originated ~2 Ga ago (Carney et al., 1994). The Kalahari Line defines the western edge of the Kapvaal Craton while the Makgadikgadi Line, the north-western edge of the Zimbabwe Craton (Carney et al., 1994; Key & Ayres, 2000; Pouliquen et al., 2008). The Tsau Line is a series of thrust faults along the strike of the Ghanzi meta-sediments (Ramokate et al., 2000). The Zoetfontein Fault is regional fault zone structures developed during major orogenic episodes in the Lower Proterozoic Era (Smith, 1984). Previous studies by Dietvorst et al. (1991) and Bureau de Recherches Géologiques et Minières (BRGM) (1991) have clearly indicated that movement of pre-existing structures subsequent to lithification in the Zoetfontein Fault, together with the development of the complex fracture pattern, plays a significant role in the hydrogeology of the Karoo strata and has a major influence on the yields of boreholes around it.

2.1.3 Hydrogeology

The hydrogeological regime of the CKB is significantly influenced by geology. The principal aquifers in the CKB are: Ecca Aquifer, Lebung Aquifer and the Ghanzi Aquifer (Table 2-1). It is remarkable that, despite deep occurrence of

groundwater (typically >60 meters below ground surface), in majority of the CKB, the main regional groundwater flow (Figure 2-4) follows the topography, i.e. it is directed from the higher elevated areas along the water divides in the west, south and east, towards lowest depression area around Makgadikgadi Pan (de Vries et al., 2000). There are no permanent surface water bodies in the study area, thus de Vries et al. (2000) characterized the CKB as a closed surface water basin with an internal groundwater drainage system, outflowing towards a natural discharge area of Makgadikgadi Pans (Figure 2-4).

Groundwater replenishment by diffuse recharge is of paramount importance in the CKB since that recharge dictates the amount of groundwater safe yield that can be extracted sustainably from aquifers. However, the high potential evapotranspiration rates due to large vapour pressure deficit, the thick (typically >60m) sandy unsaturated zone and abundant 'thirsty' Kalahari plants, very efficient in taking up unsaturated zone moisture (Lubczynski, 2009; Obakeng et al., 2007), do not favour aquifer replenishment. Such environmental conditions prompted researchers to challenge occurrence of groundwater recharge. For example de Vries (1984) had ruled out groundwater recharge in the Kalahari, stating that the current piezometric surface is a residual-fossil feature, resulting from its decay since the last fluvial period, which ended 12 millennia ago. However, later in his other studies, he admitted recharge of few mm per annum, occurring at the CKB fringes (de Vries et al., 2000). Also Mazor (1982) showed active recharge in the Kalahari fringes, i.e. in Morwamusu and Kweneng areas, despite the thick Kalahari Sand of about 100 m. These observations were confirmed by recent environmental tracers and groundwater flow modelling studies, which stated that CKB recharge is present but only incidentally, being restricted to very wet years/seasons (such as for example 1999-2000), occurring every 5-10 years (Obakeng et al., 2007); in the eastern fringe of the CKB, where the mean annual rainfall is ~ 450 mm, the mean annual recharge is in order of 5-10 mm yr^{-1} while in the central CKB where the mean annual rainfall is ~ 350 mm, the mean annual recharge is < 1 mm (de Vries et al., 2000; de Vries & Simmers, 2002; Gieske, 1992; Lubczynski, 2006, 2009; Obakeng et al., 2007; Selaolo, 1998). The recharge in the far western CKB in Namibia, has not been investigated yet.

Groundwater, wellfield abstractions from the CKB aquifers, are located in the inhabited fringes of the CKB (Figure 2-4) as documented by (SMEC & EHES, 2006). The main groundwater abstractor in the CKB is the Debswana Diamond Mining Company (DDMC), at three locations; Jwaneng, Letlhakane and Orapa

mines.

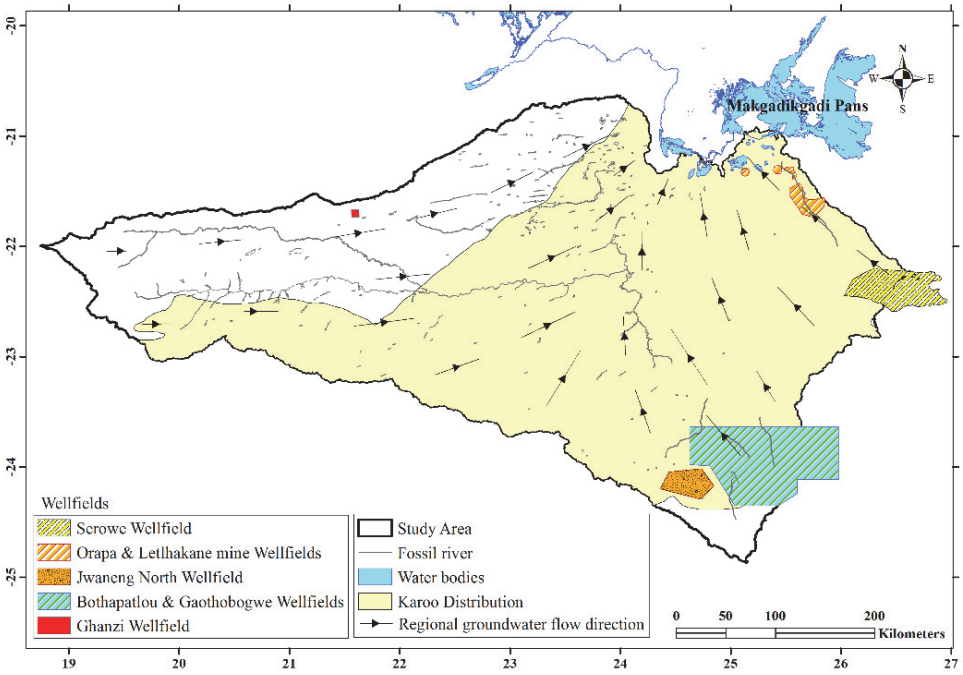

Figure 2-4: General inter-layer groundwater flow pattern and major wellfields in the Central Kalahari Basin.

The Jwaneng mine in the South-Eastern part of CKB, utilizes the Jwaneng North Wellfield (Figure 2-4) where groundwater is abstracted from the Ecca aquifer. The Orapa and Letlhakane mines, in the North-Eastern part of the CKB, have a series of wellfields where groundwater is abstracted from the Lebung Aquifer. Water supply abstraction for major villages from the Ecca Aquifer in the southern part of the CKB, takes place at Gaothobogwe Wellfield, adjacent to the Jwaneng North Wellfield and at the recently developed Bothapatlou Wellfield. In the eastern part of the CKB, at the Serowe Wellfield, groundwater abstraction is from the Lebung Aquifer and in the North-Western, at Ghanzi Wellfield, the abstraction is from the Ghanzi Aquifer (SMEC & EHES, 2006). There are also some minor abstractions from all the three aquifers for settlement water supply and livestock watering.

Chapter 3 : Hydrogeological conceptual model of large and complex sedimentary aquifer systems – the Central Kalahari Basin.

This chapter is based on:

Lekula M, Lubczynski MW, Shemang EM (2018) Hydrogeological conceptual model of large and complex sedimentary aquifer systems – Central Kalahari Basin Physics and Chemistry of the Earth, Parts A/B/C DOI https://doi.org/10.1016/j.pce.2018.05.006

3.1 Abstract

Successful groundwater resources evaluation and management is nowadays typically undertaken using distributed numerical groundwater models. Such models largely rely on hydrogeological conceptual models (HCMs). The conceptual models summarize hydrogeological knowledge of an area to be modelled and thereby providing a framework for numerical model design. In this study, an efficient data integration method for developing HCM of the large and hydrogeologically-complex, Central Kalahari Basin (CKB) aquifer system, was undertaken. In that process, suitability of 3-D geological modelling with RockWorks code in iterative combination with standard GIS (ArcGIS) was tested. As a result, six hydrostratigraphic units were identified, their heads and related flow system interdependencies evaluated and hydraulic properties attached. A characteristic feature of the CKB is a thick unsaturated Kalahari Sand Unit (KSU), that restricts the erratic recharge input to <1 mm yr^{-1} in the centre to about 5-10 mm yr^{-1} in the eastern fringe. The analysis of the spatial distribution of topological surfaces of the hydrostratigraphic units and hydraulic heads of the aquifers, allowed to identify three flow systems of the three aquifers, Lebung, Ecca and Ghanzi, all three having similar radially-concentric regional groundwater flow patterns directed towards discharge area of Makgadikgadi Pans. That pattern similarity is likely due to various hydraulic interconnections, direct or through aquitard leakages, and also due to the presence of the overlying unconfined, surficial KSU, hydraulically connected with all the three aquifers, redistributing recharge into them. The proposed 3-D geological modelling with RockWorks, turned to be vital and efficient in developing HCM of a large and complex multi-layered aquifer systems. Its strength is in simplicity of operation, in conjunctive, iterative use with other software such as standard GIS and in flexibility to interface with numerical groundwater model. As a result of conceptual modelling, fully 3-D, 6-layer numerical groundwater model, with shallow, variably-saturated saturated, unconfined layer is finally recommended as transition from conceptual into numerical model of the CKB.

3.2 Introduction

The successful groundwater resources evaluation and management is nowadays typically done using distributed numerical groundwater models. The reliability of such models is largely determined by realistic hydrogeological conceptual models (HCMs), which summarize hydrogeological knowledge of a site to be modelled and thereby providing a framework for numerical model design. According to Anderson et al. (2015), hydrogeological "conceptual model is a qualitative representation of a groundwater system that conforms to hydrogeological principles and is based on geological, geophysical, hydrological, hydrogeochemical and other ancillary information"; hence it includes both, the hydrogeological framework and hydrological system characterization. HCM is usually presented in a series of cross sections, fence diagrams and tables showing distribution of hydrostratigraphic units and boundary conditions with groundwater flow directions and hydrogeological parameter estimates. All these, are reconstructed from surface and subsurface data to help hydrogeologists understand the hydrogeological system behaviour and support quantitative modelling (Frances et al., 2014). The subsurface geological data such as lithology, structural geology and stratigraphy, are difficult to schematize due to geological heterogeneity and data scarcity (Trabelsi et al., 2013). Even more difficult is to characterize hydrostratigraphy, hydrogeological parameters, flow systems with their piezometric surfaces and interactions, all these assessed in this study.

HCM setup usually involves analysis and integration of relevant geological and hydrogeological data using database tool such as a geographical information system (GIS) (Anderson et al., 2015; Trabelsi et al., 2013), although there is no standard widely accepted methodology in that respect (Brassington & Younger, 2010). The 3-D geological modelling (Hassen et al., 2016) has not been frequently used in environmental studies in the past century due to a number of reasons, among them being high cost of software packages, necessary powerful hardware and often shortage of borehole information. However, only recently, the 3-D geological modelling has increasingly been used as a tool for synthesizing all available data types, leading to better understanding and more realistic presentation of a geological settings (Hassen et al., 2016). The demand for 3-D geological modelling and rapid increase of computer power, resulted in advancement in the 3-D modelling packages, which allowed development of efficient 3-D geological models on standard desktops (Royse, 2010), making them available to a wider scientific and commercial community (Raiber et al., 2012). Also this advancement has enabled 3-D geological models to move from the sole use in petroleum and mining industry to geological disciplines (Royse, 2010), including hydrogeology (Gill et al., 2011). In groundwater studies, 3-D geological modelling is used to evaluate complexity of structural geological and hydrogeological subsurface

heterogeneity, which is generally the basis for any HCM and therefore a very important step towards building a numerical distributed groundwater flow models (Bredehoeft, 2002; Robins et al., 2005; Tam et al., 2014). The 3-D geological models also assist in providing a check on the logic of the hydrogeological conceptualization (Gill et al., 2011), especially important in areas with high hydrogeological heterogeneity (Tam et al., 2014).

The usefulness of 3-D geological models in hydrogeological conceptualization of aquifers has been demonstrated worldwide, but only few of such models address Africa, especially semi-arid regions where groundwater is the only source of potable water. For example, in the Northern Africa, Hassen et al. (2016) constructed 3-D geological model of the Kasserine Aquifer System in Tunisia, which was further used in the development of HCM and for future development of the 3-D numerical groundwater flow model. In Southern Africa, Lindenmaier et al. (2014) integrated all available geological information in a 3-D geological model to refine the hydrostratigraphy and to develop a 3-D aquifer map within the Cuvelai-Etosha Basin in Namibia. However, there has not been presented any regional HCM of the Central Kalahari Basin (CKB) (Figure 2-1), especially not based on the 3-D geological model solution, addressing the complex, multi-layered, geological and hydrogeological CKB system heterogeneity. So far, only local studies within small parts of the CKB, summarised in the Botswana National Water Master Plan Review (SMEC & EHES, 2006), have been investigated using 3-D geological modelling.

The CKB is very important hydrogeologically to Botswana and neighbouring Namibia, as it hosts the most productive and exploited transboundary Karoo System Aquifers. A lot of research in the CKB has been carried out on the Karoo System depositional environment and for possible occurrence of oil and coal bedded methane gas, rather than for groundwater potential. These researches included, for example, studies by Bordy et al. (2010), where they analysed the depositional environment of the Mosolotsane Formation and other exploration works by international companies like for example Shell Oil Company. Hydrogeological studies in the CKB have been limited. Farr et al. (1981) evaluated groundwater resources in Botswana, including the CKB, but their study did not cover spatial distribution of hydrostratigraphic units. Considering CKB hydrogeology, only few recharge-related studies are published, all referring to CKB fringes (e.g. de Vries & Simmers, 2002; Mazor, 1982; Obakeng et al., 2007; Stadler et al., 2010). There are also some local, consultancy studies (e.g. Geotechnical Consulting Services (Pty) Ltd, 2014; Water Surveys Botswana (Pty) Ltd, 2008; Water Surveys Botswana (Pty) Ltd & Aqualogic (Pty) Ltd, 2007; Wellfield Consulting Services (Pty) Ltd, 2001, 2007, 2009, 2012), presenting local hydrogeological conditions of the CKB, based on borehole data. However, none of them attempted to integrate spatially all the available, fragmented data, to develop HCM of the CKB.

The main objective of this study was to develop an efficient method of integrating data from various sources and scales, to develop HCM of a large and complex multi-layered aquifer system, such as the CKB. Specific objectives of this study were: 1) to test suitability of 3-D geological modelling tool in: i) integration of data from various sources and scales; ii) modelling of hydrostratigraphic units in large and complex multi-layered aquifer systems; iii) its interfacing with GIS and numerical model; 2) to improve CKB understanding of: i) the spatial distribution of the hydrostratigraphic units and their hydraulic properties; ii) flow systems, their boundaries and interactions between different hydrostratigraphic units; 3) to adapt the HCM to its smooth transition into regional, numerical model.

3.3 Methodology of setting up CKB conceptual model

The hydrostratigraphic unit modelling, system parameterization, flow system analysis, preliminary water balance and hydrogeological boundary conditions were used as steps in development of an efficient method of integrating data from various sources at various scale and setting up HCM of a large and complex, CKB multi-layered aquifer system.

3.3.1 Borehole and spatial data

Borehole information, spatial geological data (including shapefiles), geological bulletins and hydrogeological reports done by groundwater consults were sourced from Botswana Geoscience Institute (BGI, former Department of Geological Survey) and Department of Water Affairs (DWA). The geological shapefiles for Namibia were downloaded online. Water levels were sourced from DWA, DDMC and Directorate of Water Resources Management in Namibia (DWRM). The digital elevation model (DEM) at 90 m spatial resolution was obtained from Shuttle Radar Topography Mission (SRTM) (Jarvis et al., 2008). The developed borehole database contained altitudes, lithological logs, water strikes and rest water levels. The published national geological map of Botswana by Key and Ayres (2000) as well as hydrogeological reports from groundwater consultants (e.g. Geotechnical Consulting Services (Pty) Ltd, 2014; Pacific Consultants International & SANYU Consultants INC, 2002a, 2002b; Water Surveys Botswana (Pty) Ltd, 2008; Water Surveys Botswana (Pty) Ltd & Aqualogic (Pty) Ltd, 2007; Wellfield Consulting Services (Pty) Ltd, 2001, 2007, 2012) provided additional geological information and hydrogeological data, like aquifer transmissivity and hydraulic conductivity.

3.3.2 Geological modelling and hydrostratigraphic units

The RockWorks version 17 software package (RockWare, 2017), further referred to as RockWorks, was used for geological and hydrogeological data

analysis and management, and for modelling topological surfaces and visualization of hydrostratigraphic units and cross-sections. The RockWorks, an easy to use software for 3-D modelling of subsurface geology and hydrostratigraphy (Trabelsi et al., 2013), handles spatial surfaces and subsurface data, providing several borehole data gridding and interpolating methods, including inverse distance, kriging, distance to point and triangulation, to build a 3-D spatial model. In this study, the five km node spacing and the inverse distance interpolation method with power two was chosen due to its ability to optimally interpolate faulted surfaces by giving less weight to far distant points, thus representing faulted surfaces better.

A six hydrostratigraphic units' schematization (Anderson et al., 2015) for the CKB system (right column of the Table 2-1) was deduced and proposed, based on detailed analysis of borehole data and related geological formations, subsurface lithology and groundwater occurrence. For example, in Mmamabula Sub-Basin, the stratigraphic Lebung Group consisting of Ntane and Mosolotsane Formations, was split into two hydrostratigraphic units, the Lebung Aquifer represented by Ntane Sandstone Formation and the Inter-Karoo Aquitard represented by argillic Mosolotsane Formation combined with underlying Thabala Formation of the Beaufort Group characterized by similar argillic composition. After systematic identification of the six hydrostratigraphic units, spatial definition of these units was further elaborated in the RockWorks.

Individual borehole coordinates, elevations, hydrostratigraphic unit intervals, deduced from borehole lithological logs and digitised major faults from geological shapefiles were added to RockWorks "Borehole Manager tool" for interpolation. The 3-D solid model of hydrostratigraphic units was then generated and analysed. This was an iterative process, carried out until the satisfactory hydrostratigraphic thicknesses, replicating their known spatial representation, were achieved. Different fault angles were also tested and a 90^0 block faulting angle was set for all the regional faults. Also spatial location of boreholes used for hydrostratigraphic unit modelling were considered adequate to address issues of aquifer wedging and hydrostratigraphic displacement due to faulting as some of them were beyond the CKB model domain. Where borehole lithological logs were insufficient, spatial extent of the hydrostratigraphic units was constrained by geological shapefiles, which have been deduced using geophysical methods. For visual presentation, the vertical interval of hydrostratigraphic units were exaggerated 200 times. The resultant, 2-D cross sections, drawn along sections of interest, were then used to visualize the spatial extent of hydrostratigraphic units.

The thicknesses of individual hydrostratigraphic units were exported from the 3-D geological model as XYZ files and further used to display and examine their

spatial extent using ArcGIS 10.4 GIS software, further referred to as ArcGIS. That data export was done with ArcGIS, because of its superior visual display.

3.3.3 System parameterization

The CKB aquifer transmissivity data (*T*) were extracted from 358 pumping tests documented in groundwater consultant reports (Geotechnical Consulting Services (Pty) Ltd, 2000, 2014; Pacific Consultants International & SANYU Consultants INC, 2002a, 2002b; Water Surveys Botswana (Pty) Ltd & Aqualogic (Pty) Ltd, 2007; Wellfield Consulting Services (Pty) Ltd, 2001, 2007, 2012). As log-normally distributed spatial property, the *T* data were interpolated using inverse distance of power two. That interpolation was carried out in ArcGIS software. The aquifer hydraulic conductivities (*K*) were derived by dividing *T* by corresponding aquifer thicknesses deduced from Rockworks. The aquifer storage parameters were extracted from 116 piezometric pumping test data and lithology of borehole logs, documented in groundwater consultant reports. The data to estimate aquitards' *K* and unsaturated zone parameters were also assigned based on groundwater consultancy reports and general literature guidelines addressing hydraulic conductivities of semi-permeable lithological units (Brassington, 1998; Freeze & Cherry, 1979).

3.3.4 Flow system analysis

Flow system of multi-layered CKB is complex, despite the fact, there are no surface water bodies interacting with groundwater; there are only ephemeral rivers and streams, infiltrating water into subsurface shortly after intense rains. Consequently there is only diffuse rain-recharge, which is erratic and on average in order of only few millimetres per year at most and only following a wet year (de Vries et al., 2000; Obakeng et al., 2007). Hydraulic heads for each aquifer were defined from the borehole groundwater level data acquired from DWA, DDMC and DWRW. The hydraulic heads of each aquifer were spatially interpolated using kriging method in ArcGIS, despite sparsely distributed boreholes in some parts of the CKB. In locations with large separation distances between boreholes, fictitious control points were used. The interpolated heads defined potentiometric maps, which further determined groundwater flow directions. The aquifer flow systems, locally connected with overlying unconfined Kalahari Sand Unit (KSU) are: i) Lebung Aquifer (LA); ii) Ecca Aquifer (EA); iii) Ghanzi Aquifer (GA). In the flow system analysis, particular attention was dedicated not only to aquifer interactions with KSU but also to interrelations between the three aquifer flow systems, each interaction pair regulated by leakance of an intra-aquitard.

3.3.5 Preliminary water balance

It is hypothesised that the only input of water in the CKB is precipitation. The main output is evapotranspiration and other two small output contributors are groundwater abstraction for habited areas and for wildlife and groundwater outflow towards Makgadikgadi Pans discharge area (Figure 2-4).

3.3.6 Hydrogeological boundary conditions

In definition of boundary conditions, first physical boundaries such as spatial extent of hydrostratigraphic units, surface topography and major tectonic structures were analysed. Next, the result of that analysis was cross-referenced with the regional potentiometric maps, extending outside the CKB, to deduce regional flow directions. In case of no distinct physical boundaries, that analysis allowed to delineate external groundwater outflow boundaries, external no-flow boundaries along (parallel to) major streamline directions and characterize internal boundaries such as preferential flow lines along major fault systems and barriers of groundwater flow.

3.4 CKB conceptual model

3.4.1 Geological modelling and hydrostratigraphic units

The six-hydrostratigraphic units within the Karoo Super Group Formation and the Pre-Karoo rocks were identified based on lithological and hydrogeological analysis and are marked by different colors in Table 2-1: i) Kalahari Sand Unit (KSU); ii) Stormberg Basalt Aquitard (SBA); iii) Lebung Aquifer (LA); iv) Inter-Karoo Aquitard (IKA); v) Ecca Aquifer (EA); and vi) Ghanzi Aquifer (GA). They are also presented spatially in series of hydrostratigraphic cross-sections in Figure 3-1 and Figure 3-2.

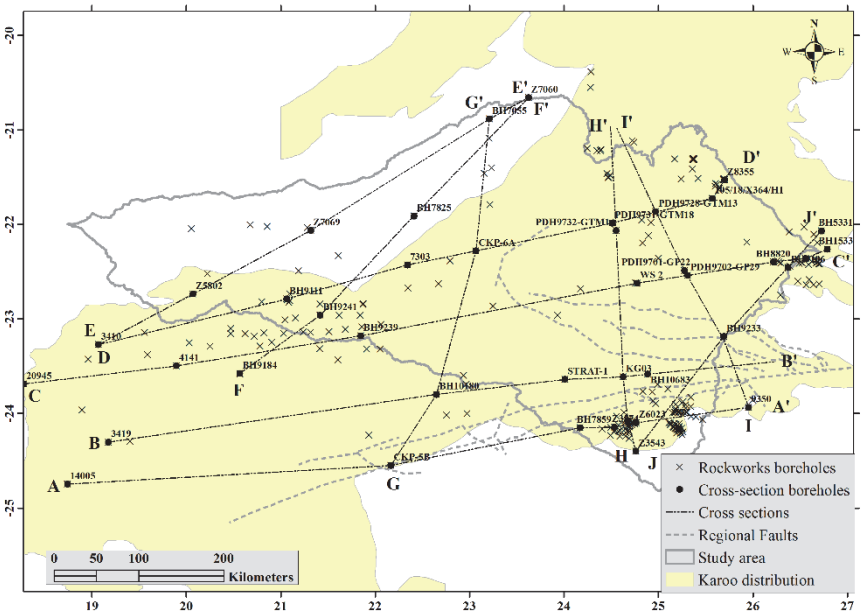

Figure 3-1: Spatial distribution of boreholes used in RockWorks database and locations of 10 selected hydrostratigraphic cross-sections in the study area.

These cross-sections present spatial extent and thicknesses of the hydrostratigraphic units, geometric and inter-hydrostratigraphic relationships, particularly around the regional faults.

Kalahari Sand Unit (KSU)

The KSU, is the first, surficial unit, composed of sandy, unconsolidated to semi-consolidated deposits. It is the only hydrostratigraphic unit with continuous spatial extent in the whole CKB. Its thickness is spatially variable, ranging from 6 m in the western part to more than 100 m in the central and northern parts of the CKB (Figure 3-2 and Figure 3-3a). The characteristic feature of this unit is that 80-100% of its thickness is unsaturated so only its bottom part is locally saturated. If directly underlain by any of the aquifers, i.e. Lebung, Ghanzi or Ecca, then it is in hydraulic contact with that aquifer. The KSU is not productive within the CKB, therefore it is not referred as an aquifer, even though perched saturated units occur in its profile.

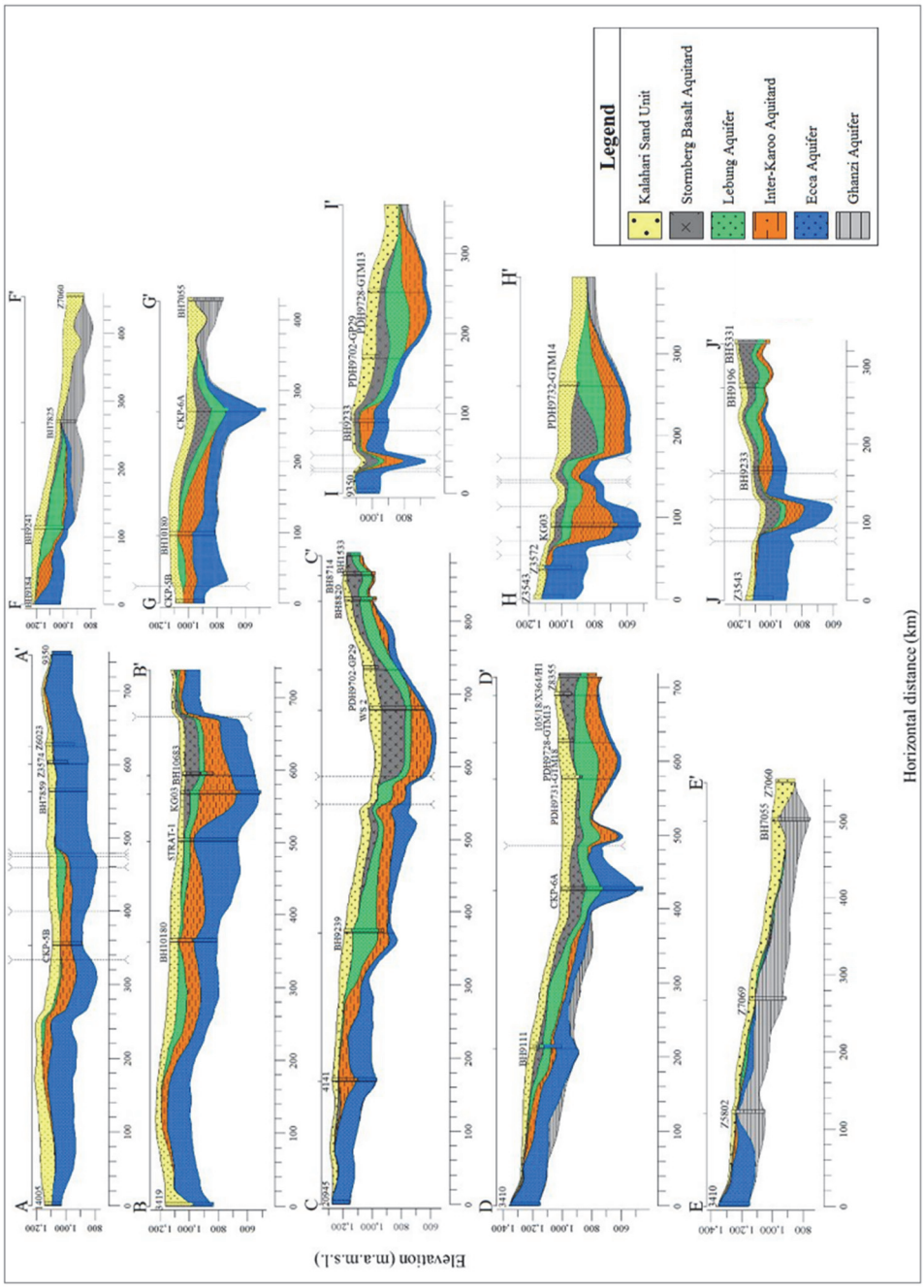

Figure 3-2: Hydrostratigraphic cross-sections-locations presented in Figure 3-1. Vertical dashed lines show locations of faults.

Stormberg Basalt Aquitard (SBA)

The SBA is non-uniformly distributed in the CKB, composed of sparsely-fractured basalt (Figure 2-3). Its thickness is spatially variable ranging from 0 to ~ 200 m, due to the block faulting and basin morphology (Figure 3-2 and Figure 3-3b). The SBA has been eroded in the southern part of the Zoetfontein Fault (Figure 2-3), where significant uplifting occurred resulting in a horst structure as seen in Figure 3-2 sections H-H, I-I and J-J. The thickest SBA block of more than 200 m is in the CKB centre. That block is likely a result of sufficient space release after deepening of the basin (Figure 3-2 sections C-C' and H-H' and Figure 3-3b) and its basalt infillment. Similarly, the thick SBA in central part of Zoetfontein Fault zone can be attributed to significant down-faulting of the graben structure, thus preserving the original stratigraphy of the basin. The SBA is considered as highly heterogeneous aquitard mainly because of localised, dense fracture occurrences.

Lebung Aquifer (LA)

The LA, is one of the most productive aquifers in the CKB. It is composed of dual porosity sandstone characterized with spatially varying thickness, ranging from zero meters in the north-western part of the CKB where it wedges out and also in the southern part of the Zoetfontein Fault where it has been eroded as a result of significant uplifting, to ~230 m in the north-eastern and south-western parts of the CKB (Figure 3-3c). The depth of the top of the LA is also spatially variable, being significantly influenced by deepening of the basin towards the CKB centre and by regional faulting, mainly by Zoetfontein Fault (Figure 3-2), being the deepest in the central part of the CKB where it also coincides with the thickest SBA. Where overlain by SBA, the LA is confined but where the SBA is missing, it is hydraulically connected with the overlying KSU, creating one unconfined aquifer (provided KSU is saturated at its bottom part) as can be seen in Fig 3-2 sections B-B',C-C' and H-H'. In the western part of CKB, where Inter-Karoo Aquitard is absent, the LA is hydraulically connected with the underlying Ecca aquifer.

Inter-Karoo Aquitard (IKA)

The IKA, is composed of inter-changing low permeability mudstones and siltstones, underlying the LA and overlying the Ecca Aquifer. It has low, spatially variable permeability, ranging from nearly impermeable to semi-permeable. Its thickness is spatially variable, ranging from zero meters in the north-western and southern part of the CKB, to ~250 m in the central part (Figure 3-3d). The depth to the top of the IKA is also spatially variable and significantly controlled by deepening of the basin towards central CKB and also by regional faults (Figure 3-2). The low permeability of this unit ensures a low groundwater exchange between the LA and the underlying Ecca Aquifer, thus acting as an aquitard confinement to the Ecca aquifer (SMEC & EHES, 2006).

Where the IKA is absent, the Ecca Aquifer is in hydraulic contact with the overlying LA, but in locations where the LA and the SBA are missing, the Ecca Aquifer is hydraulically connected with the KSU.

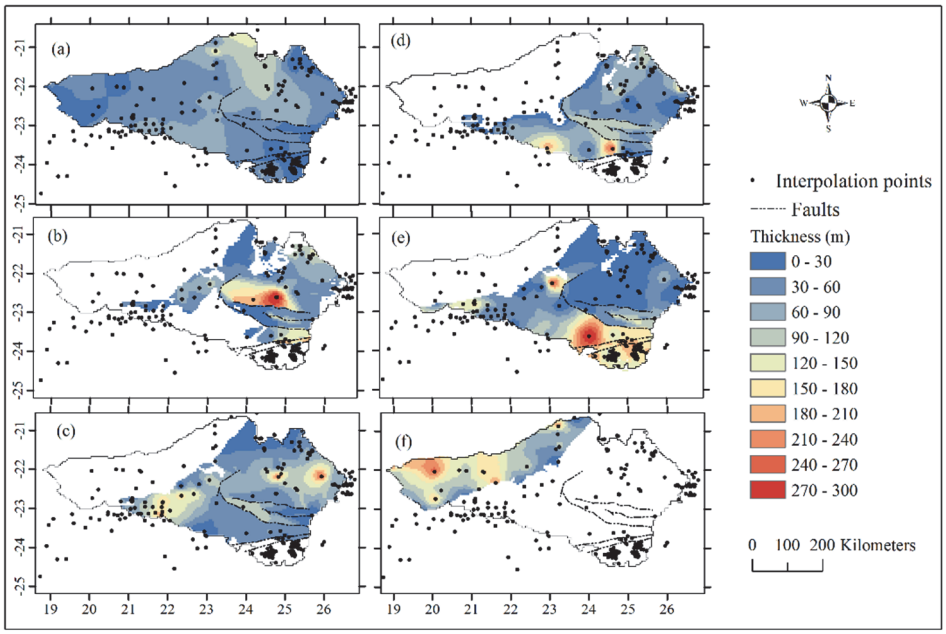

Figure 3-3: Thickness of the six hydrostratigraphic units in the Central Kalahari Basin. Alphabetic letters denotes: a) Kalahari Sand Unit; b) Stormberg Basalt Aquitard; c) Lebung Aquifer; d) Inter-Karoo Aquitard; e) Ecca Aquifer; f) Ghanzi Aquifer.

Ecca Aquifer (EA)

The EA is composed of an alternating sugary-grained sandstone with coal seams, characterized by smooth transition between different formations (Smith, 1984). It has a spatially varying thickness ranging from zero in the north-western CKB where it wedges out, to ~290 m in the southern part of the Zoetfontein Fault, where significant uplifting was followed by erosion of the SBA, LA and even IKA (Figure 3-3e) so that EA is directly overlain by KSU. The thickness of the EA in the north-eastern part of the CKB is uncertain due to limited amount of borehole data penetrating the whole EA thickness. Depth to the top of the EA is spatially variable and is largely controlled by deepening of the basin towards central CKB and the graben and horst structures of the Zoetfontein Fault zone (Figure 3-2). The EA is the deepest in the southern part of the CKB around the Zoetfontein graben structure, where all the stratigraphic units of the Karoo Super Group are present, representing the original Karoo sedimentation (SMEC & EHES, 2006). The EA is confined where overlain by IKA (Figure 3-2). Where the IKA is absent, the EA is hydraulically connected with the overlying LA and where the LA and the SBA are missing, it is hydraulically connected with the KSU, creating one unconfined aquifer (Figure 3-2). The

direct hydraulic contact between EA and LA can be seen in Figure 3-2 in sections D-D' and I-I' while between EA and KSU in section H-H' and J-J'.

Ghanzi Aquifer (GA)

The GA is a sandwich of fractured arkosic sandstones, siltstone, mudstone and rhythmite; nearly all its spatial extent is directly overlain by the KSU, the two being in hydraulic contact. The GA is only present in the north-western part of the CKB (Figure 3-3f). Its thickness is spatially variable, ranging from zero due to wedging towards centre of CKB, to ~230 m (Figure 3-2 and Figure 3-3f) towards the north-western CKB. The depth to the top of the GA is also spatially variable, shallow where the KSU is the only overlying hydrostratigraphic unit and deeper towards the basin centre, as can be seen in Figure 3-2 sections E-E' and F-F'.

Basement Aquiclude

Basement aquiclude is represented by the impermeable unit underlying the deepest aquifer unit in a given location of the flow system. It can be Dwyka, Waterberg, Transvaal, Gaborone Granite, Kanye Formation or Okwa Complex (Table 2-1).

3.4.2 System parameterization

The KSU is not a productive aquifer in the CKB, so there are no parametric estimates from pumping tests. However, that sandy, permeable and relatively homogeneous unit, plays an important role in redistribution but also restriction of groundwater recharge to underlying aquifers because of its large thickness and "thirsty" Kalahari trees, being able to uptake water from large depth. The horizontal and vertical hydraulic conductivities of the KSU, obtained from SMEC and EHES (2006), range from 1.0 to 15.0 md^{-1} and from 0.1 to 2.0 md^{-1} respectively. The SBA is represented by a secondary porosity basalt rock type that has negligible storage (SMEC & EHES, 2006) and low, fracture-based, vertical hydraulic conductivity in order of $3.0x10^{-4}$ md^{-1} (Brassington, 1998; Freeze & Cherry, 1979). The *K* of the LA presented in Figure 3-4a, varies from less than 0.1 to more than 10.0 md^{-1}, the range typically associated with sandstones (Brassington, 1998; Freeze & Cherry, 1979) while the *T*, from 10.0 to 100.0 m^2d^{-1} (Figure 3-4d). The relatively uniform *K* and *T* of LA in the central part of the CKB, are uncertain due to data limitation, hence need to be optimised during the numerical model simulation. The IKA is composed of semi-permeable layer-sequence of siltstones and mudstones, which can be characterized by a horizontal hydraulic conductivity ranging from $8.6x10^{-7}$ to $1.2x10^{-3}$ and vertical hydraulic conductivity ten times lower than the horizontal (Brassington, 1998; Freeze & Cherry, 1979). The low IKA vertical *K* ensures limited hydraulic contact between EA and LA. The K and *T* of the EA (Figure 3-4b and Figure 3-4e, respectively) are highly spatially variable, ranging from

low values in the eastern side of the CKB, to large values in the western side, where locally K>10 md^{-1} and T>500 m^{2}d^{-1}. The large area with T in range 100-500 m^2 d^{-1} in the north-eastern part of CKB is uncertain due to limited amount of data, hence it needs to be optimised during the numerical model simulation.

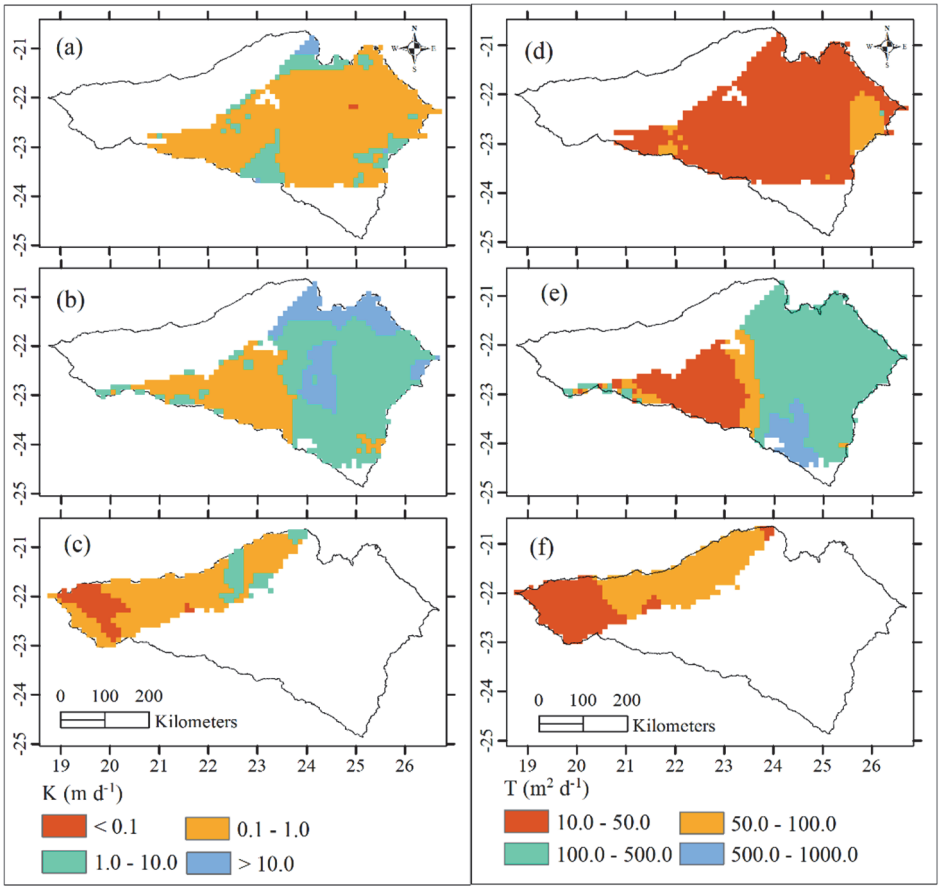

Figure 3-4: Aquifer hydraulic conductivity (K) and transmissivity (T) in the Central Kalahari Basin: a) Lebung Aquifer K; b) Ecca Aquifer K; c) Ghanzi Aquifer K; d) Lebung Aquifer T; e) Ecca Aquifer T; f) Ghanzi Aquifer T.

The GA is hydraulically connected with KSU. Like in the case of EA, the K and T of the metamorphic, fractured-arkosic rock composition of GA, changes spatially from low values in the western part to higher in the eastern (Figure 3-4c and Figure 3-4f, respectively), with K ranging from less than 0.1 to 10.0 m d^{-1} and T from 10.0 to 100.0 m^2 d^{-1}, respectively.

3.4.3 Flow system, water balance and hydrogeological boundary conditions

3.4.3.1 Kalahari Sand Unit (KSU)

The potentiometric map of the Kalahari Sand Unit is presented in Figure 3-5. This map considers number of possibilities regarding KSU hydraulic relation with underlying units. Where the KSU is underlain by either LA, EA or GA, and the potentiometric surface is above the KSU bottom, then the lowest part of the KSU is saturated (continuous isolines); if the potentiometric surface is below the KSU bottom, then the KSU profile is entirely unsaturated (dashed isolines). If the KSU is underlain by aquitard or aquiclude and the potentiometric surface is above the KSU bottom, then the lowest part of the KSU is saturated, as unconfined layer isolated from the bottom; otherwise, the KSU is entirely unsaturated.

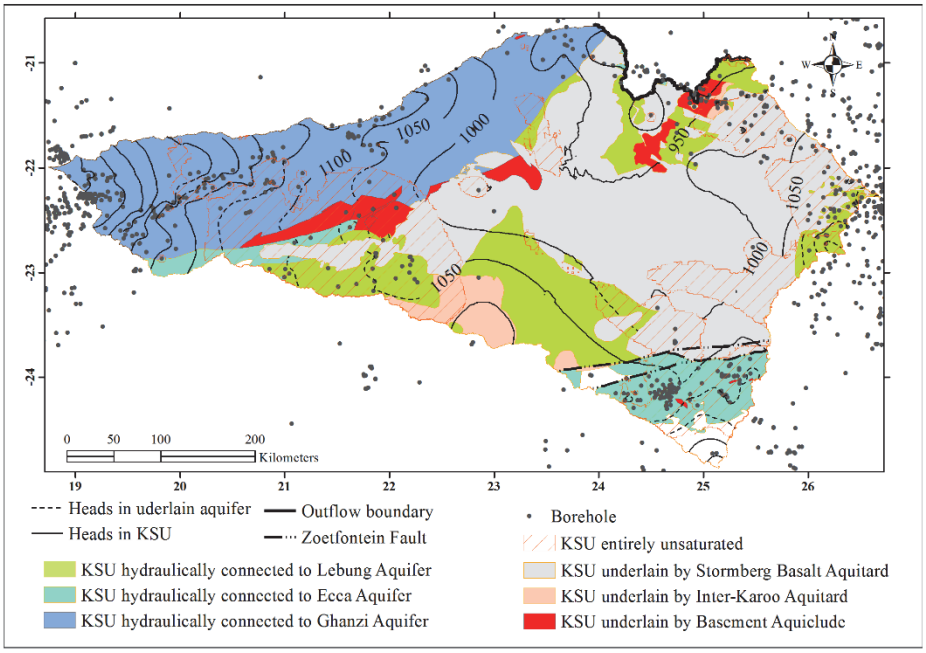

Figure 3-5: Hydraulic heads and boundary conditions of an unconfined Kalahari Sand Unit (KSU) and Ghanzi Aquifer.

The flow pattern of the KSU is radially-concentric (Figure 3-5). It converges from western, eastern and southern no-flow boundaries defined along the CKB watershed divides, towards the northern, Makgadikgadi Pans groundwater outflow boundary. That pattern, matches also the flow pattern of underlain aquifers and the regional pattern of groundwater flow, postulated by de Vries (1984) and de Vries et al. (2000). In the central-eastern part of the CKB, the

KSU is saturated, being either on top of the SBA or hydraulically connected with underlain LA. In the north-western part of the CKB, the KSU is in hydraulic connection with GA, while the connection with EA occurs only within a little strip in the western area.

The thickness of the saturated part of the KSU profile, vary spatially from zero (stripped areas in Figure 3-5) to 25 m (KSU saturation-thickness map not presented), hence the saturated thickness of the KSU is non-uniformly distributed. Regarding temporal variability of the saturated KSU thickness, it has to be noted that after substantial recharge, that thickness gently increase, but gently, afterwards gradually declining mainly due to downward leakage and/or groundwater evapotranspiration. In the KSU, there are also localised, perched layers, which however play negligible role in the CKB flownet system, eventually only redistributing recharge; therefore, the Kalahari perched layers are neglected in the regional CKB groundwater flow model.

3.4.3.2 Lebung Aquifer (LA)

The Lebung Aquifer has a spatially limited extent. Like the KSU, its hydraulic heads show a radially-concentric pattern, converging from western, southern and eastern no-flow boundaries, towards the northern Makgadikgadi Pans groundwater outflow boundary (Figure 3-6). In the peripheral zone of the CKB, where the LA is directly overlain by KSU (Figure 3-6), they both create one hydraulically connected, unconfined aquifer. That hydraulic connection allows for recharge from the KSU into the LA. In the remaining area, the LA is confined by overlaying SBA although according to Smith (1984), there is localized leakage across the SBA due to localised fracture systems. It is interesting that the directions of the vertical leakages across the overlying SBA and the underlying IKA, are spatially variable. Those leakage directions depend on the potentiometric surface of the LA relative to the overlying KSU and underlying EA, while the leakage rates across the SBA and IKA depend on the respective leakances and head differences.

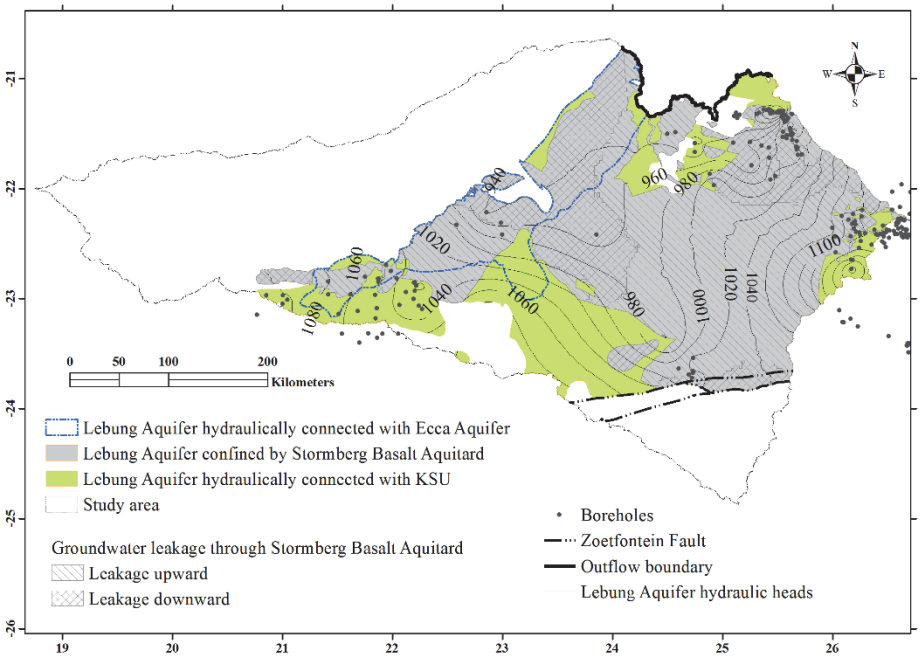

Figure 3-6: Hydraulic heads and boundary conditions of Lebung Aquifer.

At the southern part of the CKB, the groundwater flow system of the LA is delimited by graben and horst discontinuity structures of the Zoetfontein Fault zone, schematic of which is presented in Figure 3-7.

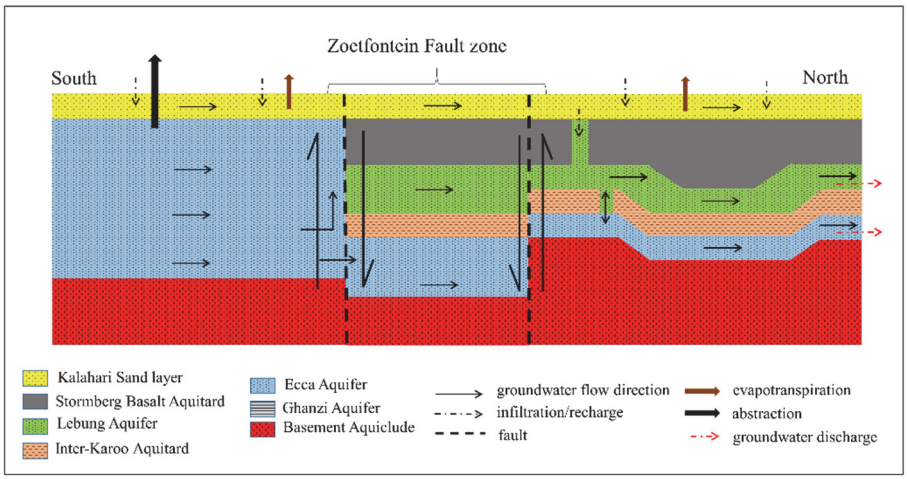

Figure 3-7: Schematic of flow system adjacent to Zoetfontein Fault.

Considering structural position of the LA at the northern side of the fault, it is likely that this aquifer is in hydraulic contact across the fault, with the EA at the southern side, although that connection requires additional investigations.

The radially-concentric groundwater flow pattern in the LA (and in KSU) implies its relatively simple water balance, where the Darcian lateral flow originated from water exchanges with overlying and underlying layers, is discharged at the northern outflow boundary and also by groundwater evapotranspiration as well as some well abstractions.

3.4.3.3 Ecca Aquifer (EA)

The flow pattern of the Ecca Aquifer is similar to the flow patterns of the LA and KSU, i.e. the hydraulic heads show a radially concentric pattern, converging from western, southern and eastern no-flow boundaries towards the northern outflow boundary at the Makgadikgadi Pans (Figure 3-8). That similarity is influenced by good hydraulic EA connections with: i) KSU in the southern part, towards south of Zoetfontein Fault (Figure 3-5, Figure 3-7 and Figure 3-8) and in the western part (Figure 3-8); with ii) LA wedging at the north-western part (Figure 3-8 as well as the cross-sections in Figure 3-3); and with iii) GA towards north-west.

The majority of the EA within the CKB is confined by IKA separating it from LA. The spatially variable vertical, upward or downward, leakage in the IKA, as presented in Figure 3-8, is constrained by relative positions of the potentiometric surfaces of the EA and LA and by IKA leakance. It is hypothesized that the EA (like LA) represents laterally closed system. It exchanges groundwater only with overlying layers (and losses some water by groundwater evapotranspiration and abstractions at wellfields located south of the Zoetfontein Fault, see Figure 2-4), so that nearly-all the EA groundwater is discharged at the northern outflow boundary as the external boundaries are no-flow boundaries. The physical, wedging boundaries at the north-western and southern limits are reliable no-flow boundaries. The remaining external boundaries can be assigned as hydraulic no-flow boundaries along streamlines, in directions perpendicular to equipotential lines; however, some sections of these boundaries, particularly those under thick IKA, are uncertain as not sufficiently documented by adjacent boreholes.

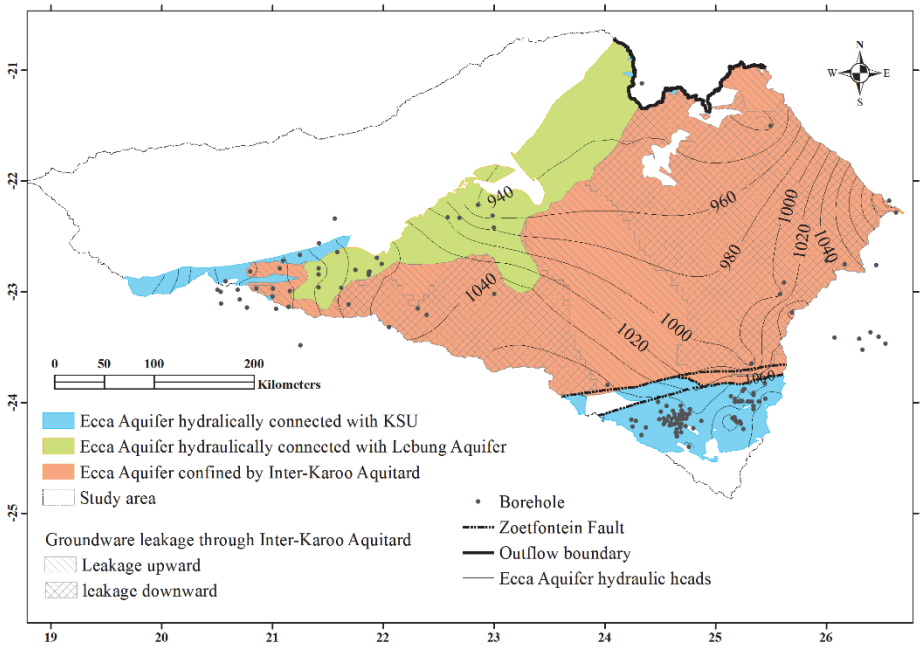

Figure 3-8: Hydraulic heads and boundary conditions of Ecca Aquifer.

Nevertheless, if there is some flow across these boundaries, it is expected that it is negligible although at the current state of knowledge that hypothesis cannot be proved or rejected. Once numerical model is setup and calibrated, that hypothesis can be tested.

3.4.3.4 Ghanzi Aquifer (GA)

The Ghanzi Aquifer (Figure 3-5), is the only aquifer present in the north-western CKB. In the large part of the CKB extent, it is directly overlain by KSU, so prone to recharge, and it is hydraulically connected with saturated KSU (continuous isolines) forming jointly one unconfined aquifer. The GA groundwater flow pattern, like of all other aquifers, is directed towards the northern outflow boundary of the Makgadikgadi Pans. In the south-eastern direction, the GA is hydraulically connected with the EA (Figure 3-2 section E-E' and Figure 3-5) and possibly also with LA (Figure 3-2, G-G). Considering that groundwater flow direction is parallel to the contacts with EA and LA (Figure 3-5), it is expected that the groundwater exchange with these aquifers is negligible. This means that all the water recharged through KSU into the GA, except of groundwater evapotranspiration loses and Ghanzi Wellfield abstraction, is discharged at the northern outflow boundary.

3.5 Discussion

Systematic integration of various Central Kalahari Basin (CKB) data sets from various sources in the 3-D geological model, resulted in development of the HCM of the CKB (Table 2-1 and Figure 3-9). The first important step in the model setup, was the definition of hydrostratigraphic units. Such definition requires good geological and hydrogeological knowledge. In this study, geology was pretty well defined from investigation boreholes and from geological studies of Key and Ayres (2000), Carney et al. (1994) and Smith (1984), although conversion of stratigraphic and lithological units into hydrostratigraphic units was still challenging due to not always clear regional meaning of Groups, Sub-basins and Formations and their inter-dependencies. The Table 2-1, attempted to regulate that issue, proposing six hydrostratigraphic units, namely: Kalahari Sand Unit, Stormberg Basalt Aquitard, Lebung Aquifer, Inter-Karoo Aquitard, Ecca Aquifer and Ghanzi Aquifer.

Classification of the hydrogeological system of the CKB into six hydrostratigraphic units was crucial for the development of the 3-D, CKB hydrostratigraphic model, presented in the form of cross-sections in Figure 3-2. A comprehensive analysis of the geological formations (Table 2-1), lithological information from borehole logs and potential groundwater occurrences, were used not only as the basis for identifying hydrostratigraphic units but also for defining their spatial extents. This was in contrast to the study by Allen et al. (2008), where hydrostratigraphic units and their spatial extents, were deduced from borehole lithological descriptions only. In locations with inadequate borehole information, the geological shapefiles (Figure 2-3) were used to constrain the spatial distribution of the hydrostratigraphic units and to fill in the missing information in spaces between borehole logs. This process was achieved through flexible, iterative modelling, applying combination of RockWorks and ArcGIS software.

Utilisation of 3-D geological modelling codes such as RockWorks, is particularly suitable for 3-D hydrostratigraphic models of large scale and complex aquifer systems such as the proposed in this study, because it conveniently integrates available data of lithology, stratigraphy, structural geology, tectonics and most importantly hydrogeology, providing opportunity of exporting any topological data of any required surface for follow up numerical model. The RockWorks code, seems to be handier than software-based, hydrostratigraphic conceptualization, built-in numerical modelling environments, such as the Groundwater Modelling System (GMS), for example used by Gurwin and Lubczynski (2005). This is mainly, because 3-D modelling codes such as the RockWorks, are simpler in operation, require much less time to learn while maintaining comparable capability i.e.: i) flexibility in data processing (e.g. database and conceptual model can be easily upgraded with new available data

at any processing stage), particularly needed for the assessment of hydrostratigraphic information; ii) suitability for handling large data sets without compromising their computation time (Allen et al., 2008); iii) easy interfacing with any follow up numerical modelling code.

In HCMs, hydraulic properties reflect spatial heterogeneity of a system and determine aquifer flows and aquitard leakages. Therefore, spatial system heterogeneity has to be defined carefully by assigning hydraulic parameters applying all information available for each hydrostratigraphic unit separately. Those parameters are further used in a numerical model, so will further be confirmed, eventually adjusted, during numerical model calibration (not part of this study). For the CKB aquifers, hydraulic parameters were assigned mainly based on pumping tests while for the KSU and for aquitards, based on lithology description of borehole logs. All the assigned hydraulic parameters fell in the ranges of their standard ranges as described in Freeze and Cherry (1979) and Brassington (1998).

In numerical model simulations, so also in setting up conceptual models, the shallowest, unconfined layer, is often meant as the one that is responsible for redistribution of recharge but not having large importance in lateral groundwater flow (Gurwin & Lubczynski, 2005; Hassan et al., 2014). Such layer, as in the CKB is the KSU, can be optimally modelled by variably-saturated numerical solutions, for example offered by unsaturated-zone flow (UZF1) Package (Niswonger et al., 2006) integrated in MODFLOW-NWT (Niswonger et al., 2011). In that solution, the net recharge (R_n) is inherently estimated, based on driving forces of precipitation and potential evapotranspiration and parameterization of the surface, unsaturated and saturated zones. In the case of the CKB, the parameterization of the unsaturated zone, nearly entirely embedded within the KSU, is uncertain because of its large thickness (typically more than 60 m) and little hydraulic information about it, as the majority of investigation studies focusses on layers below the KSU.

The large thickness of unsaturated zone, and pretty dense and "thirsty" Kalahari vegetation with world-deepest tree roots and large potential evapotranspiration, imply large interception, transpiration and evaporation processes (Lubczynski, 2000, 2009), all three restricting the R_n replenishment of groundwater resources. As a result, the R_n is erratic and if present, then very low, i.e. in order of few mm per year only. Considering that spatial distribution of Kalahari woody vegetation is relatively uniform and that the Kalahari soil is quite homogeneous (Obakeng et al., 2007), it can be assumed that the KSU thickness, plays a major role in spatio-temporal redistribution of subsurface fluxes so also in net recharge. That thickness, as defined in RockWorks, varies spatially from ~6 m at the eastern fringe, through more than 100 m at the central part of the CKB where recharge is unlikely, to less

than 10 m at the western edge of the CKB, where the largest recharge, possibly more than 10 mm y^{-1} is expected, although to our knowledge, that recharge has not been validated yet.

In a HCM setting, it is important to characterize all groundwater flow systems of a study area. As the saturated part of the KSU is pretty thin (or not present) and underlain by any of the aquifers, Lebung, Ecca or Ghanzi (Figure 3-5), then they jointly create flow system with that underlying aquifer. This means that in total there are three flow systems in the study area, Lebung, Ecca and Ghanzi, each of them eventually hydraulically connected with saturated bottom part of the KSU. It is remarkable that all the three flow systems, have similar radial flow pattern, with groundwater moving from external boundaries towards northerly located Makgadikgadi Pans discharge area (Figure 2-4, Figure 3-5, Figure 3-6 and Figure 3-8). Such pattern was also postulated by de Vries et al. (2000).

Despite similar patterns of the three flow systems, there are substantial differences between their hydraulic heads. Such differences do represent driving forces of the vertical leakages across the aquitards. The shallowest, SBA aquitard, is spatially limited. It confines LA, separating it from KSU. That confinement and related leakage depend on SBA leakance, i.e. on thickness and vertical hydraulic conductivity of the SBA, i.e. fracture openings and density of fractures (Figure 3-6). The IKA has also important hydraulic role constraining leakage between LA and EA emphasized by locally large head difference. The IKA is composed of semi-permeable siltstone and mudstone so its vertical hydraulic conductivity is dependent on the lithological composition, i.e. mainly on the contribution of sandy fraction. It is remarkable that at the majority of the IKA extent, there is downward leakage because of the higher LA heads than the EA heads while the opposite leakage direction occurs only in the central part of the basin (Figure 3-8). Such pattern follows Toth flownet system concept (Toth, 1963) and is typical for the hydraulics of sedimentary basins (Verweij, 1993). Considering parameterization of the two aquitards for the future numerical model setup, the leakances are unknown, so the preliminary-assigned, lithology-based leakances, have to be calibrated within the numerical model.

The reliability of HCMs are limited by available data quantity and quality. For example, in the CKB, the EA thickness is generally uncertain because of limited number of boreholes penetrating the whole Ecca sequence. This particularly refers to the locations from central, towards the north and north-eastern part of the CKB, where large deepening of the basin takes place. In these locations, most of the boreholes are terminated either within the IKA or just after they intersect the Ecca. This problem is mitigated by presence of sparsely distributed deep exploration boreholes, penetrating the whole Karoo sequence, although such boreholes are pretty scarce. Nevertheless, Voss (2011) have

argued that it is not necessary to bring all the complexity of geology into a descriptive groundwater model system just because real geology "looks" complicated thus bringing more uncertainties, hence the use of the sparsely distributed deep exploration borehole logs is deemed adequate.

Conceptual models serve as the critical background step for assembling numerical models. Therefore a transition between the two should be as smooth as possible. For that purpose, a simplified schematic diagram of the CKB hydrogeological conceptual model next to the corresponding, simplified proposal of numerical model schematization is presented in Figure 3-9. In that proposal, the only source of water input into the CKB is precipitation. The main water output is evapotranspiration with other two, much smaller output contributors being groundwater abstraction for inhabited areas and wildlife, and lateral groundwater outflow towards Makgadikgadi Pans' discharge area.

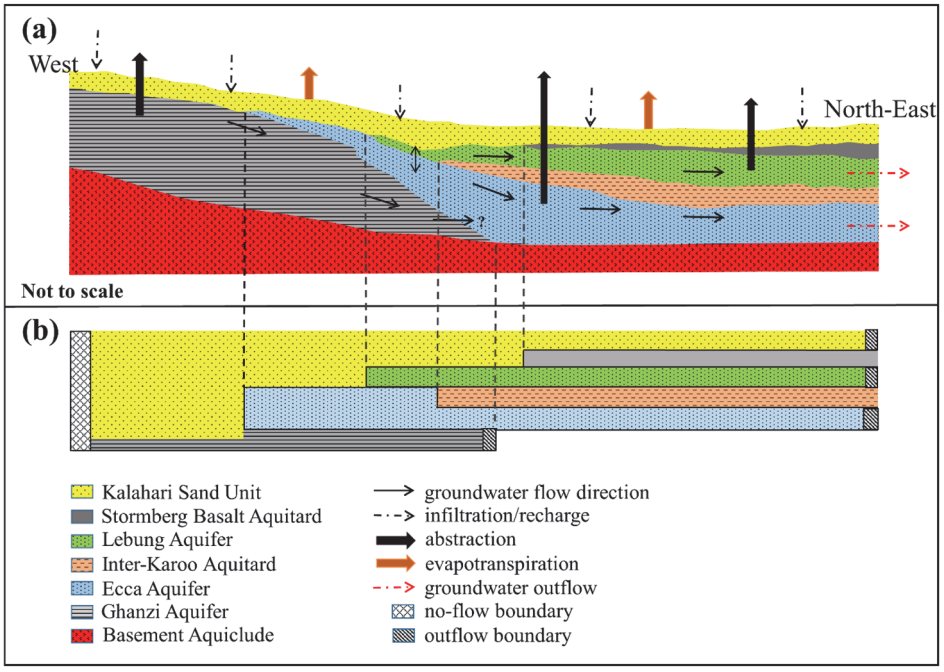

Figure 3-9: Schematic diagrams of: a) hydrogeological conceptual model of the Central Kalahari Basin; b) numerical model schematisation.

Transition of HCMs into numerical models is not straightforward. It varies with software packages and with their interfacing requirements (Cox et al., 2013). The proposed transition of the CKB conceptual model (Figure 3-9a) into numerical model is presented in Figure 3-9b. Considering that transition, still choice can be made for either quasi 3-D or full 3-D numerical model schematization (not part of this study). In quasi 3-D solution, there are only lateral flows in the aquifers and vertical leakages in the aquitards, the latter

assumed not to have any storage. According to Anderson et al. (2015), the quasi 3-D numerical models have been surpassed by time because of such simplifying assumptions. In the case of the CKB, the main disadvantage of the quasi 3-D schematization is that it does not permit for realistic simulation of the spatial aquifer wedging typical in the CKB and also not for particle tracking option to determine groundwater residence time. As such, for the numerical modelling of the CKB, a fully 3-D numerical schematization is recommended.

3.6 Conclusions

This study has shown that a systematic approach of using 3-D geological modelling code such as RockWorks, is vital when developing hydrogeological conceptual models of complex-multi layered aquifer systems. Its strength is in simplicity of operation and iterative conjunctive use with other GIS-type of software. The RockWorks code supported in this study by ArcGIS, was useful in improving understanding of the spatial distribution of the CKB hydrostratigraphic units and their hydraulic properties. Besides, it allowed to define flow system interactions and contributed to definition of external and internal physical CKB boundaries. Therefore, the methodology presented in this study is highly recommended for development of conceptual models, particularly of large sedimentary, multi-layered hydrogeological systems.

Chapter 4 Validation of satellite-based rainfall in Kalahari

This chapter is based on:

Lekula M, Lubczynski MW, Shemang EM, Verhoef W (2018) Validation of satellite-based rainfall in Kalahari. Physics and Chemistry of the Earth, Parts A/B/C DOI https://doi.org/10.1016/j.pce.2018.02.010

4.1 Abstract

Water resources management in arid and semi-arid areas is hampered by insufficient rainfall data, typically obtained from sparsely distributed rain gauges. Satellite-based rainfall estimates (SREs) are alternative sources of such data in these areas. In this study, daily rainfall estimates from FEWSNET RFE~11km, TRMM-3B42~27km, CMOPRH~27km and CMORPH~8km were evaluated against nine, daily rain gauge records in Central Kalahari Basin (CKB), over a five-year period, 01/01/2001-31/12/2005. The aims were to evaluate the daily rainfall detection capabilities of the four SRE algorithms, analyse the spatio-temporal variability of rainfall in the CKB and perform bias-correction of the four SREs. Evaluation methods included scatter plot analysis, descriptive statistics, categorical statistics and bias decomposition. The spatio-temporal variability of rainfall, was assessed using the SREs' mean annual rainfall, standard deviation, coefficient of variation and spatial correlation functions. Bias correction of the four SREs was conducted using a Time-Varying Space-Fixed bias-correction scheme. The results underlined the importance of validating daily SREs, as they had different rainfall detection capabilities in the CKB. The FEWSNET RFE~11km performed best, providing better results of descriptive and categorical statistics than the other three SREs, although bias decomposition showed that all SREs underestimated rainfall. The analysis showed that the most reliable SREs performance analysis indicator were the frequency of "*miss*" rainfall events and the "*miss-bias*", as they directly indicated SREs' sensitivity and bias of rainfall detection, respectively. The Time Varying and Space Fixed (TVSF) bias-correction scheme, improved some error measures but resulted in the reduction of the spatial correlation distance, thus increased, already high, spatial rainfall variability of all the four SREs. This study highlighted SREs as valuable source of daily rainfall data providing good spatio-temporal data coverage especially suitable for areas with limited amount of rain gauges, such as the CKB, but also emphasized SREs' drawbacks, creating avenue for follow up research.

4.2 Introduction

Rainfall data with good temporal and spatial coverage is important not only to weather forecasters and climate scientists, but also to a wide range of decision makers including hydrologists, as it is the main driving force of hydrological models. However, in semi-arid to arid areas, particularly in developing countries, such data is lacking due to limited spatial coverage of rain gauges (Kenabatho et al., 2017). The alternative source of such rainfall data is remotely-sensed, satellite-based rainfall estimates (SREs), which have the advantage of providing large spatial and temporal rainfall data coverage. These SREs include among others, Famine Early Warning Systems Network Rainfall Estimate (FEWSNET RFE) (Herman et al., 1997), Tropical Rainfall Measuring Mission (TRMM) sensor package (Kummerow et al., 1998), Climate Prediction Center (CPC) Morphing Technique (CMORPH) (Joyce et al., 2004) and Precipitation Estimates from Remotely Sensed Information Using Artificial Neural Networks (PERSIANN) (Sorooshian et al., 2000).

SREs have been investigated worldwide with various objectives. Various studies investigated rainfall detection capabilities of SREs to define the best performing one, either to be used as independent data source, or to complement limited rain gauge data as input in hydrological models (Arias-Hidalgo et al., 2013; Bauer et al., 2006; Milzow et al., 2009; Milzow et al., 2011), or to assess the rainfall spatial and temporal variability (Ringard et al., 2015; Zhang et al., 2017). However, SREs are known to exhibit inaccuracies in the form of systematic (bias) and random errors, which need to be investigated and corrected, where possible, before being used in hydrologic models (Habib et al., 2014; Nicholson et al., 2003). These errors might be due to different factors, among them being SREs algorithm estimation through cloud top reflectance, thermal radiance estimation, infrequent satellite over-passes, orbital drifts, topography and precipitation retrievals (AghaKouchak et al., 2009; Dinku et al., 2008; Joyce et al., 2004; Kummerow et al., 2004). Large SREs' biases are frequently reported, also over the African continent (Nicholson et al., 2003). These biases are particularly distinct when comparing daily SRE with daily rain gauge data (Artan et al., 2007), but decline when analyzing monthly or longer timescales because of temporal data accumulation (Dembele & Zwart, 2016).

SREs can be corrected for systematic errors; appropriate methods are well documented in literature. For example, Habib et al. (2014) investigated the effect of bias correction of SREs on runoff simulation at the source of the Upper Blue Nile applying three multiplicative bias correction schemes: Time and Space Variable, Time Variable and Space Fixed and Time and Space Fixed. They used these three bias correction schemes to analyze the spatio-temporal variability of CMORPH bias and to identify critical aspects of such variability from a hydrologic perspective.

Validation of various SREs using rain gauge data have been conducted worldwide. However, little of such work has been done in Africa due to limited spatial coverage of rain gauges. Few examples include study by Adeyewa and Nakamura (2003), who used systematic and random error statistics to validate TRMM radar rainfall algorithm over main climatic regions in Africa at monthly and seasonal time scales. Their results showed that the random and systematic errors were sensitive to the seasonal rainfall difference and spatial location. Dinku et al. (2010) used descriptive and categorical statistical validation methods to evaluate the performance of CMORPH~27 km, TRMM-3B42 and TRMM-3B42RT in rainfall detection over mountainous regions of Ethiopia (also Colombia) at daily time scale. In that study, CMORPH~27 km performed better than TRMM-3B42 and TRMM-3B42RT, even though performances of all the SREs were low. Romilly and Gebremichael (2011) evaluated the accuracy of CMORPH, PERSIANN, TRMM-TMPA and TRMM-3B42RT over six river basins in Ethiopia through bias ratio, spatial pattern and dependence of bias ratio of SREs on elevation at monthly and seasonal time scales. Results of that study showed that CMORPH, TRMM-TMPA and TRMM-3B42RT outperformed PERSIANN. Haile et al. (2013) investigated the accuracy of 1-hourly, 8 km spatial resolution CMORPH algorithm over Gilgel Abbay Basin, also in Ethiopia. Their results showed a significant rainfall variation across the basin, although that variability was poorly correlated to gauge observations, not only in spatial but also in temporal manner. Their validation methodology included descriptive and categorical statistical verification.

Few SREs related studies have been carried out in Southern Africa where this study took place. They include a study by Liechti et al. (2012), who compared and evaluated TRMM-3B42 v6, FEWSNET RFE 2.0 and CMORPH 0.25^0 against daily, decadal and monthly rain gauge data, to choose one that could be used as input for hydrological model of the Zambezi Basin. In that study, FEWSNET RFE 2.0 and TRMM-3B42 had better comparative performances than CMORPH. Despite better performance of FEWSNET RFE 2.0, the TRMM-3B42 with a daily time step was finally chosen because of its longest data record. Tote et al. (2015) evaluated the performance of TAMSAT African Rainfall Climatology and Time-series (TARCAT 2.0), FEWSNET RFE 2.0, and Climate Hazards Group Infrared Precipitation with Stations (CHIRPS) by comparing their decadal estimates with ten days rain gauge data for drought and flood monitoring in Mozambique using categorical statistics. In that study, FEWSNET RFE 2.0 and CHIRPS performed better than TARCAT 2.0, because they both had been inherently bias corrected using the Global Telecommunication Station (GTS) rain gauge data network. Finally, in the south-eastern Botswana, Kenabatho et al. (2017) evaluated the daily performance of TRMM and spatial rainfall from the Generalized Linear Models (GLMs) (Chandler & Wheater, 2002) on rainfall detection in the Notwane catchment area using quantitative (descriptive) and

categorical statistics. Their results indicated the potential of SREs in augmenting the limited rain gauged data in semi-arid areas.

This study was motivated by the lack of systematic evaluation of different SRE rainfall detection performances in the Kalahari area to date. The Kalahari area has sparse rainfall monitoring network but large demand for valuable spatio-temporal rainfall data by governmental and non-governmental offices of the Kalahari countries, i.e. Botswana, Namibia and South Africa. Such data can be provided by SREs, however in different parts of the world different SREs perform optimally, so the need for this study.

The objectives of this study were then formulated as following: 1) to evaluate daily rainfall detection capabilities in the CKB of the following four SREs: i) FEWSNET RFE 2.0 with ~11 km spatial resolution; ii) TRMM-3B42 v7 with ~27 km spatial resolution; iii) CMORPH v1 with 8 km spatial resolution; and iv) CMORPH v1with ~27 km spatial resolution; 2) to analyze and present spatio-temporal variability of rainfall in the CKB; 3) to perform bias correction to the four SREs and evaluate if the bias correction scheme adequately addressed the SREs' systematic errors; 4) advise on the optimal SRE for daily rainfall assessment in the CKB.

4.3 Datasets

This study was carried out using five-year daily data, from 01/01/ 2001 to 31/12/2005.

4.3.1 Meteorological data

Daily rainfall data of twelve rain gauge stations for the five-year study period were sourced from the Botswana Department of Meteorological Services (DMS). After screening, only nine stations were left to be used in this study (Figure 2-1 and Table 4.1).

Table 4-1: Availability of daily rain gauge data (01/01/2001-31/12/2005).

Station	Longitude	Latitude	Elevation [m a.m.l]	Mean Annual Rainfall (MAR) [mm]	Missing data [%]
Sua	25.98^0	-20.63^0	903	389	0
Maun	23.42^0	-19.98^0	947	356	5
Letlhakane	25.58^0	-21.42^0	992	343	10
Sir Seretse Khama Int. Airport (SSKA)	25.92^0	-24.70^0	1000	367	0
Mahalapye	26.83^0	-23.12^0	1014	469	20
Serowe	26.70^0	-22.38^0	1138	377	0
Kang	22.75^0	-23.75^0	1139	356	0
Ghanzi	21.63^0	-21.68^0	1148	383	10
Jwaneng	24.80^0	-24.58^0	1192	478	0

The three stations removed exhibited many data gaps. The remaining nine stations were also affected by data gaps (Table 4-1), although the percentage of missing data was considered low. This data was used as a reference for the assessment of the SREs, neglecting days when stations had data gaps.

4.3.2 Satellite data

Time series of four daily SREs for the five-year study period were downloaded online; their properties and sources are summarized in Table 4-2. All the SREs' grids attributed to each of the nine rain gauge locations are scale-projected in Figure. 4-1 – note that TRMM and $CMORPH_{27}$ grids coincide.

Table 4-2: Satellite rainfall estimates (SREs) used in this study, data sources and spatial and temporal information.

Product	Adopted abbreviation in Thesis	Source	Spatial resolution	Temporal resolution
FEWSNET RFE 2.0	RFE	http://earlywarning.usgs.gov/fews	0.1^0 (~11 km)	1 day
TRMM-3B42 v7	TRMM	http://mirador.gsfc.nasa.gov	0.25^0 (~27 km)	1 day
CMORPH v1	$CMORPH_{27}$	GeoNETCAST ISOD toolbox of ILWIS GIS software (http://52north.org/downloads/)	0.25^0 (~27 km)	1 day
CMORPH v1	$CMORPH_8$	GeoNETCAST ISOD toolbox of ILWIS GIS software (http://52north.org/downloads/)	0.072^0 (~8 km)	30 minutes (aggregated to 1 day)

The RFE is a blended product, based on cold cloud duration (CCD) derived from: METEOSAT thermal infrared (TIR), Special Sensor Microwave/Imager (SSM/I), Advanced Microwave Sounding Unit (AMSU) (Herman et al., 1997).

The RFE data is inherently bias-corrected, and the GTS station used for that correction, can be accessed through the FTP server ftp://ftp.cpc.ncep.noaa.gov/fews/gts/. The TRMM uses both high temporal resolution TIR and passive microwave measurements to estimate precipitation (Kummerow et al., 1998; Yang & Luo, 2014). It is also ground-validated but not over African Continent (http://trmm-fc.gsfc.nasa.gov/trmm_gv). The CMORPH products use multiple microwave and TIR sensors to derive rain rates, which are then used to infer motion fields (Joyce et al., 2004; Yang & Luo, 2014). The CMORPH products are not ground-validated. Three CMORPH, spatial and temporal are supplied in version 1: 0.0727° (8 km) every 30 minutes, 0.25^0 (27 km) 3 hourly and 0.25^0 (27 km) daily.

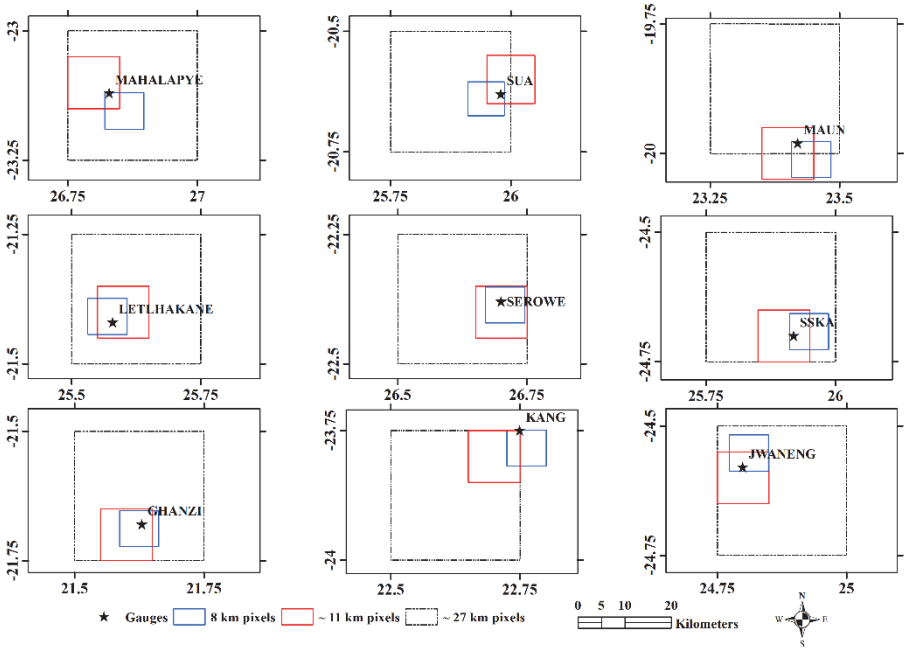

Figure 4-1: Rain gauge locations and their matching with RFE (red outline), TRMM, $CMORPH_{27}$ (black hashed outline) and $CMORPH_8$ (blue outline) grids.

4.4 Methodology

4.4.1 Satellite rainfall evaluation

Performances of RFE, TRMM, $CMORPH_{27}$ and $CMORPH_8$ in the CKB were evaluated by a suite of graphical techniques and statistical methods at a daily time step. This was done by inter-comparison of rainfalls of each of the nine reference rain gauges (Figure 2-1) with the coinciding pixel of each SRE (Figure 4-1). The evaluation methods included scatter plot analysis, descriptive statistics, categorical statistics and bias decomposition.

4.4.1.1 Scatter plots

The nine daily, pixel-extracted SREs of RFE, TRMM, $CMORPH_{27}$ and $CMORPH_{8}$ algorithms, were evaluated for their linear associations with coinciding nine daily reference rain gauge data using scatter plots. The coefficient of determination, R^2, was used as a measure. Similar scatter plots of the monthly aggregated rainfalls were also analyzed, but only for comparison purpose.

4.4.1.2 Descriptive statistics

The descriptive statistics to compare the SREs at the nine rain gauge stations with corresponding rain gauge values (Figure 4-1) included: i) Pearson's product-moment correlation coefficient (*CC*) – measure of linear association between daily SREs and the reference daily gauge data pairs; ii) mean error (*ME*) – averaged magnitude of differences between daily SREs and the reference daily gauge data; iii) mean absolute error (*MAE*) – averaged magnitude of absolute error differences between daily SREs and the reference daily gauge data; and iv) root mean square error (*RMSE*) – square root of the mean squared differences (errors) between daily SREs and the daily reference gauge rainfall, all calculated using the following equations:

$$CC = (\overline{G.S} - \bar{G}.\bar{S}) / \sqrt{(\overline{G^2} - \bar{G}^2)(\overline{S^2} - \bar{S}^2)} \quad (4\text{-}1)$$

$$ME = {}^{1}/_{n} \sum_{i=1}^{n} (S_i - G_i) \quad (4\text{-}2)$$

$$MAE = {}^{1}/_{n} \sum_{i=1}^{n} |S_i - G_i| \quad (4\text{-}3)$$

$$RMSE = \sqrt{{}^{1}/_{n} \sum_{i=1}^{n} (S_i - G_i)^2} \quad (4\text{-}4)$$

where: S – daily SRE coinciding with daily reference gauge rainfall; G – daily rain gauge data; $\bar{S}$ – daily average of SRE over the entire study period at the analyzed pixel; $\bar{G}$ – daily average rain gauge estimate over the entire study period; n – number of data pairs; i- operator. These statistics were summarized in box and whisker plots using median, minimum and maximum, and 25% and 75% quantiles of each statistical value.

4.4.1.3 Categorical statistics

The categorical statistics (Wilks, 2006), which is widely used to evaluate performance of SREs (e.g, Dinku et al., 2010; Hossain & Huffman, 2008; Kenabatho et al., 2017; Qin et al., 2014), was also used in this study to further evaluate and compare the performances of RFE, TRMM, $CMORPH_{27}$ and $CMORPH_{8}$ in rainfall detection. The categorical statistics applied in this study included: i) Probability Of Detection (*POD*); ii) False Alarm Ratio (*FAR*); iii)

Critical Success Index (*CSI*) and; iv) Frequency Bias (*FBS*), all calculated as follows:

$$POD = H/(H + M) \quad (4\text{-}5)$$

$$FAR = F/(H + F) \quad (4\text{-}6)$$

$$CSI = H/(H + F + M) \quad (4\text{-}7)$$

$$FBS = (H + F)/(H + M) \quad (4\text{-}8)$$

where: *H* is referred to as "*hit*", i.e. the satellite algorithm has successfully detected rain; *M* is "*miss*", i.e. the satellite algorithm failed to detect rain; *F* is "*false alarm*", i.e. the satellite algorithm failed to detect a no-rain case; and *C* is "*correct negative*", i.e. satellite algorithm successfully detected a no-rain case (Dinku et al., 2010; Kenabatho et al., 2017).

A contingency Table 4-3 is used to illustrate these four types of conditions. A threshold 0.5 mm day^{-1} defining a rainy day was used in this study, which is consistent with the threshold adopted by DMS (Kenabatho et al., 2017).

Table 4-3: Contingency table for comparison of occurrences of gauge and satellite rainfall events.

	Gauge rain frequency (N_g)	Gauge no rain
Satellite rain frequency (N_s)	*H*	*F*
Satellite no rain	*M*	*C*

Note $N_s = H+F$ and $N_g = H+M$

The *POD* is the fraction, which a satellite algorithm correctly estimated rainfall events as measured in the rain gauge; it ranges from 0 to 1 with a perfect value of 1; *FAR* is the fraction of falsely detected rainfall event by satellite algorithm to all satellite rainfall detected events ; it ranges from 0 to 1 with a perfect value of 0; *CIS* is a fraction, which satellite algorithm has correctly estimated rainfall but taking into account the false alarms in contrast to *POD*; it ranges from 0 to 1 with a perfect value of 1; *FBS* is a fraction comparing the frequency of estimated rainfall (N_s) with the frequency of gauge-measured rainfall (N_g); it ranges from 0 to ∞ and the perfect value is 1. These statistics were also summarized in box and whisker plots using median, minimum and maximum, and 25% and 75% quantiles of each statistical values.

4.4.1.4 Bias decomposition

The total rainfall bias reported by the four SREs was decomposed into three components *Hit Bias* (*HB* – Equation 4-9), *Miss Bias* (*MB* – Equation 4-10) and

False Bias (*FB* – Equation 4-11). This bias analysis gives an insight into the possible sources of SREs' algorithm errors, while the *Total Bias* (TB_c – Equation 4-12) i.e., cumulative difference between the SREs and gauge data, is based on aggregation of differences in rainfall volumes over the entire sample, so does not provide information on the sources of such differences (Habib et al., 2009; Haile et al., 2013; Tian et al., 2009). The three bias components and the *Total Bias* are respectively presented below:

$$HB = \sum_{i=1}^{n}(S_i - G_i) : (S > 0 \,\&\, G > 0) \tag{4-9}$$

$$MB = \sum_{i=1}^{n} G_i \; : (S = 0 \,\&\, G > 0) \tag{4-10}$$

$$FB = \sum_{i=1}^{n} S_i \; : (S > 0 \,\&\, G = 0) \tag{4-11}$$

$$TB_c = HB - MB + FB \tag{4-12}$$

where subscript *c* denotes 'categorical'; *i* – operator and *n* – number of valid conditions.

The value of *HB* can either be positive or negative, *MB* is always negative while *FB* is always positive. If it can be assumed that the rain gauge measurement represents the correct rainfall over the satellite pixel area in which that gauge is located (Figure 4-1), then the negative *HB* signify that the satellite algorithm underestimated correctly detected rainfall, while positive, overestimated. In such case, the total bias is constrained by the sign and magnitude of *HB* while the *MB* and *FB* almost cancel each other.

4.4.2 Spatio-temporal variability of rainfall in CKB

Analysis of the spatio-temporal variability of rainfall in the CKB was conducted using SREs' annual rainfall, evaluating: i) the mean annual rainfall (*MAR*); ii) the standard deviation of the *MAR* (σ); iii) the coefficient of variation of the *MAR* (*CV*); and iv) the spatial correlation functions, using an array of points with a 27 km Computational Separation Distance (CSD) for SREs extraction, which matches the spatial resolution of TRMM and CMORPH$_{27}$. The *MAR*, σ and *CV* are expressed as follows:

$$MAR = \sum_{i=1}^{n} {}^{S_i}/_{n} \tag{4-13}$$

$$\sigma = \sqrt{{}^{1}/_{n}\,(S_i - \bar{S})^2} \tag{4-14}$$

$$CV = {}^{\sigma}/_{MAR} \tag{4-15}$$

The spatial correlation function can be used for both descriptive and predictive purposes. When used in a descriptive mode, it infers dominant meteorological process (Gebremichael & Krajewski, 2004) while in a predictive mode, it is used in spatial estimation of the meteorological process (Haile et al., 2009). For the CKB, the spatial correlation function was developed in a predictive mode, in two-steps. In the first step, the *CC*s for each point pair combinations were calculated. In the developed array of points, there were different point-combinations with equal Euclidian separation distances, but different *CC*s. For this study the minimum *CC*s per point pairs with equal Euclidian separation distances were used, as a worst case scenario. In the second step, these minimum *CC*s, were plotted against their Euclidian separation distances and an analytical, three-parameter exponential function model was then fitted into the obtained graph. The analytical expression of that model function is as follows:

$$CC = C_0 exp\left[-\left({}^{d}/_{d_0}\right)^2\right] \tag{4-16}$$

where d is the Euclidian separation distance between any two points in linear units and the three model parameters are as follows: c_o - correlation value for the near-zero distance (nugget parameter); d_o – correlation distance known as the scale parameter (Haile et al., 2009) and s - shape parameter. Initially, all the three parameters, d_o, c_o and s were optimized by minimizing the root mean square error (*RMSE*) between the model and calculated *CC*. The sensitivity of d_o was then assessed by varying (constraining) c_o, starting from the earlier optimized c_o until the maximum $c_o = 1$ using the same procedure as above but optimizing only d_o and s.

4.4.3 Bias correction

Bias correction of the four SREs was conducted using the adopted Time Variable and Space Fixed (TVSF) bias correction scheme developed by Habib et al. (2014). That bias correction scheme choice was based on the sparse spatial distribution of rain gauges in and around the CKB. For example, other, more sophisticated Time and Space Variable bias correction scheme performed best in CMORPH bias correction study by (Habib et al., 2014), but it requires good spatial coverage of rain gauge data to create an interpolated reference rain gauge raster data. Unfortunately, in the case of this study, use of such bias correction schema would be highly uncertain due to only nine available rain gauges in the large CKB area, implying large separation distances between the gauges. It was also assumed that the impact of the CKB topography on rainfall is minimal, as topographic gradient in majority of the study area was <0.001. The TVSF scheme was developed at a daily time step by dividing the daily sum of all rain gauge data (G_i) by daily sum of their corresponding SRE (S_i) values using Equation 4-17, to get the daily bias factor *BF.*

$$BF = \sum_{i=1}^{n} G_i \Big/ \sum_{i=1}^{n} S_i \qquad (4\text{-}17)$$

where *i* is the gauge location index and *n* is the total number of rain gauges analyzed.

The TVSF scheme was then applied by multiplying each daily SRE pixel value by the daily value of *BF*, resulting in a new bias-corrected SREs. In case the daily SREs sum was zero (denominator in Equation 4-17), the *BF* was assigned zero. The performance of the bias-corrected SREs, were assessed using descriptive and categorical statistics in the same way as uncorrected SREs. Spatial correlation functions for the corrected SREs were developed to assess their spatial variability.

4.5 Results and discussion

4.5.1 Satellite rainfall evaluation

Graphical comparisons between RFE, TRMM, $CMORPH_{27}$, $CMORPH_8$ SREs and rain gauge data are presented through scatter plots of daily values in Figure 4-2. The correlation between daily rain gauge data and their corresponding daily SREs vary from station to station for each algorithm. The RFE displayed the highest R^2 in the majority of the rain gauge stations. The relatively better R^2 displayed by RFE than by the other three SREs, is likely due to its inherent bias-correction during image processing (Brown, 2008).

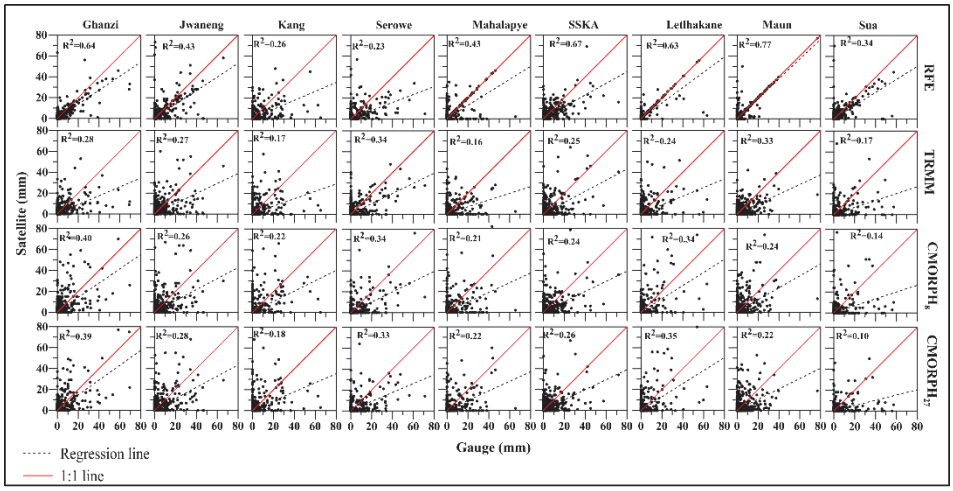

Figure 4-2: Scatter plots of daily RFE, TRMM, $CMORPH_{27}$ and $CMORPH_8$ SREs against daily reference rain gauge data over a five year (01/01/2001-31/12/2005) study period.

However, even that correlation is not much better than for other SREs because GTS stations used by the RFE, sometimes, failed to report rainfall, hence no

inherent bias correction in such days (Brown, 2008). This for example, can be observed at the Kang, Serowe and SSKA stations, where there is weak correlation between rain gauge data and RFE rainfall (Figure 4-2). The R^2 displayed by TRMM and $CMORPH_{27}$ are lower than that of RFE, while TRMM in general is superior to $CMORPH_{27}$, likely because of its ground validation. The reason why $CMORPH_8$ has the lowest correlation against the rain gauge data is not only because its processing does not incorporate any rain gauge data (Joyce et al., 2004), but also it has the finest spatial resolution so it benefits the least from spatial data accumulation (AghaKouchak et al., 2012). In contrast to daily correlations, the correlations of monthly-aggregated SREs versus the monthly aggregated rain gauge data, was substantially better (Figure 4-3) as shown by significant improvement of R^2. That improvement was mainly because of temporal data aggregation. The better performance of SREs at coarser temporal resolution is similar to the results by Dembele and Zwart (2016), who observed the same trend in their study in in Burkina Faso.

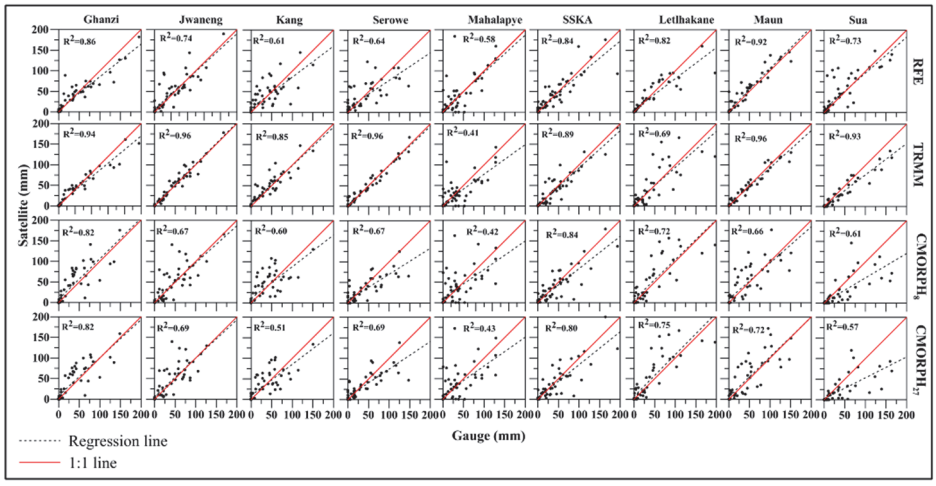

Figure 4-3: Scatter plots of monthly RFE, TRMM, $CMORPH_{27}$ and $CMORPH_8$ SREs against monthly reference rain gauge data over a five year (01/01/2001-31/12/2005) study period.

The descriptive statistics as presented in Figure 4-4 was used to further evaluate the daily rainfall performance of RFE, TRMM, $CMORPH_{27}$ and $CMORPH_8$.

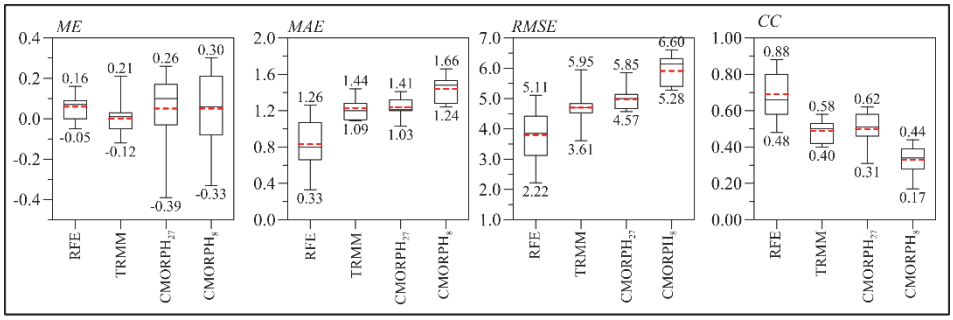

Figure 4-4: Box and whisker plots of descriptive statistics for RFE, TRMM, $CMORPH_{27}$ and $CMORPH_8$ SREs. The whisker's smallest and the largest values are labelled; the red dash-line denotes the mean value.

The RFE had *ME* close to zero, lower *MAE*, lower *RMSE* and higher *CC* than the other three SREs, suggesting better rainfall detection in the CKB. The categorical statistics provides information about the frequency of daily-events but not the quantitative information. For example in the case of *hit*, where SRE is 0.5 mm d^{-1} and the rainfall in the corresponding gauge 5 mm d^{-1}, both records indicate one *hit*, despite large (-4.5 mm d^{-1}) hit bias (*HB*) as per Equation 4-9. The averaged frequencies of daily RFE, TRMM, $CMORPH_{27}$ and $CMORPH_8$ *hit* (*H*), *miss* (*M*) and *"false"* (*F*), over the five-year study period, are presented in Figure 4-5. The RFE had the highest average *H* (9.6%), lowest averaged *M* (2%) and also lowest averaged *F* (6.8%). In the categorical statistics, the best criterion to select the best performing SRE seems to be the *M* as it refers to detection of the true rainfall occurring on the ground, but not detected by satellite algorithm, directly indicating sensitivity of the satellite algorithm to rain detection. That criterion is best fulfilled by RFE, which has the lowest averaged frequency of missed rain (Figure 4-5). Slightly less reliable than *miss* (but still valuable), is the *hit* criterion, because it is possible that different showers are detected by a satellite algorithm than by a gauge in a given observation time, in this study during a day. Considering the *hit* criterion, also the RFE performed better than other SREs. The "*false*" expression as described by Wilks (2006) in categorical evaluation might not be an adequate term, but an issue of spatial rain gauge representativeness within the satellite algorithm pixel. Rain gauge represents nearly point measurement, so when a rain cloud path would cover only part of the pixel but not the rain gauge, then SRE might even better represent the true rainfall of the whole pixel area than the rain gauge. However, this issue could be assessed only if there was more than one rain gauge in an SRE algorithm pixel, which unfortunately was not the case in this study. Another reason of "*false*" rainfall occurrence can be associated with semi-arid climate condition of the study area, where low rainfall intensity rain drops can evaporate before reaching the ground, resulting in no rain recorded in a rain gauge but recorded by satellite (Dinku et al., 2011; Moazami et al., 2013).

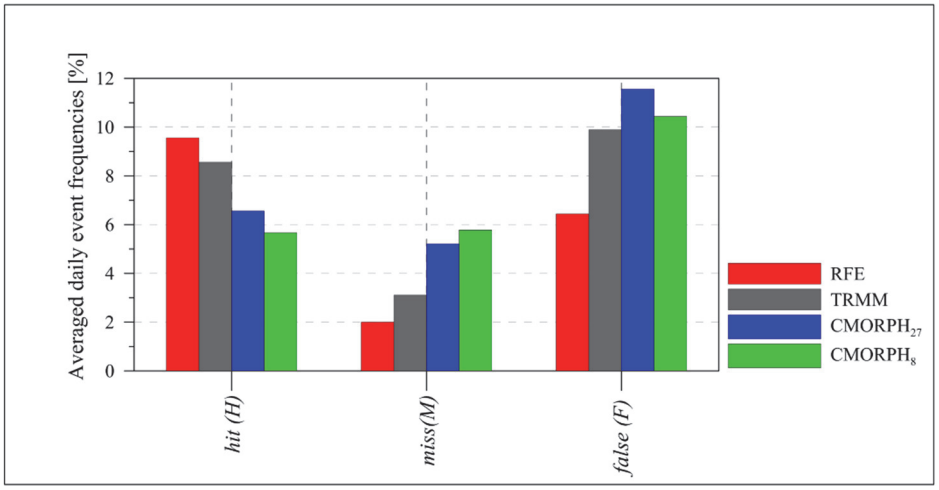

Figure 4-5: The averaged frequencies of hit (*H*), miss (*M*) and false (*F*) for RFE, TRMM, $CMORPH_{27}$ and $CMORPH_8$ over five-year (01/01/2001-31/12/2005) study period.

The *H*, *M* and *F* frequencies for RFE, TRMM, $CMORPH_{27}$ and $CMORPH_8$ were also used to calculate categorical statistics as presented in Figure 4-6. The RFE had the highest *POD*, the lowest *FAR*, the highest *CSI*, and the *FBS* closer to 1 than any of the other three SREs. The $CMORPH_8$ had the higher *FAR* than the other three SREs, which could be due to gauge representation in the satellite algorithm pixel and also because it benefited the least form spatial data aggregation as explained earlier. In authors' opinion, the *POD* is the most valuable categorical statistic when comparing validity of SREs as it is not dependent on *F* but inversely dependent on *M* and moderated by *H* (as *H* occurs in the numerator and in the denominator), the latter two being reliable categorical measures.

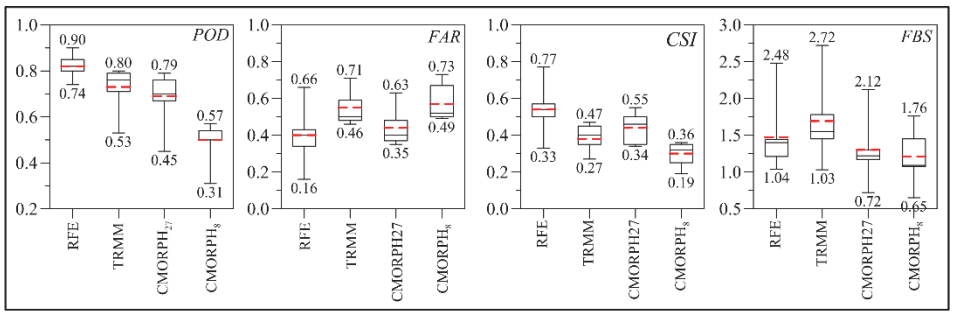

Figure 4-6: Box and whisker plots of categorical statistics for RFE, TRMM, $CMORPH_{27}$ and $CMORPH_8$ SREs. The whisker's smallest and the largest values are labelled; the red dash-line denotes the mean value.

The *FBS* is also an important categorical statistic as it gives information on the ratio of SREs rain days (N_s) against observed ones (N_g). For the CKB, N_s was larger than N_g as shown by the average *FBS*>1 (Figure 4-6), which means that

SREs generally recorded more frequently rainfall events than the gauges, which is also emphasized (Equation 4-8) by larger number of false rainfall events (*F*) than missed events (*M*) (Figure 4-5). However, the *FBS* does not provide quantitative information whether a satellite rainfall algorithm overestimates or underestimates rainfall.

The overall results of the categorical statistical validation of the four SREs indicate that the RFE algorithm better detected daily rainfall in the CKB than TRMM, $CMORPH_{27}$ and $CMORPH_{8}$. These results are comparable with those of Liechti et al. (2012), who found that RFE (and TRMM) had better rainfall detection capabilities than CMORPH in the Zambezi Basin. Also Tote et al. (2015) found that RFE (and CHIRPS) performed better than TARCAT in Mozambique. The consistently advantageous performance of RFE, was largely because of its inherent-bias correction. The poor performance of the CMORPH SREs was likely due to rainfall retrieval errors, which were compounded by the lack of inherent bias correction during processing. The relatively poor TRMM performance in this study was because of limited ground validation and none of them covering Southern Africa continent. Milzow et al. (2011) also chose RFE over TRMM, as it performed better in their study in the Okavango Basin.

4.5.2 Bias decomposition

To evaluate the performances of RFE, TRMM, $CMORPH_{27}$ and $CMORPH_{8}$ in quantitative manner, their total biases were decomposed into hit bias (*HB*), miss bias (*MB*) and false bias (*FB*). All the composite biases and the total bias are presented in Figure 4-7 as percentages of the total gauge rainfall over the five-year study period.

Even quick visual inspection of the Figure 4-7 indicates that RFE biases (Figure 4-7a) are lower than of TRMM and much lower than of $CMORPH_{27}$ and $CMORPH_{8}$ (Figure 4-7b, Figure 4-7c and Figure 4-7d). The TB_c at each of the four SREs varied from negatives (SRE underestimation) to positives (SRE overestimation). It is remarkable that nearly all *HB* components of the four SREs are negative, except of Maun site for RFE and SSKA site for $CMORPH_{8}$. This is an indication that the SREs generally underestimated the gauge-detected daily rainfall. The much lower *MB* in RFE as compared to the TRMM and two CMORPH SREs, means that RFE missed much less rainfall detected at gauges than the other three SREs, so performed better. Cases of SREs' daily rainfall underestimation, i.e., -*HB* or *MB*, are likely due to limitation of TIR sensor used by RFE, TRMM and CMORPH, which uses cloud top temperature to estimate rainfall and because of that is unable to provide information beneath the top of the cloud (Dinku et al., 2011; Dinku et al., 2010). Therefore, when rain is formed while the top of the cloud has not reached the minimum temperature threshold for rainfall detection (warm clouds) yet, the rain will not

be recorded or it will start to be recorded later, in either ways resulting in rainfall underestimation.

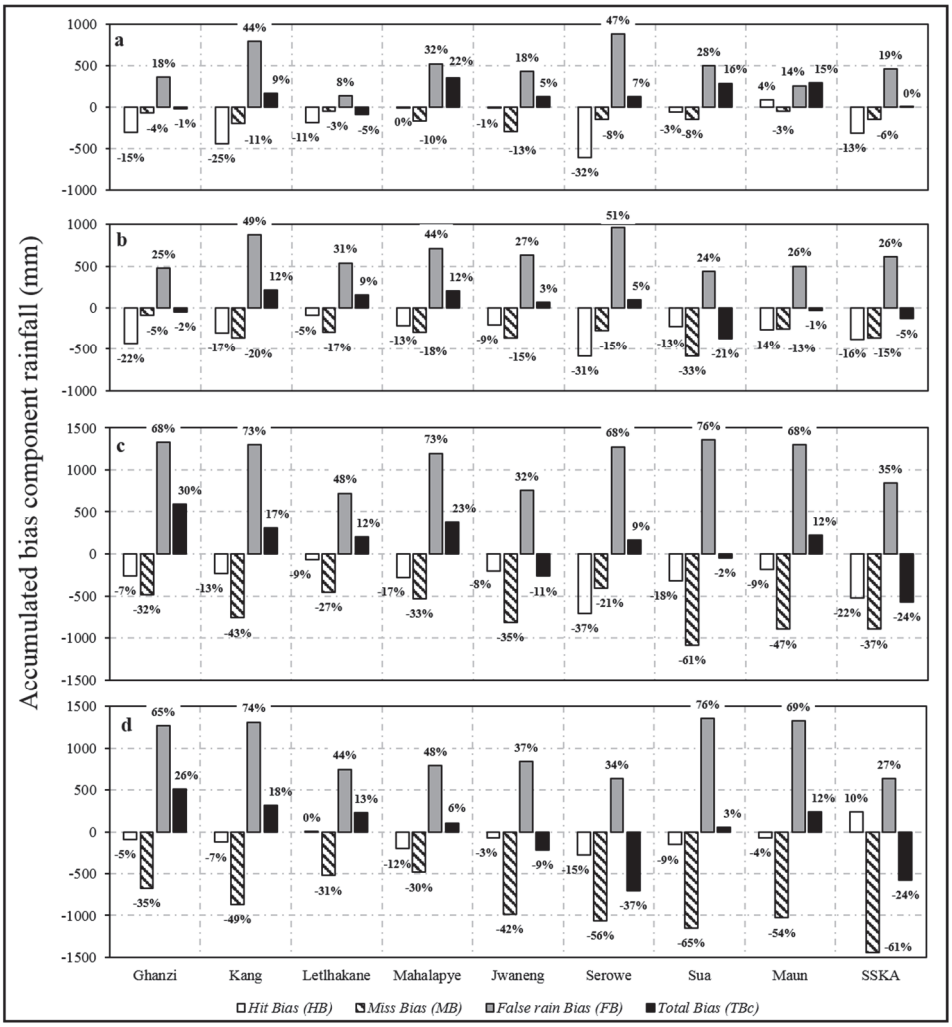

Figure 4-7: Total bias (TB_c) decomposition of: a) RFE; b) TRMM; c) $CMORPH_{27}$; and d) $CMORPH_8$ SREs, into *hit* (*HB*), *miss* (*MB*) and "*false*" (*FB*) rain biases over the five year (01/01/2001-31/12/2005) study period. Percentages above and below the bars, represent bias component contributions to the total rain.

Kalahari region seems to be particularly vulnerable to "warm cloud" effect due to the high temperatures of summer rainy seasons, which can go even up to 40°c. The third bias component of the TB_c, i.e. *FB*, was also lower in the RFE as compared to the TRMM and two CMORPH SREs, but as earlier explained in the context of false alarm events (*F*), the *FB* is not conclusive regarding validation of the SREs, although it influences the total accumulated rainfall.

The risk in using TB_c as per Equation 4-12 for the evaluation of the accumulated bias is in cancellation of the positive and negative biases (*MB* is always negative, *FB* is always positive and *HB* can have either signs), which creates wrong impression of TB_c being much lower than in reality, whereas the individual biases could be, and in some cases in this study, were, even larger than the TB_c itself.

The bias decomposition and particularly the analysis of its individual components as presented above, is a very beneficial, quantitative SREs assessment, as it provides valuable information for SRE validation, especially the *MB* and *FB* as discussed above, on individual contributions of different biases to TB_c. The same criteria of evaluating contributions of different bias components to TB_c, was successfully used by Habib et al. (2009) in South Louisiana, United States of America, on their study validating NEXRAD multi-sensor precipitation estimates by experimental dense rain gauge network. In Africa, Haile et al. (2013) also successfully used bias decomposition study to evaluate CMOPRH rainfall product on hourly time scales over the source of the Blue Nile River; they found, similarly to this study, that the *MB* and *HB* were negatively large but the resultant smaller TB_c was neutralized by the large positive *FB*.

4.5.3 Spatio-temporal variability of rainfall in the CKB

The small amount of rain gauges in the CKB and its surrounding was inadequate to assess the spatio-temporal rainfall variability (Figure 2-1). Therefore, analysis of the spatio-temporal variability of rainfall in the CKB was done utilizing the four SREs. That analysis was done by evaluating their mean annual rainfall (*MAR*), annual rainfall standard deviation (σ) and coefficient of variation *CV* as per Equations 4-13 to 4-15. The result of that analysis is presented in Figure 4-8.

The *MAR* of the four SREs was low in the south-western and high in the north-eastern part of the CKB, creating evident SW-NE rainfall gradient (except of the small patch of low rainfall around Makgadikgadi Pans, which could be an art-effect resulted by high reflectance of soda ash). This rainfall gradient is in agreement with results from other studies in the CKB such as for example by Porporato et al. (2003), who identified similar direction of the regional, Kalahari rainfall gradient. The σ and *CV* as defined over the five-year study period, were also spatially variable (Figure 4-8). The high σ displayed by RFE in the western CKB indicates it's large deviation of annual rainfall from *MAR*, also confirmed by large *CV*, all translating into high temporal rainfall variability of RFE in that area. The large *CV* of the TRMM, $CMORPH_{27}$ and $CMORPH_8$ in the north-eastern edge of the CKB, also shows their high temporal rainfall variability. The observed differences between similar TRMM, $CMORPH_{27}$ and $CMORPH_8$ statistical patterns and the RFE patterns are likely due the inherent-bias

correction of the latter during its processing although that issue need to be further investigated. However, regardless of the differences observed, all the statistical patters of the four SREs investigated indicate that rainfall in the CKB is highly spatially and temporally variable, which is characteristic for semi-arid environments and is in agreement with the previous studies by Bhalotra (1987) and Obakeng et al. (2007).

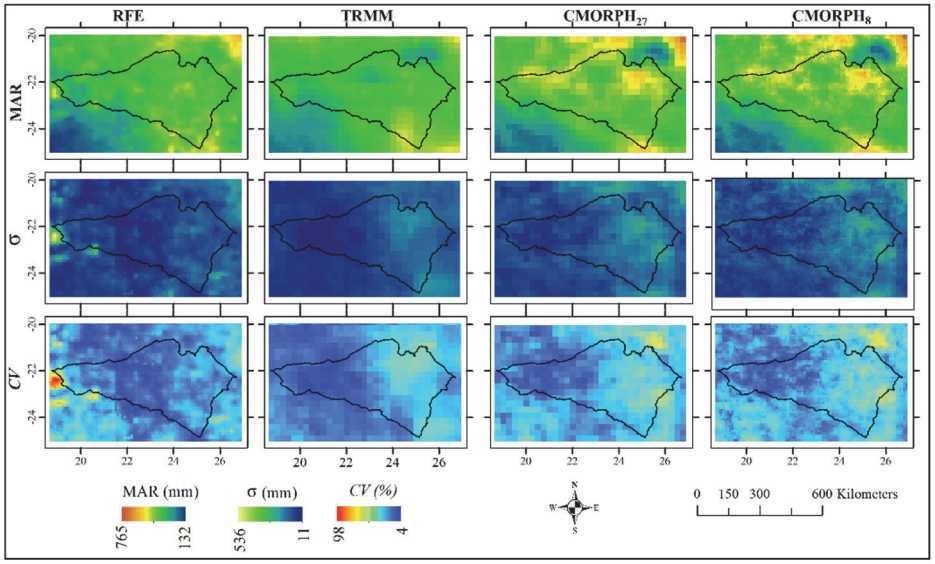

Figure 4-8: Mean annual rainfall (*MAR*), standard deviation (σ) and coefficient of variation (*CV*) for RFE, TRMM, $CMORPH_{27}$ and $CMORPH_8$ SREs in the CKB over the five year (01/01/2001-31/12/2005) study period.

To further investigate the spatial variability of rainfall in the CKB, the spatial correlation functions for all the four SREs were developed using Equation 4-16; the results are presented in Figure 4-9.

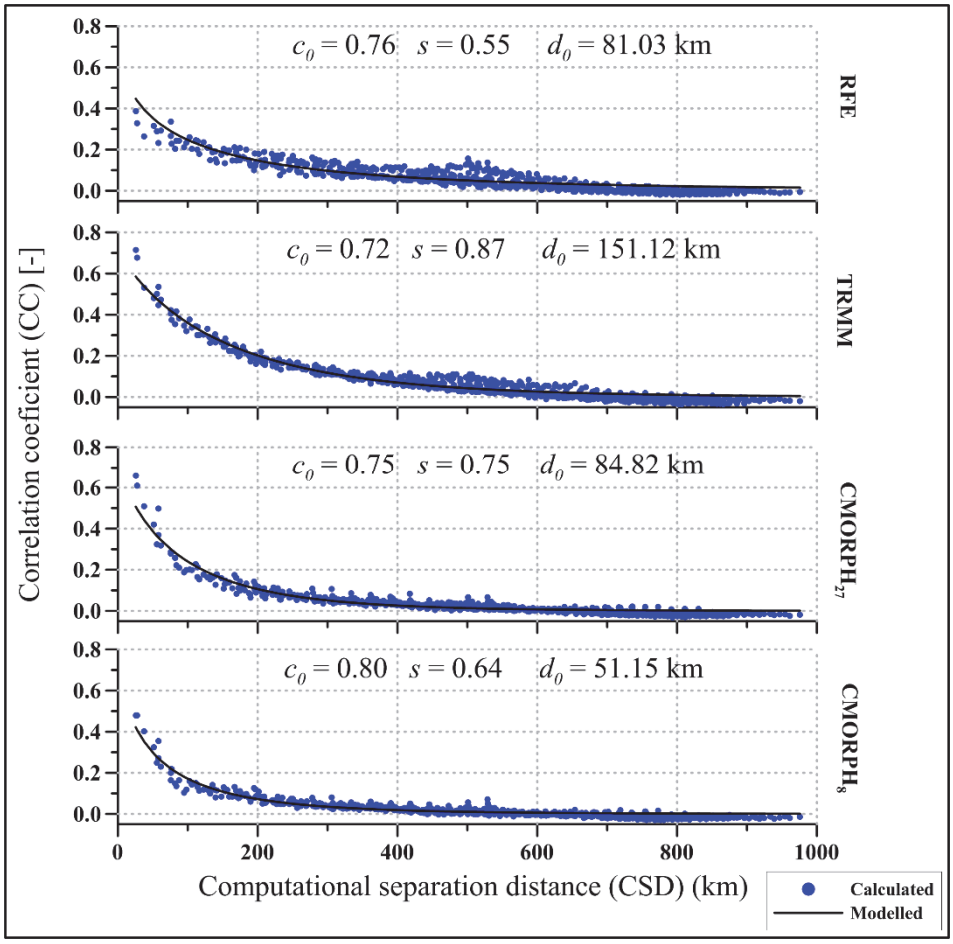

Figure 4-9: Spatial correlation functions for RFE, TRMM, CMORPH$_{27}$ and CMORPH$_8$ in the CKB. The parameters, c_o, s and d_o follow the Equation 4-16

As expected, there is a decrease in the correlation between rainfall data pairs, with the increase in their computational separation distance (CSD). The TRMM, is characterized by the smoothest spatial variability as documented by its largest d_o (correlation distance), followed by CMORPH$_{27}$, RFE and then CMORPH$_8$. This can also be observed in Figure 4-10, which presents sensitivity analysis of d_o where for given c_o, the d_o is the largest for TRMM in all the cases, meaning better correlation of any two points at larger separation distances than for the other three SREs.

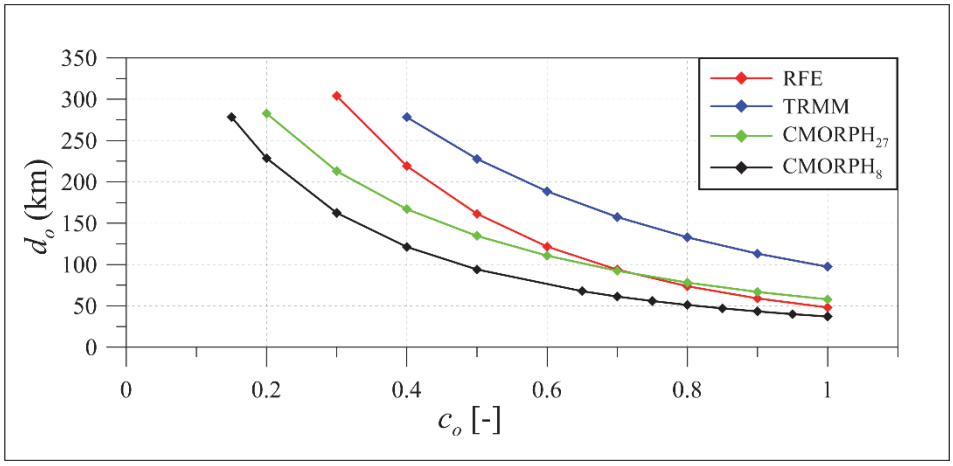

Figure 4-10 :Sensitivity analysis of d_o for RFE, TRMM, CMORPH$_{27}$ and CMORPH$_8$ in the CKB

The generally high spatio-temporal variability of rainfall in the CKB (Figures 4-8 to 4-10) is in agreement with the results from studies by Bhalotra (1987) and Obakeng et al. (2007) carried out in the same area. Among the four SREs investigated in this study, the TRMM indicated the lowest spatial rainfall variability, having the largest d_o as defined by spatial correlation functions presented in Figure 4-9 and Figure 4-10. Unfortunately, to our knowledge, there is no other published study applying spatial correlation function analysis, so it is not possible to compare correlation distances and related spatial variability of rainfall.

4.5.4 Bias correction

A Time Variable Space Fixed (TVSF) bias correction scheme (Equation 4-17) was applied to RFE, TRMM, CMORPH$_{27}$ and CMORPH$_8$ daily SREs, to correct their systematic (bias) in the CKB. In order to assess if there was improvement in the SREs after applying the TVSF-bias correction scheme, the bias-corrected SREs were evaluated using the scatter plots, descriptive statistics and categorical statistics. Spatial correlation functions were also developed for the TVSF, bias-corrected SREs, to assess their spatial variability.

The scatter plots of the corrected four SREs against rain gauge data are presented in Figure 4-11. It can be observed that the TVSF bias correction scheme improved the linear association of the four SREs with the reference rain gauge data, as observed through the increase in the R^2. For example, the R^2 of the uncorrected four SREs at Ghanzi, ranged from 0.18 to 0.19 (Figure 4-2) but after bias-correction improved to 0.20 to 0.81 (Figure 4-11). The same trend was observed in other, eight rain gauge sites.

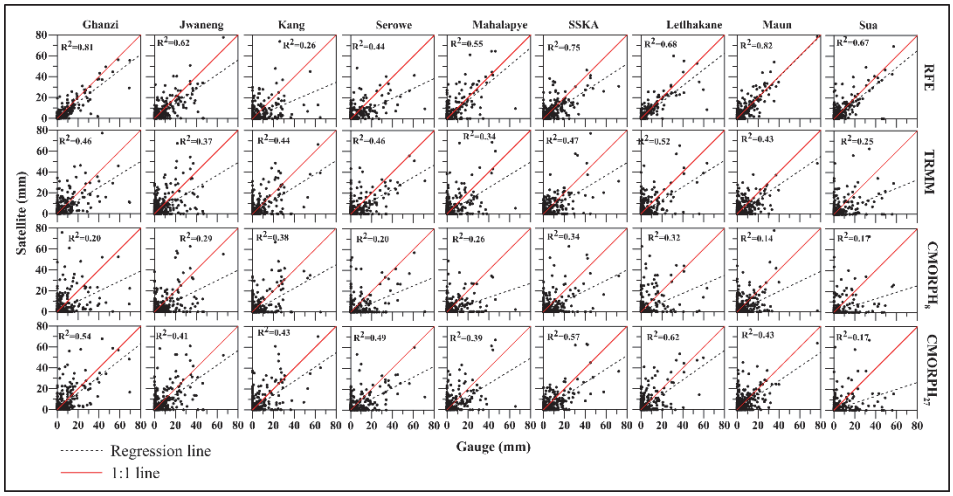

Figure 4-11: Scatter plots of corrected daily RFE, TRMM, $CMORPH_{27}$ and $CMORPH_{8}$ SREs against reference rain gauge rates over the five year (01/01/2001-31/12/2005) study period.

The descriptive statistics, i.e. *CC*, *MAE*, *ME* and *RMSE* for the TVSF, bias-corrected four SREs is presented in Figure 4-12. It can be observed that the *CC* increased in all the nine investigated sites, pointing at the improvement of the linear agreement between daily SREs and gauged rainfall. Also the *MAE* and *RMSE* were reduced in the corrected sites. After bias correction, *ME* better converged to zero. Concluding, the TVSF satellite rainfall bias-correction improved correlation of SREs with reference daily rain gauges and reduced the magnitude of differences between the daily corrected SREs and gauge measurements.

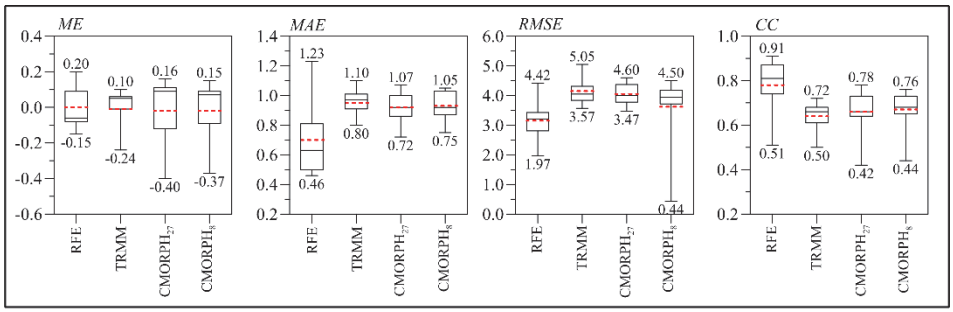

Figure 4-12: Box and whisker plots of descriptive statistics for RFE, TRMM, $CMORPH_{27}$ and $CMORPH_{8}$ SREs. The whiskers smallest and the largest values are labelled; the red dash-line denotes the mean value.

The categorical statistics of the four, TVSF bias-corrected SREs is presented in Figure 4-13. The results show that: i) *POD* remained constant because *M* and *H* did not change (Equation 4-5); ii) *FAR* has decreased because *F* was reduced (Equation 4-6); iii) *CSI* decreased due to the reduction of *F* (Equation 4-7) iv)

FBS also decreased due to better agreement between N_s and N_g (Equation 4-8). These results show that application of TVSF bias scheme to the four SREs has improved their daily rainfall detection in the CKB by reducing the false rain events (*F*).

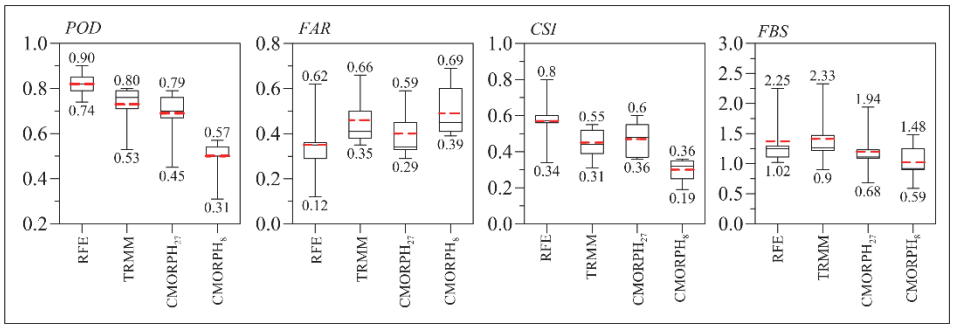

Figure 4-13: Box and whisker plots of categorical statistics for TRMM, $CMORPH_{27}$ and $CMORPH_8$ SREs. The whiskers extend to the smallest and the largest values (labelled) and the red dash-line denotes the mean value.

The spatial variability of TVSF, bias-corrected SREs were assessed using spatial correlation functions and their results are presented in Figure 4-14. The applied TVSF bias-corrected scheme increased the spatial variability of the four SREs, as documented by consistently lower d_o for all bias-corrected SREs (Figure 4-14), than for the uncorrected SREs (Figure 4-9). This might be due to limited number of rain gauges and the applied, spatially-fixed, TVSF bias correction scheme, which was developed using averaged rain gauge data with large separation distances to calculate the daily bias factor (*BF*).

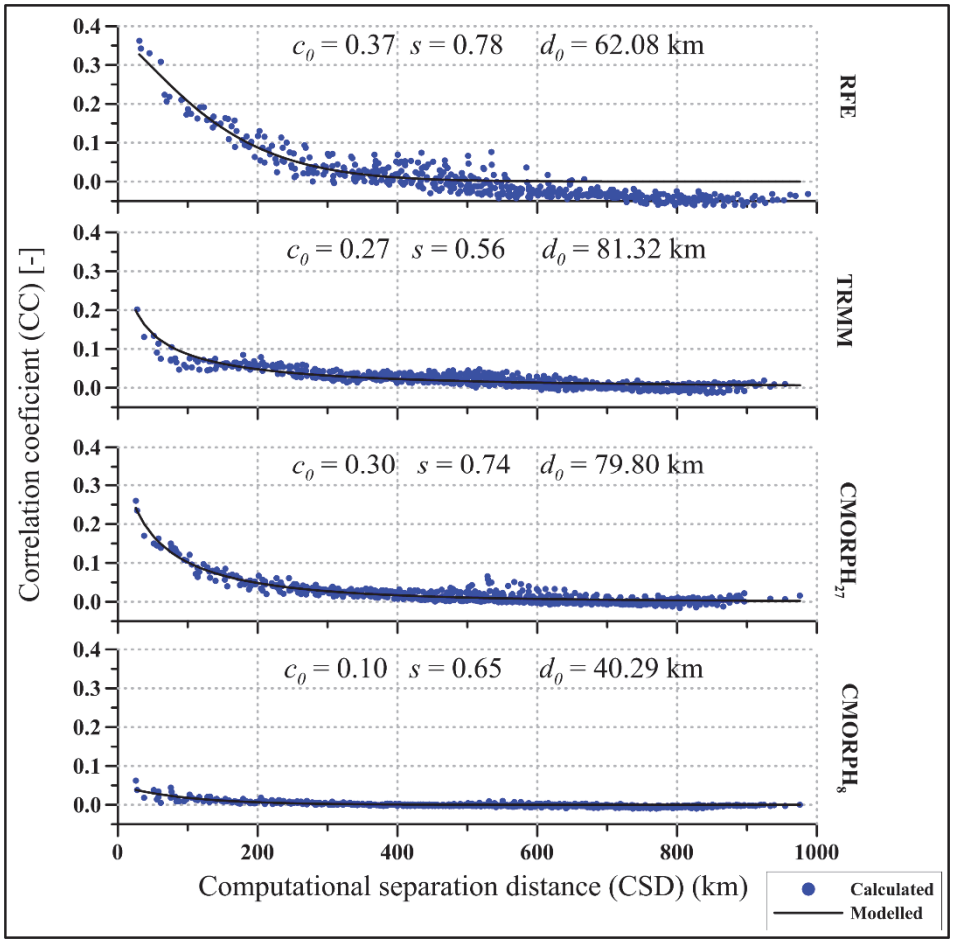

Figure 4-14: Spatial correlation functions for the bias-corrected RFE, TRMM, CMORPH$_{27}$ and CMORPH$_8$ SREs in the CKB. The parameters, c_o, s and d_o follow the Equation 4-16

4.6 Conclusions

Evaluation of the performances of RFE, TRMM, CMORPH$_{27}$ and CMORPH$_8$ of daily rainfall detection in the Central Kalahari Basin (CKB) over a five year period (2001-2005), using nine, well-distributed rain gauges, was conducted using four types of analysis: i) scatter plots; ii) descriptive statistics; iii) categorical statistics; and iv) bias decomposition methods. The four SREs were then bias-corrected by applying Time Varying and Space Fixed (TVSF) scheme. Finally, the spatio-temporal rainfall variability in the CKB was evaluated and compared between SREs, before and after bias-correction applying spatial correlation function analysis, mean annual rainfall, annual rainfall standard deviation and coefficient of variation. From this study, the following can be concluded:

1. The use of SREs (e.g. in water resources management) is particularly important in areas where rain gauges are scarce, such as the CKB, as the SREs provide alternative source of rainfall data with good spatial and temporal coverage.
2. Results of this study underlined the importance of validation of SREs at various climatic condition, because different SREs have different rainfall detection capabilities in different climatic areas.
3. The RFE displayed better daily rainfall detection capability than TRMM, $CMORPH_{27}$ and $CMORPH_{8}$.
4. It is remarkable, that the four SREs recorded more rainfall events than the gauges, but underestimated rainfall as compared to gauged rainfall. The larger rainfall frequency recorded by SREs was due to high frequency of false rain than the missed rain events, while the rainfall underestimation, likely due to limitation of TIR sensor used by the RFE, TRMM and CMORPH algorithms, which uses cloud top temperature to estimate rainfall and sometimes, start recording rainfall a bit later than when it occur in the case of warm clouds.
5. The most reliable indicator of the SREs performance analysis seems to be the frequency of "miss" rainfall events and the amount of the "miss-bias" rainfall, that both are expected to be the lowest possible, as the miss directly indicates satellite algorithm sensitivity to rainfall detection and miss-bias quantifies it.
6. The limited amount (9) of reliable reference rain gauge data available in the large Central Kalahari Basin (~195000 km^2), in combination with the scale difference between large-scale SREs' pixels and small-scale, rain-gauge area of influence, created uncertainty in the evaluation of the four, daily SREs as presented in this study.
7. The Time Varying and Space Fixed (TVSF) bias correction scheme applied in this study improved some error measures but resulted in the reduction of the spatial correlation distance, thus increased the spatial rainfall variability of all the four SREs. To be able to apply other, more sophisticated, spatio-temporally variable bias-correction schemes, more reference rain gauges are needed, which were not available in this study.
8. The analysis of the SREs of this study highlight the high spatial and temporal variability of rainfall, in the CKB.
9. Daily SREs have been rarely evaluated; this study confirmed that such evaluation is very challenging, but as demand for daily rainfall data rapidly increases, more research on daily satellite rainfall is needed.

Chapter 5 : Coupling remote sensing with long term in-situ data in coupled surface-groundwater flow modelling of the Central Kalahari Basin

This chapter is based on:

Lekula M, Lubczynski MW Coupling remote sensing with long term in-situ data in coupled surface-groundwater flow modelling of the Central Kalahari Basin. Hydrogeology Journal, in review.

5.1 Abstract

Distributed numerical models, considered nowadays as optimal tool for groundwater resources management, have always been constrained by availability of spatio-temporal input data. This problem is particularly distinct in arid and semi-arid developing countries, characterized by large spatio-temporal variability of water fluxes but scarce ground-based monitoring networks. That problem can be mitigated by remote sensing (RS) methods, which nowadays are applicable for modelling not only surface water resources but also groundwater resources, through rapidly increasing applications of integrated hydrological models (IHMs). This study shows implementation of various RS products in the IHM of Central Kalahari Basin (CKB, ~200Mm^2) multi-layered aquifer system, characterized by semi-arid climate and thick unsaturated zone, both enhancing evapotranspiration. It also analyses spatio-temporal water flux dynamics, providing 13-year (2002-2014), daily and annual, water balances, to evaluate groundwater resources dynamics and replenishment in the CKB. The MODFLOW-NWT model, applying UZF1 package, accounting for variably saturated flow was calibrated in transient, throughout 13.5 years (6 months warm-up, 13-year simulation) using borehole hydraulic heads as state variables and RS-based daily rainfall and potential evapotranspiration as driving forces. Other RS input data included: digital elevation model, land-use/land-cover and soils datasets. The model showed dominant role of subsurface evapotranspiration restricting gross recharge to only few mm/year and typically negative net recharge (median -1.5mmy^{-1}), varying from -3.6 (2013) to +3.0 (2006) mmy^{-1} with rainfalls 287 and 664 mmy^{-1} respectively, implying water table decline. The amount and temporal distribution of rain, unsaturated zone thickness and vegetation type/density, were primary determinants of the spatio-temporal net recharge distribution in the CKB.

5.2 Introduction

Groundwater is often the only, but vulnerable, source of potable water in arid and semi-arid areas, hence it must be well-evaluated and managed. Nowadays, distributed integrated hydrological models (IHM), coupling surface with groundwater processes, are considered an optimal tool for groundwater resources management, but their reliability is largely constrained by availability and quality of input data (Meijerink et al., 2007). The largest data problem refers to arid and semi-arid areas, where this study was carried out, because in such areas, ground-based monitoring networks are scarce (Brunner et al., 2007; Leblanc et al., 2007), so there are large areas without any monitoring point. That problem can be mitigated by remote sensing (RS) methods.

In recent years, RS has played an increasing role in providing spatio-temporal information for water resources evaluation and management (Coelho et al., 2017). Its applications in surface hydrology, including surface water modelling, are already well known and typically include: digital elevation derivatives, land cover, spatio-temporal rainfall and evapotranspiration evaluations (Schmugge et al., 2002). However, the RS contribution to groundwater hydrology and groundwater resources evaluation is less distinct so less known.

The standard RS applications in groundwater hydrology involved: assessment of groundwater recharge (e.g. Awan et al., 2013; Brunner et al., 2004; Coelho et al., 2017; Jasrotia et al., 2007; Khalaf & Donoghue, 2012), surface-groundwater interaction (e.g., Bauer et al., 2006; Hassan et al., 2014; Leblanc et al., 2007; Sarma & Xu, 2017), groundwater storage (resources) evaluation and change (e.g. Henry et al., 2011; Rodell et al., 2007; Rodell & Famiglietti, 2002; Taniguchi et al., 2011; Yeh et al., 2006). With recent advancement of IHMs, the RS contribution to such models is rapidly increasing, largely because of continuously increasing amount of downloadable RS products, such as for example rainfall or potential evapotranspiration.

Among the IHMs, there are complex models based on 3-D solution of Richards' equation and models simplifying Richards' equation. Examples of former, are proprietary HYDRUS-3D (Šimůnek et al., 2012) and free for academia HydroGeoSphere (Brunner & Simmons, 2012; Therrien, 1992), both computationally demanding and both requiring fine spatial and temporal discretization due to large nonlinearity of Richards' equation (Downer & Ogden, 2004; Sheikh et al., 2009). Models simplifying Richards' equation are more robust. For example, used worldwide in lots of surface/groundwater interaction studies MIKE SHE (Danish Hydraulic Institute, 1998), simplifies Richard's equation to 1-D, although it is still a very complex code, requiring a variety of skills such as hydrogeology, soil science, agronomy, computational hydraulics (Refsgaard, 2010) and many kinds of data for spatial heterogeneity description

(Ma et al., 2016). Besides, it is a proprietary software. Relatively simpler and more computationally efficient are models simplifying Richard's equation, not only to 1-D but also simplifying vertical, variably saturated flow as driven only by gravity potential gradient, i.e. ignoring negative potential gradients (Harter & Hopmans, 2004; Niswonger & Prudic, 2004; Smith & Hebbert, 1983). Such solution, applying kinematic wave (KW) approximation of Richards' equation solved by the method of characteristics, is for example proposed within the widely used Unsaturated-Zone Flow (UZF1) Package (Niswonger et al., 2006) under MODFLOW-NWT (Niswonger et al., 2011). In the regional scale modelling, as in this study, such simplification, can even be advantageous, because the errors introduced by averaging or upscaling soil hydraulic parameters, makes the KW and Richards' equations comparable in accuracy, while the KW equation requires less input data and much less computational power (Bailey et al., 2013; Hassan et al., 2014; Morway et al., 2013). Besides, the MODFLOW related codes, are public domain.

MODFLOW-NWT with its surface-groundwater interaction packages, including UZF1 package (El-Zehairy et al., 2018), have already been applied worldwide, either directly or within the GSFLOW (Markstrom et al., 2008) IHM. Most of these applications focused on simulation of hydrological processes of surface-groundwater interactions (e.g. El-Zehairy et al., 2018; Hassan et al., 2014) and climate change impact on groundwater resources (e.g. Gong et al., 2012; Hay et al., 2010; Huntington & Niswonger, 2012; Surfleet & Tullos, 2013; Surfleet et al., 2012). However, none of such applications has ever been dedicated to simulation of a regional, multi-layered aquifer system with a very thick unsaturated zone, integrating RS data and long-term in-situ hydro-meteorological time-series data.

The main objective of this study was to present the use of various RS products coupled with long term in-situ monitoring data, as input of a regional scale, distributed, numerical IHM of the CKB and characterize spatio-temporal flux dynamics of this semi-arid, multi-layered aquifer system with very thick unsaturated zone, providing long-term, quantitative water balance estimate.

As study area, the Central Kalahari Basin (CKB; Figure 2-1) has been chosen, as it complies with the above characteristics, but also because it hosts the most productive, important and exploited transboundary groundwater resources of the Karoo System Aquifer (SMEC & EHES, 2006), the focus of interest of Botswana and potentially also of Namibia.

5.3 Numerical model

The MODFLOW-NWT model with active UZF1 Package, further referred as MOD-UZF, was chosen as the IHM to be use in this study because: i) it is relatively simple, but still integrated solution, allowing to compute groundwater

fluxes (gross recharge, groundwater evapotranspiration and groundwater exfiltration) internally, based on unsaturated zone parameterization and external input driving forces, such as rainfall reduced by interception and potential evapotranspiration (Figure 5-1), rather than assigning them arbitrary, as it is the case in a standard, standalone groundwater models (Hassan et al., 2014); ii) the study area is pretty flat with poor drainage network, active only shortly after long heavy rains, which justifies the use of MOD-UZF rather than more sophisticated modelling solution involving surface, precipitation-runoff sub-model coupled with groundwater model, as for example GSFLOW or even one of the 3D Richards' equation models; iii) it is computationally efficient solution, optimal for large areas such as the CKB (~200000 km^2); iv) it is public domain software with extensive web materials.

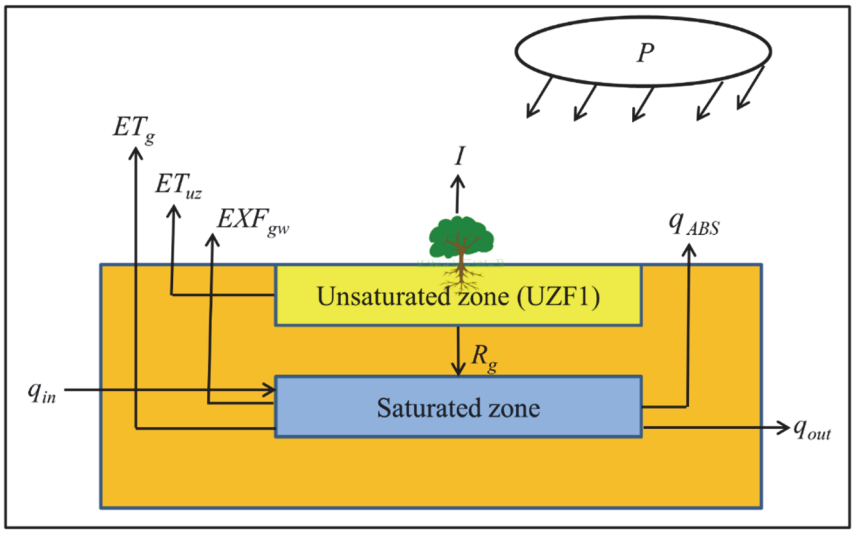

Figure 5-1: Schematic diagram of MOD-UZF setup for the CKB, where: *P* – precipitation; *I* – interception; q_{ABS} – groundwater abstraction; ET_g – groundwater evapotranspiration; ET_{uz} – unsaturated zone evapotranspiration, EXF_{gw} – groundwater exfiltration to land surface; R_g – gross recharge; q_{in} – lateral groundwater inflow; q_{out} – lateral groundwater outflow.

For pre- and post-processing of the MOD-UZF, the ModelMuse graphical user interface (Winston, 2009) was used because: i) it is a public domain software with support from developers; ii) it is easy and straightforward software with good technical support. Post-processing of cell by cell water budgets for each model layer or a specific part of the model was evaluated with the ZONEBUDGET (Harbaugh, 1990).

5.3.1 Model setup

A 3-D, six-layer, regional numerical model was built over the CKB area, following the hydrogeological conceptual model (HCM) (Figure 4-9) of Lekula et al. (2018a), where the six model layers directly corresponded to the six hydrostratigraphic units (HUs) (Table 2-1). The top model boundary represented by topographic surface, was assigned using 90 m spatial resolution digital elevation model data obtained from Shuttle Radar Topography Mission (SRTM) (Jarvis et al., 2008). Each subsequent layer boundary was defined by subtraction of the interpolated HU thicknesses using borehole log data and was imported from the 3-D geological model developed in Rockworks 17 software (RockWare, 2017), further referred to as Rockworks. Where HUs pinched out (Figure 4-9), layers were extended throughout the model domain, applying a fictitious, 1 m thick layer, with hydraulic properties representative of the overlying layer, in order to have continuous hydraulic connections in all the six layers, as per solution proposed by Anderson et al. (2015) and for example implemented by Masterson et al. (2016).

In the first, top layer representing KSU, 1-D-vertical, variably-saturated flow between land surface and water table, was simulated by the UZF1 package. All the six model layers, including the upper, partially unsaturated one, were set as "convertible" to be able to simulate spatio-temporally varying groundwater flow in either confined or unconfined conditions, depending on the head position. A quadratic 5x5 km square grid, consistent with the WGS84 ARC System Zone 10 coordinate system was used for consistency, because the CKB falls within both, WGS 1984 UTM Zone 34 and 35. Such grid resolution was found to be a trade-off between model computational time and model accuracy.

5.3.2 Model input

The input data for the CKB consisted of driving forces, parameters and state variables. Rainfall diminished by interception, further referred as effective precipitation (P_e), is the main driving force of the MOD-UZF model. In this study, the spatio-temporally variable, daily satellite rainfall of Famine Early Warning System Network Rainfall Estimate v2 (Herman et al., 1997), further referred as RFE, was downloaded from the Unites States Geological Survey (USGS) Famine Early Warning System Network (FEWSNET) data portal https://earlywarning.usgs.gov/fews/datadownloads for the period from 1 June 2001 to 31 December 2014. The choice of RFE, was because of its superior daily rainfall detection capability in the CKB (Lekula et al., 2018b). The RFE of 0.1^0 (~11 km) spatial resolution was resampled in ArcGIS to 5 km spatial resolution to match the model grid size, then converted to ASCII format and finally imported into ModelMuse.

The interception loss was assigned as spatially variable based on 1x1 km spatial resolution Land Use Land Cover (LULC) map by Loveland et al. (2000). Five land cover types were defined using information from Le Maitre et al. (1999), Miralles et al. (2010) and Werger and van Bruggen (1978), each with attributed interception rates defined in percentages of rainfall: bare soil and water bodies, 0%; grasslands, 2%; shrubs, 4%; savannah (a mixture of grassland, shrubs and forest), 6%; forest, 12%. That map was reclassified according to the corresponding interception loss classes and resampled to 5x5 km spatial resolution, all done in ArcGIS. Finally, for each day of simulation, the interception map was subtracted from the rainfall map to obtain spatio-temporally variable infiltration rate, also known as effective precipitation (P_e), applied as model input for each simulation day.

The second, important driving force of the MOD-UZF is potential evapotranspiration (*PET*). The spatio-temporally variable daily *PET* data at 1^0 (~110 km) spatial resolution was downloaded from the same USGS FEWSNET data portal as the rainfall and for the same period as rainfall. The FEWSNET *PET* was chosen as it is the only RS *PET* product available at daily time step for the CKB. FEWSNET *PET*, further referred to as *PET*, was resampled in ArcGIS to 5 km spatial resolution to match the model grid. The resampled daily *PET*, was finally converted to ASCII format and imported into ModelMuse.

The third driving force of the model were well abstractions, sourced from the two Debswana Diamond Mining Company Wellfields (Orapa and Jwaneng) and Water Utilities Corporation Wellfields (Greater Ghanzi and Gaothobogwe areas). The abstraction rates were arranged according to the daily simulation time step.

The parameterization of the unsaturated and saturated zones is presented in Table 5-1.

Table 5-1: CKB system parameterization: C – parameters that were estimated from available data and adjusted during calibration; L – parameters that were sourced from literature; F – parameters estimated and averaged from available field tests; θ_i - soil initial water content; θ_r - soil residual water content; θ_s – soil saturated water content; *EXTWC* – evapotranspiration extinction water content; *EXTDP* – evapotranspiration extinction depth; K_h – horizontal hydraulic conductivity; K_v – vertical hydraulic conductivity; S_y – specific yield; S_s – specific storage; *Cond* – conductance; UPW - upstream weighting package.

ZONE	Parameter	Minimum value	Maximum value	Unit	MOD-UZF packages	Source
Unsaturated zone	θ_s	0.37	0.43	m^3m^{-3}	UZF1	L
	θ_r	0.05	0.15	m^3m^{-3}	UZF1	L
	θ_i	0.05	0.15	m^3m^{-3}	UZF1	L
	EXTWC	0.06	0.16	m^3m^{-3}	UZF1	L
	EXTDP	1	25	m	UZF1	L
	ε	3.5	3.5	-	UZF1	L
	K_v	1.1	1.96	m d^{-1}	UZF1	C
Saturated zone	K_h *(layer 1)*	11	19.6	m d^{-1}	UPW	C
	K_h *(layer 2)*	3.1E-05	0.009	m d^{-1}	UPW	L
	K_h *(layer 3)*	0.42	0.95	m d^{-1}	UPW	C
	K_h *(layer 4)*	1.02E-07	0.004	m d^{-1}	UPW	L
	K_h *(layer 5)*	0.132	0.67	m d^{-1}	UPW	C
	K_h *(layer 6)*	0.585	0.96	m d^{-1}	UPW	C
	S_y *(layer 1)*	0.22	0.33	-	UPW	F
	S_y *(layer 2)*	1.0E-05	1.0E-05	-	UPW	F
	S_y *(layer 3)*	0.02	0.08	-	UPW	F
	S_y *(layer 4)*	1.0E-06	1.0E-06	-	UPW	F
	S_y *(layer 5)*	0.03	0.04	-	UPW	F
	S_y *(layer 6)*	0.01	0.06	-	UPW	F
	S_s *(layer 2)*	1.0E-09	1.0E-09	m^{-1}	UPW	L
	S_s *(layer 3)*	2.0E-06	8.0E-06	m^{-1}	UPW	C
	S_s *(layer 4)*	1.0E-09	1.0E-09	m^{-1}	UPW	L
	S_s *(layer 5)*	2.0E-06	4.8E-06	m^{-1}	UPW	C
	S_s *(layer 6)*	1.2E-06	6.5E-06	m^{-1}	UPW	F
	Cond	0.5	67	m^2 d^{-1}	GHB	C
	Cond	2	307	m^2 d^{-1}	DRN	C

The relation between unsaturated hydraulic conductivity and the unsaturated zone water content was defined by Equation 5-1 of Brooks and Corey function (Brooks & Corey, 1966).

$$K(\theta) = K_v \left[{\theta - \theta_r}/{\theta_s - \theta_r} \right]^{\varepsilon} \quad (5\text{-}1)$$

where $K(\theta)$ - unsaturated hydraulic conductivity, K_v - vertical saturated hydraulic conductivity, θ - current volumetric water content, ε - Brooks and Corey exponent

In the UZF1 Package, continuity between the unsaturated zone and saturated zone in the top unconfined aquifer is maintained through S_y estimated as $\theta_s - \theta_r$, where θ_r in fact approximates specific retention (Niswonger 2006). The θ_r and θ_s (Table 5-1) were defined as spatially variable input, with help of the 1x1 km resolution Africa soil map data (Jones et al., 2013); for each soil class, θ_r and θ_s were assigned following studies by Carsel and Parrish (1988) and Joshua (1991) and then spatially aggregated into 5x5 km grid. The evapotranspiration extinction water content (*EXTWC*) was assigned as θ_r + 0.01 and initial water content (θ_i) as equal to θ_r. The UZF1 vertical hydraulic conductivity (K_v) was assigned as ten times lower than K_h of the first layer (Domenico & Schwartz, 1998; SMEC & EHES, 2006) and was adjusted in the calibration process. The Brooks and Corey exponent (ε) was kept as default (Table 5-1).

The spatial distribution of evapotranspiration extinction depth (*EXTDP*) was defined for different vegetation types, following the 1x1 km spatial resolution LULC classification by Loveland et al. (2000). The values of the *EXTDP* classes were then assigned based on maximum rooting depths deduced from Obakeng et al. (2007), Kleidon (2004) and Canadell et al. (1996) as: bare soil and water bodies, 0 m; grasslands, 2 m; shrubs, 6 m; savannah (a mixture of grassland, shrubs and forest), 12 m; forest, 25 m. The 1x1 km *EXTDP* was imported to ModelMuse and averaged within the 5x5 km grid.

The system parameterization (Table 5-1) was based on the spatial distribution of aquifer parameters obtained from previous studies (Lekula et al., 2018a). The vertical hydraulic conductivity (K_v) of all the layers was assigned as ten times lower than K_h (Domenico & Schwartz, 1998) and was adjusted in the calibration process as per Table 5-1. The K_h were derived from the aquifer transmissivity data, extracted from pumping tests of projects executed in the CKB and aquifer thicknesses deduced using Rockworks (Lekula et al., 2018a). These were the basis for demarcating internally homogeneous and isotropic *K*-zones for the aquifers, i.e. for layer 1 - 26 zones, for layer 3 - 26 zones, for layer 5 - 27 zones and for layer 6 - 11 zones. The Stormberg Basalt and Inter-Karoo aquitards (layer 2 and 4) were assigned with spatially uniform *K*-values (Table 5-1). The zones of aquifer storage parameters, i.e. specific yield (S_y) and specific storage (S_s), were delineated the same way as *K*-zones while their values were assigned following borehole lithology and various literature sources elaborated in Lekula et al. (2018a). The S_y and S_s were further

calibrated in the transient simulation following expansion of the cones of depressions around wellfields.

Based on the HCM of Lekula et al. (2018a), the following, external boundary conditions (Figure 5-2) were assigned for the CKB numerical model: i) no-flow boundaries all around the CKB, matching the Okwa-Mmone River Catchment for the first KSU, while for the subsequent units, either at the contact with impermeable unit or along groundwater flowlines (Lekula et al., 2018a); ii) the head dependent inflow/outflow boundary assigned using MODFLOW General Head Boundary (GHB) Package (McDonald & Harbaugh, 1988), to simulate potential lateral groundwater inflow or outflow (Figure 5-2); and iii) the head dependent outflow boundary assigned using MODFLOW Drain (DRN) Package (McDonald & Harbaugh, 1988) to simulate groundwater outflow representing lateral CKB discharge to the Makgadikgadi Pans in the northern part of the study area (Figure 5-2).

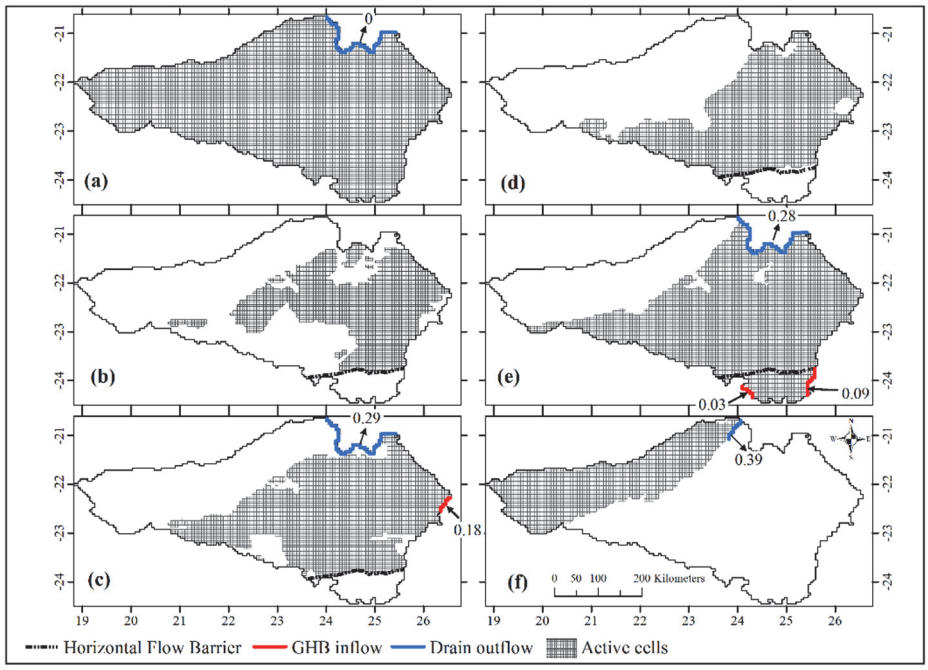

Figure 5-2: Boundary conditions and layer pinch-out of the six layers: a) Kalahari Sand unconfined layer; b) Stormberg Basalt Aquitard; c) Lebung Aquifer; d) Inter-Karoo Aquitard; e) Ecca Aquifer; f) Ghanzi Aquifer. Arrow and a number indicate flow direction and 13-year mean flow magnitude in $mmyr^{-1}$ (referenced to the whole study area).

There is also an internal model boundary along the regional Zoetfontein Fault (Figure 2-1 and Figure 5-2), which is prominent structural feature of the fifth unit (EA), simulated using the Horizontal Flow Barrier (HFB) Package (Hsieh & Freckleton, 1993), applying thickness of 3 m and hydraulic conductivity adjusted during the calibration process.

Groundwater levels converted to hydraulic heads were sourced from Department of Water Affairs (Botswana), Water Utilities Corporation (Botswana), Debswana Diamond Mining Company (Botswana) and Directorate of Water Resources Management (Namibia). The hydraulic heads were used as state variables in the model calibration. In the calibration, all the water levels in investigation boreholes (see Figure 4-5) were used, while in transient, only monitoring boreholes (Figure 2-1).

5.3.3 Model calibration and sensitivity analysis

First, a steady-state model was developed and calibrated using 13-year means of daily driving forces and state variables (from 1st June 2001 to 31st August 2014) to initialize the transient model. The steady-state simulation did not provide satisfactory initial hydraulic heads and initial water contents (θ_i) to start transient simulation, resulting in unrealistically large gross recharge. Similar problem was also observed by Niswonger et al. (2006). To fix it, a 6 months warm-up (spin-up) period, lasting from 1st June 2001 until December 31st 2001, was applied. Hence, the final transient model was calibrated with data from 1st January 2002 till 31st December 2014 applying daily stress periods and daily time steps.

For model calibration, Newtonian (NWT) solver was used, applying the option of "calculating groundwater heads even if below cell bottom" to prevent drying cells. The head tolerance was adjusted to 0.5 m, the flux tolerance to 5000 m^3 d^{-1} and the model complexity was set to "complex". All the remaining solver criteria were left as default setting. The model was calibrated manually because of its complexity; using optimisation codes such as PEST (Doherty & Hunt, 2010) or UCODE (Hill & Tiedeman, 2006) was computationally and time-wise too demanding. Besides, manual calibration allows users to better understand the model behaviour (Hassan et al., 2014).

The steady-state and transient model calibrations aimed at minimising the mean absolute error (*MAE*) and the root mean square error (*RMSE*) of the differences between the simulated and measured groundwater heads and water balance discrepancies at each time step as per Equation 5-2 and Equation 5-3. The calibration process was done in all six simulated layers, adjusting the initially assigned zone hydraulic conductivities (K_h), mainly those with scarcity of pumping test data. In the same way, also zones of specific yield (S_y) and specific storage (S_s) were adjusted (Table 5-1).

$$MAE = {}^{1}/_{n} \sum_{i=1}^{n} |H_{obs} - H_{sim}| \quad (5\text{-}2)$$

$$RMSE = \sqrt{{}^{1}/_{n} \sum_{i=1}^{n} (H_{obs} - H_{sim})^2} \quad (5\text{-}3)$$

where H_{obs} – observed heads; H_{sim} – simulated heads; n – number of data pairs; i- operator.

The sensitivity analysis mainly focused on testing sensitivity of fluxes representing water exchange between unsaturated and saturated zone i.e. unsaturated zone evapotranspiration (ET_{uz}), groundwater evapotranspiration (ET_g), gross recharge (R_g) and net recharge (R_n), to changes in parameters. Various parameters were tested in that respect, to find those influencing the most surface-groundwater exchange; finally three parameters were selected to be tested, i.e.: vertical hydraulic conductivity (K_v) of the Kalahari Sand Unit (1st layer), evapotranspiration extinction depth (*EXTDP*) and soil saturated water content (θ_s).

5.3.4 Water balances

Water balancing of the multi-layered aquifer system, particularly when simulated with variably saturated models, can be a complex issue because of many interacting unsaturated and saturated zone components (Figure 4-9). The water balance of the whole CKB model domain can be expressed as follows:

$$P + q_{GHB} = ET_{ss} + q_{ABS} + q_{DRN} \pm \Delta S \quad (5\text{-}4)$$

where: P – precipitation, q_{GHB} – lateral groundwater inflow into the modelled area across the GHB boundary, q_{DRN} - lateral groundwater outflow out of the modelled area across the DRN boundary, I – canopy interception, ET_{ss} – subsurface evapotranspiration, q_{ABS} – groundwater abstraction, and ΔS – total change in storage.

The ET_{ss} and ΔS can be expressed as follow:

$$ET_{ss} = ET_{uz} + ET_g \quad (5\text{-}5)$$

$$\Delta S = \Delta S_{uz} + \Delta S_g \quad (5\text{-}6)$$

where: ET_{uz} - unsaturated zone evapotranspiration; ET_g - groundwater evapotranspiration; ΔS_{uz} – storage change in unsaturated zone; and ΔS_g – storage change in the saturated zone.

The unsaturated zone water balance is expressed as:

$$P_a = P_e + EXF_{gw} = R_g + ET_{uz} \pm \Delta S_{uz} \quad (5\text{-}7)$$

where: P_e – effective precipitation ($P_e = P - I$), EXF_{gw} – groundwater exfiltration; R_g - gross recharge; P_a - actual infiltration (El-Zehairy et al., 2018)

The saturated zone water balance for all the simulated four layers can be expressed as follows:

$$R_g + q_{GHB} = q_{ABS} + q_{DRN} + ET_g + EXF_{gw} \pm \Delta S_g \quad (5\text{-}8)$$

The net recharge (R_n) is expressed as follows (Hassan et al., 2014):

$$R_n = R_g - EXF_{gw} - ET_g \quad (5\text{-}9)$$

5.4 Results and discussion

5.4.1 Model calibration

The calibrated MOD-UZF hydraulic parameters are presented in Table 5-1. Figure 5-3 shows the comparison between simulated and measured groundwater heads for the 13-year calibration period for the selected representative boreholes as in Figure 2-1. In general, there is a good match of the simulated with the measured, temporal head patterns. The mean absolute errors (*MAE*) for the control points ranged from 0.02 to 2.70 m and the root mean square error (*RMSE*) from 0.02 to 3.13 m. The likely explanations for discrepancies between the simulated and measured heads include: (i) averaging of the simulated heads within the 25 km^2 model cell; (ii) potential errors in the abstraction data of piezometers/boreholes affected by wellfield groundwater abstraction (TP34J, W14J, WF6_OB18O, WF5_OB10O, W47J, WF2_OB1O and WF2_OB3O) (iii) unrepresented heterogeneity within the 25 km^2 model cell; (iv) uncertainty in the measured water levels; (v) eventual errors in model parameterization.

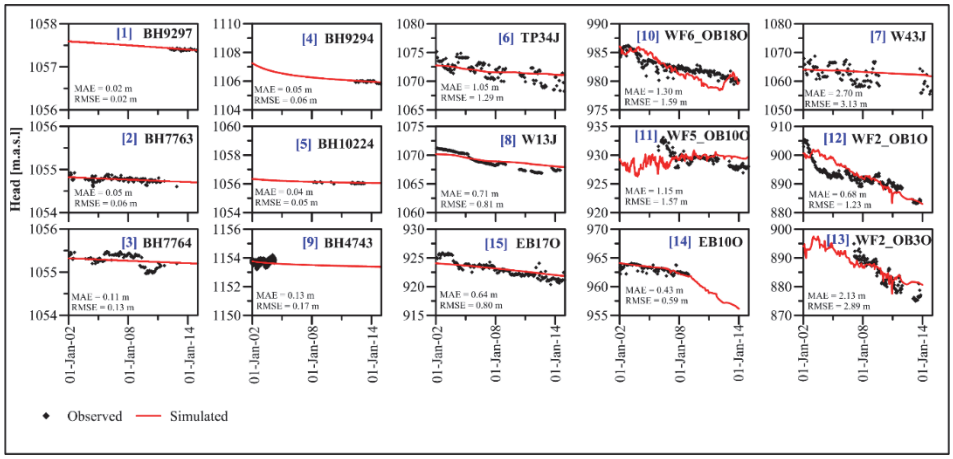

Figure 5-3: Simulated and observed daily variability of the selected groundwater piezometric heads; the locations of monitoring boreholes can be found in Figure 2-1. The calibrated piezometers are grouped into 5 columns; note, in each column, the head ranges are the same, but between columns, different.

It can be seen in Figure 5-3 that there are wide ranges of slopes of the head declines. The declines are steeper in major abstraction areas than in locations without abstractions. The particularly steep declines of groundwater levels are observed in boreholes W13J, W43J and TP34J located in the wellfield operated by Debswana Diamond Mining Company (DDMC) in Jwaneng and in boreholes EB17O, WF2_OB10 and WF6_OB18O, also operated by DDMC in Orapa. The heads in areas outside wellfields' influences (BH4743, BH7763, BH7764, BH9294, BH9297 and BH10224), also decline but with gentle slope. These declines are because the Kalahari area is affected by substantial ET_{uz}, due to large *PET* and thick unsaturated zone restricting infiltration and recharge and also because of considerable ET_g due to groundwater uptake by deep rooted acacia trees (Obakeng, 2007) and possibly also to direct groundwater evaporation from water table (Balugani et al., 2016), both reducing net recharge and as such reducing also groundwater resources. Throughout of 13-year simulation period, the relatively low R_g was not able to compensate the groundwater discharge, occurring mainly by ET_g (Lubczynski, 2000, 2009) and marginally by abstractions for livestock watering and EXF_{gw}. In Kalahari, substantial replenishment of groundwater resources occurs only once per decade in response to exceptional rainfall years (Lubczynski, 2009, 2011; Obakeng et al., 2007; Wanke et al., 2008) and within this study period, there was no such rainfall year.. The last exceptional rainfall year in Kalahari and aquifer replenishment was in the wet season of 1999/2000 characterized by rainfall of 970 mm yr^{-1} (Obakeng et al., 2007), i.e. before this study simulation period. Since then, the CKB heads have the declining trend as can be seen in Figure 5-3.

5.4.2 Water balances

The yearly mean water balance of the whole model domain per each of the 13 simulated hydrological years, is presented in Table 5-2 while the 13-year means per each layer are presented in the schematic block-diagram in Figure 5-4. Note that in the CKB, the hydrological year starts from 1 September of the previous year and ends 31 August of the analysed year. The 13-year mean water balance of the whole model domain as per Equation 5-4 consists of: P = 458.91 mm yr^{-1}, I = 9.18 mm yr^{-1} (2.00% of P), q_{GHB} = 0.30 mm yr^{-1} (0.07% of P), ET_{ss} = 436.36 mm yr^{-1} (95.09% of P), q_{ABS} = 0.22 mm yr^{-1} (0.05% of P), q_{DRN} = 0.94 (0.20% of P) and the positive, mean ΔS = 12.52 mm yr^{-1} (2.73% of P).

As the EXF_{gw} in the CKB was negligible, the input into unsaturated zone (Equation 5-7), consists mainly of P_e (449.73 mm yr^{-1}). As such the P_a is comparable with P_e, which is characteristic for the investigated CKB study area, but likely also for other, similar study areas with thick unsaturated zone. The

output of the unsaturated zone water balance (Equation 5-7) is dominated by ET_{uz} (433.24 mm yr^{-1}, 96.33 % of P_e), so only 1.87 mm yr^{-1} (0.42% of P_e) percolates down and recharges the saturated zone as R_g, while the ΔS_{uz} (14.62 mm yr^{-1}) accounts for 3.19 % of P_e. Such dominance of the ET_{uz} as compared to R_g, is due to thick unsaturated zone, favouring ET_{uz} and limiting R_g to extremely wet seasons with large rain showers.

The input of the saturated zone water balance (Equation 5-8) consists of R_g (1.87 mm yr^{-1}) and q_{GHB} (0.30 mm yr^{-1}), while the output is dominated by ET_g (3.12 mm yr^{-1}), followed by q_{DRN} (0.94 mm yr^{-1}) and groundwater abstraction (q_{ABS} ; 0.22 mm yr^{-1}). In the 13 investigated years, in the CKB, there was dominance of groundwater output as compared to input, which is reflected by the negative mean ΔS_g (-2.11 mm yr^{-1}) as only in one hydrological year 2006 with the largest rainfall of 664.45 mm yr^{-1}, the ΔS_g was positive. This also explain the declining water table within the 13 simulated years, replenished approximately once per decade or even less (Wanke et al., 2008)

The R_n was estimated as R_g - ET_g (Equation 5-9) because $EXF_{gw} \sim 0$, therefore the positive R_n indicates $R_g > ET_g$ and otherwise. Throughout the 13 hydrological year of model simulation (Table 5-2), the R_n was typically negative, except of the two years with rainfall distinctly above-average, i.e. 2006 when P = 664.45 mm yr^{-1} and R_n = 3.42 mm yr^{-1} and 2014 when P = 605.90 mm yr^{-1} and R_n = 0.98 mm yr^{-1}. However, these two years, could not compensate the remaining eleven years with negative R_n so the 13-year mean R_n = -1.25 mm yr^{-1}. It is interesting that the largest yearly R_n (2006) coincided with the largest P and R_g while the lowest yearly R_n (2002) not with the lowest P and R_g but with the highest ET_g. In that year 2002, the ET_g was highest because at the beginning of the simulation period the water table was still pretty high after the substantial replenishment in the extremely wet season of 2000 (Obakeng et al., 2007), which enhanced ET_g. Unfortunately, there was no sufficient data available in this study to start the model simulation from that year 2000 or earlier to show that.

Table 5-2: A 13 hydrological year annual water balance of the whole Central Kalahari Basin as per Equation 5-4, Equation 5-7 and Equation 5-8. All values are in mm yr^{-1}. The CKB hydrological year starts from 1 September of the previous year and ends 31 August of the analysed year.

Hydrological Year	P	P_e	I	ET_{ss}	ET_{uz}	ET_g	R_g	R_n	q_{GHB}	q_{DRN}	q_{ABS}	ΔS	ΔS_{uz}	ΔS_g
2002	445.40	436.49	8.91	413.34	408.00	5.34	1.88	-3.46	0.30	0.94	0.22	22.29	26.61	-4.32
2003	357.29	350.14	7.15	364.99	361.10	3.88	0.66	-3.22	0.30	0.94	0.22	-15.70	-11.63	-4.08
2004	439.49	430.70	8.79	419.82	416.91	2.91	1.42	-1.49	0.30	0.95	0.22	10.02	12.37	-2.35
2005	386.60	378.87	7.73	383.38	380.57	2.82	0.97	-1.85	0.30	0.94	0.22	-5.38	-2.67	-2.71
2006	664.45	651.16	13.29	553.78	550.98	2.81	6.23	3.42	0.30	0.94	0.22	96.51	93.96	2.55
2007	330.48	323.87	6.61	329.45	324.67	4.78	1.52	-3.26	0.30	0.94	0.22	-6.43	-2.32	-4.12
2008	483.41	473.74	9.67	473.55	470.23	3.31	1.33	-1.98	0.30	0.94	0.22	-0.67	2.17	-2.84
2009	510.24	500.04	10.20	489.85	487.13	2.72	1.40	-1.32	0.30	0.94	0.22	9.33	11.51	-2.18
2010	556.79	545.65	11.14	543.24	540.92	2.32	1.55	-0.78	0.30	0.94	0.23	1.54	3.19	-1.65
2011	590.72	578.91	11.81	567.16	564.79	2.37	2.02	-0.35	0.30	0.94	0.22	10.89	12.11	-1.21
2012	307.21	301.07	6.14	304.30	301.38	2.92	1.29	-1.63	0.30	0.94	0.21	-4.07	-1.60	-2.48
2013	287.84	282.08	5.76	284.00	281.62	2.38	1.09	-1.29	0.30	0.94	0.21	-2.76	-0.63	-2.14
2014	605.90	593.78	12.12	545.77	543.76	2.01	2.99	0.98	0.30	0.94	0.22	47.15	47.03	0.12
Statistics														
Mean	458.91	449.73	9.18	436.36	433.24	3.12	1.87	-1.25	0.30	0.94	0.22	12.52	14.62	-2.11
Median	445.40	436.49	8.91	419.82	416.91	2.82	1.42	-1.49	0.30	0.94	0.22	1.54	3.19	-2.35
Max.	664.45	651.16	13.29	567.16	564.79	5.34	6.23	3.42	0.30	0.95	0.23	96.51	93.96	2.55
SD	122.11	119.67	2.44	99.72	100.12	0.99	1.43	1.86	0.00	0.00	0.01	29.79	28.23	1.86
Min	287.84	282.08	5.76	284.00	281.62	2.01	0.66	-3.46	0.30	0.94	0.21	-15.70	-11.63	-4.32

The lateral and vertical flux exchange through the six layers of the CKB is presented in Figure 5-4 as 13-year mean. In that diagram, each layer receives number of input and output water fluxes and the difference between them per layer, represents its storage change. The presented water balance is pretty complex because of very thick top KSU unsaturated zone layer redistributing rainfall water into various underlying layers and partitioning that water between R_g, ET_{uz} and ET_g, but also because of complex structural geology and hydrogeology of the simulated area, with step-wise pinching out of the layers underlying KSU, which implies complex flux exchanges between layers. For example, the R_g as per Figure 5-4, consists of five components, summing up to 1.87 mm yr^{-1} (Table 5-2). These are 1.49 mm yr^{-1} to KSU, 0.23 mm yr^{-1} to SBA, 0.04 mm yr^{-1} to LA, 0.03 mm yr^{-1} to EA and 0.08 mm yr^{-1} to GA, each applied to its water table, being the shallowest water table in the 6-layer flow system. The R_g to KSU was deduced directly from the MOD-UZF water budget output. However, the other R_g components were defined indirectly by delineation of water budget zones with ZONEBUDGET postprocessor in layers underlying fully unsaturated KSU and calculating the downward fluxes in those zones. This additional calculation protocol was applied because the current UZF1 package, estimates R_g only within the water table extent of the layer to which the UZF1 Package is assigned, in this study case the KSU. There was no analogic water budgeting problem with ET_g, because the *EXTDP* was everywhere less than the KSU thickness while the EXF_{gw} was negligible.

Considering external groundwater exchange, (Figure 5-2 and Figure 5-4), the lateral groundwater inflow enters LA from the east (0.18 mm yr^{-1}) and EA from two sides in the south (0.01 + .11 mm yr^{-1}). The presence of these lateral inflows (defined by application of GHB) rejected the HCM hypothesis that the CKB is a fully isolated basin, although the simulated inflows are pretty low, and possibly triggered by abstractions. The northern lateral groundwater outflows towards Makgadikgadi Pans were: i) in KSU, negligible; ii) in LA, 0.29 mm yr^{-1}, so more than lateral input; iii) in Ecca 0.28 mm yr^{-1}, so more than 3-times larger than lateral input; and iv) in GA, which did not have any lateral input, was the largest, 0.39 mm yr^{-1}. Such large GA groundwater outflow, was mainly because of the largest and positive interlayer, flux exchange with KSU (Figure 5-4), where the 13-year mean annual input from KSU to GA was 0.62 mm while the output to KSU, only 0.28 mm. The large downward input was because of peripheral, so prone to recharge, GA position within the CKB and relatively large area of the saturated KSU contacting directly with GA. In contrast the lowest interlayer flux exchange difference between different layers was observed between KSU and EA where the same 0.09 mm went in and out of the layers. The 13 year average groundwater abstractions (q_{ABS}) in all the 3 aquifers, presented as a spatial flux, looks pretty small as compared to other fluxes, because that abstraction is referenced to the whole model domain (~200 Mm^2), while these abstractions are significant at the local scales.

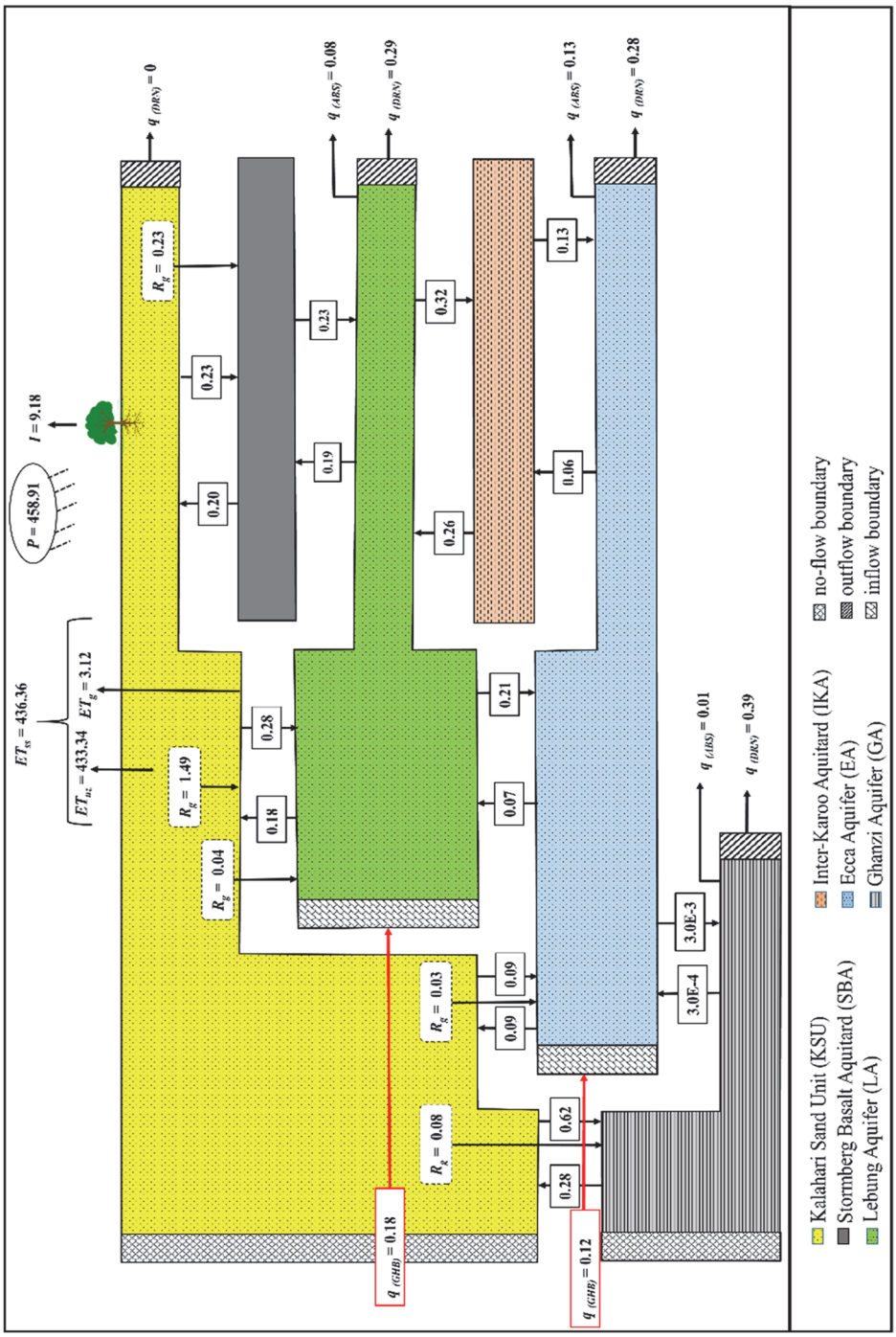

Figure 5-4: Schematic block-diagram of inter-layer water balance exchange within the Central Kalahari Basin, presented in mm y^{-1} as 13-year yearly means for the whole model domain.

5.4.3 Spatial variability of fluxes

The Figure 5-5a presents the spatial variability of R_g, ET_g and R_n in the wettest simulation hydrological year 2006, and the Figure 5-5b, in the driest 2013 (Table 5-2). It can be seen that in both years, R_g, ET_g and R_n were highly spatially variable, being limited to small areas such as fossil river channels and depressions. This is in agreement with de Vries et al. (2000), who also observed locally enhanced recharge of up to 50 mm yr^{-1} in pans and fossil valleys in the southern part of the CKB. The restriction of these fluxes to the depressions and fossil channels is mainly due to relief depressions and temporal increase of water levels and soil moisture along these locations so shallower water table, and better chance for R_g and R_n, but also higher ET_{uz} and ET_g. In the 2006 hydrological year, the R_g (6.23 mm y^{-1}) was larger and covered much bigger area than the R_g (1.09 mm y^{-1}) in 2013 (Figure 5-5b) while the ET_g in 2006 and 2013 were comparable in values (2.81 and 2.38 mm y^{-1} respectively). As such, the R_n in 2006 was generally positive (3.42 mm y^{-1}) having spatial extent similar to R_g, while the R_n in 2013 was generally negative (-1.29 mm y^{-1}) and was restricted to similar locations as ET_g. The results show that positive R_n occurs in the CKB only during wet years, as also noted by (Wanke et al., 2008) in a similar environment, north of the CKB.

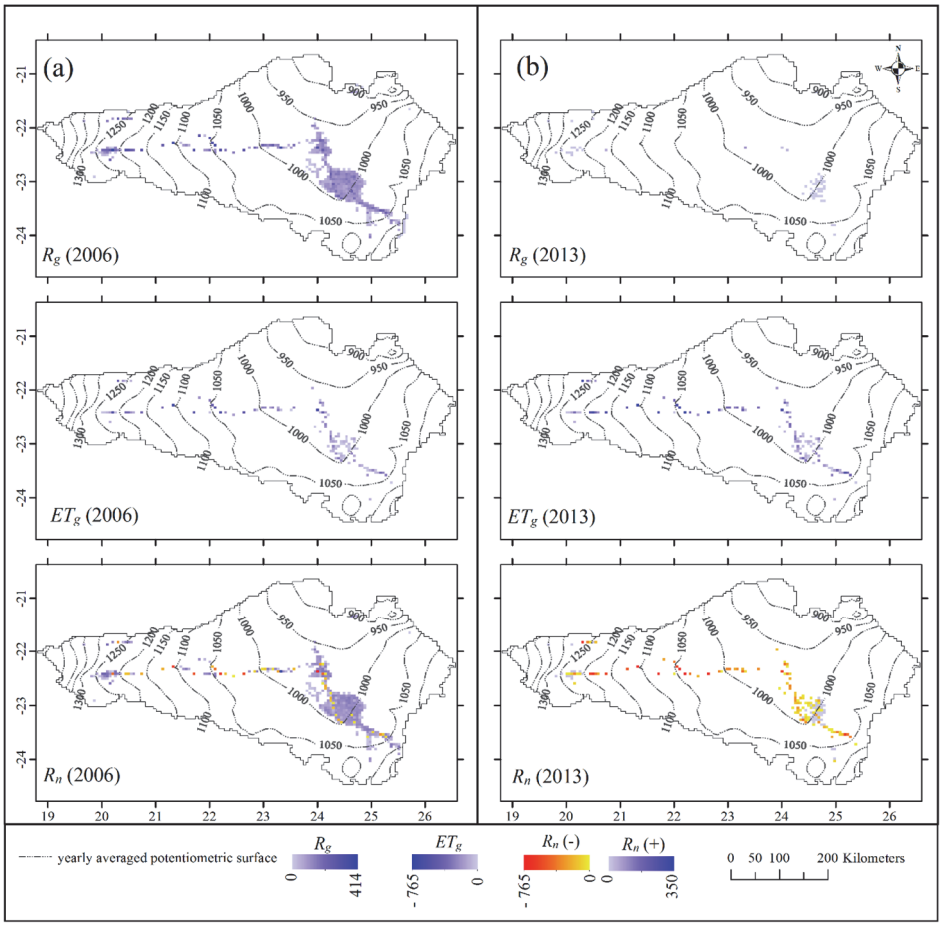

Figure 5-5: Spatial variability of gross recharge (R_g), groundwater evapotranspiration (ET_g), and net recharge ($R_n = R_g - ET_g$ as $EXF_{gw} = 0$) for: a) 2006; b) 2013, hydrological years.

5.4.4 Temporal variability of fluxes

Large temporal variability of surface and subsurface water fluxes, both on a daily (Figure 5-6) and yearly basis (Table 5-2) is observed. The CKB is characterised by erratic, restricted to wet season, high-rainfall days, relatively low interception (Table 5-2) and erratic large actual infiltration events, some of them even >20 mm d^{-1} (Figure 5-6a). However, majority of that infiltration, is removed from the unsaturated zone by generally large ET_{uz}, ranging from nearly zero in dry season even to 5 mm d^{-1} in wet season, so only small portion of rain arrives to water table. This is because of the extremely large Kalahari *PET*, the largest in the hottest wet season, and because of very thick unsaturated zone, which enhance water loss and restricts R_g to erratic episodes that in the 13 years of this study period, ranged from 0 up to 0.13 mm d^{-1} in

2006. The daily ET_g is less temporally variable, varying from 0 to 0.02 mm d^{-1} in the same manner as the water table, i.e. its peak is delayed several months with respect to the peak of wet season rains. As such, the ET_g fluctuation pattern is also offset with respect to ET_{uz}, which is mainly dependent on climatic factors, so matching *PET.*

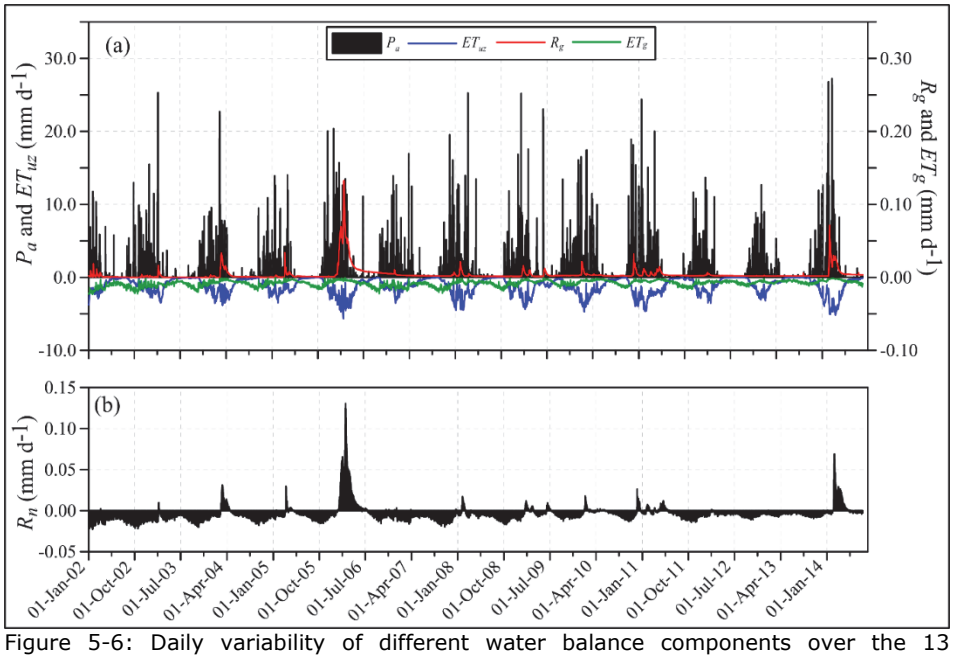

Figure 5-6: Daily variability of different water balance components over the 13 hydrological year simulation period: a) actual infiltration (P_a), unsaturated zone evapotranspiration (ET_{uz}), gross recharge (R_g), groundwater evapotranspiration (ET_g); b) net recharge (R_n).

The daily variability of R_n is presented in Figure 5-6b. As being defined by the difference between highly temporally variable R_g and moderately variable ET_g, the resultant R_n is also temporally variable, ranging from -0.02 to 0.13 mm d^{-1}. It is remarkable that on a year basis there are only relatively short R_n>0 events, occurring even not every year. The exceptions are years 2006 and 2014 with above average annual precipitation (Table 5-2), when relatively large R_g was observed resulting in positive annual R_n. In the other 11 years, the ET_g was dominant, so annual R_n<0. The annual variability of R_n as well as of other fluxes, is listed in Table 5-2. The episodic nature of recharge events in the CKB is attributed to erratic rainfall, thick unsaturated zone and very high *PET* so also large ET_{uz}. Significant recharge events occur only in response to cumulated in time, consisting of number of sequential, above average rainfall events. Similar observation was made also by Wanke et al. (2008) in a comparable environment.

The R_g and R_n dependence on precipitation is illustrated in Figure 5-7. It can be observed that below ~600 mmy^{-1} of annual rain threshold, there is nearly no change of R_g and R_n. The substantial R_g and R_n increments take place only when annual rains exceed 600 mm. Assuming linear trend of rainfall-recharge in the years with the largest rainfalls as in Figure 5-7, the estimated backward annual R_g and R_n for the exceptionally wet year 1999/2000 with 970 mm rainfall (year not simulated), were ~23 and 16 mm respectively. The above assumption of linear trend is quite modest so most likely the recharge input was even larger.

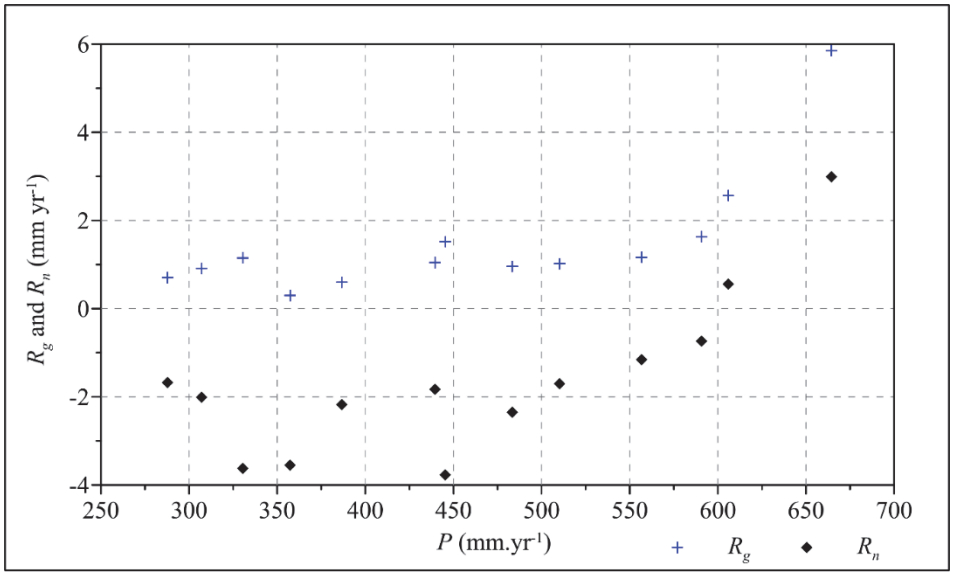

Figure 5-7: Cross-dependence of yearly means of rainfall (P) versus gross recharge (R_g) and net recharge (R_n).

5.4.5 Sensitivity analysis

The replenishment and therefore sustainability of groundwater resources, largely depends on R_n (Equation 5-9; Lubczynski, 2006, 2011). Therefore, the sensitivity analysis in this study focused on testing R_g, ET_g and EXF_{gw} and also the resultant R_n, all representing water exchange between unsaturated and saturated zone. However, after preliminary tests, the EXF_{gw} was excluded from further sensitivity analysis, as the EXF_{gw} was negligible in all analysed years due to generally deep water table depth (WTD), so also its sensitivity was not relevant for the R_n estimate. Therefore, the sensitivity analysis was carried out mainly for R_g and ET_g testing also the resultant R_n (Figure 5-8), all in the wettest within the study period, hydrological year 2006.

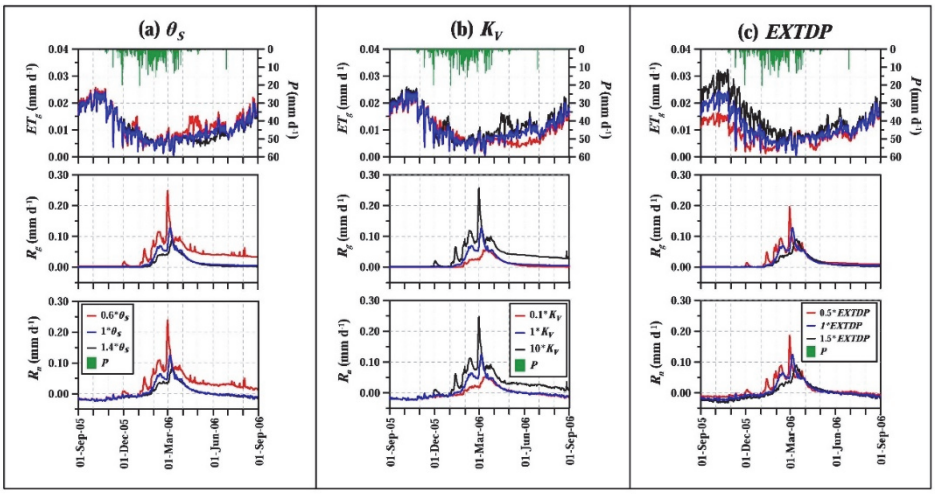

Figure 5-8: Sensitivity analysis of: (i) groundwater evapotranspiration (ET_g); (ii) gross recharge (R_g); and (iii) net recharge (R_n) in response to changes in the following model parameters: a) soil saturated water content (θ_s); b) UZF1 vertical hydraulic conductivity (K_v); c) evapotranspiration extinction depth (*EXTDP*). The sensitivity analysis is presented for the wettest hydrological year 2006.

As the R_g was substantially larger than ET_g in that year, it had generally much larger effect upon the R_n while varying unsaturated zone parameters, θ_s, K_v and *EXTDP*. In contrast, in dry years, the R_n was totally dependent on ET_g as R_g was negligible. The ET_g sensitivity to changes of θ_s was generally low, regardless of the ET_g seasonal variability, driven mainly by the water table fluctuation, characterized by peaks delayed with respect to the occurrence of the wet seasons. The little peak of the ET_g in $0.6\theta_s$ simulation at the end of April 2006, was likely attributed to the ~1.5-2.0 months delayed water table rise, in response to the R_g peak occurring around 1 March (Figure 5-8). The K_v changes had very similar impact upon ET_g, having similar little peak of ET_g in April 2006 for $10K_v$ simulation, likely due to the same reason as in $0.6\theta_s$ simulation. The sensitivity of the ET_g to *EXTDP* was different than of the other two parameters analysed. In general, the larger the ET_g itself was, the larger differences were between different *EXTDP* simulations. It is remarkable that the ET_g maxima and the largest differences between the three *EXTDP* simulations, were just before the wet season started, i.e. in October (Figure 5-8), with the largest ET_g for 1.5 *EXTDP* simulation. After that peak, the differences between the three simulations gradually declined to be negligible already in February.

In the selected example wet year 2006 (Figure 5-8), the R_g was sensitive to changes of all the three tested parameters, θ_s, K_v and *EXTDP*. The $0.6\theta_s$ and $10K_v$, as well as the $1.4\theta_s$ and $0.1K_v$ simulations, had very similar effects upon R_g, as both parameters, i.e. θ_s and K_v, similarly influence $K(\theta)$ in Equation 5-

1. In the presented R_g sensitivity patterns, remarkable is the peak around 1 March in response to wet season accumulation of rain, with clear sequence of peak occurrences, the fastest for the lowest $0.6\theta_s$ and for the largest $10K_v$, both, due to the largest $K(\theta)$. It is also remarkable that only the two simulations i.e. $0.6\theta_s$ and $10K_v$, resulted in the delayed, substantial R_g extending throughout the dry season, while in the all other θ_s and K_v simulations, R_g converged to zero, shortly after the wet season. In contrast, that non-zero R_g 'tail' extending throughout the dry season was not present in any of the *EXTDP* simulations. Considering the sequential R_g peaks, they had similar timing and pattern as the θ_s and K_v simulations. The largest R_g was attributed to the lowest *EXTDP* and otherwise, as the increment of *EXTDP* reduces the amount of water potentially available for R_g. The R_n sensitivity presented in Figure 5-8, was very similar to the R_g because of negligible impact of EXF_{gw} and small impact of ET_g.

5.4.6 Experiences of using remote sensing (RS) in data scarce Central Kalahari Basin

The recent advancement of integrated hydrological models (IHMs) creates promising "avenue" for novel RS applications not only in surface but also in groundwater studies. This is because, in contrast to standard, standalone groundwater models, where driving forces, i.e. R_g and ET_g were not quantifiable by RS, in the IHMs driving forces, i.e. rainfall and *PET* (Hassan et al., 2014), are well quantifiable by RS, while the R_g and ET_g, are estimated internally, based on surface and unsaturated zone parameterization.

One of the main challenges of integrated hydrological modelling, particularly in arid and semi-arid areas characterized by large spatio-temporal variability of water related fluxes, has been insufficient availability and quality of surface and subsurface input data. This study shows that RS can contribute to regional scale IHMs, providing various types of readily available (downloadable) RS products, most importantly, spatio-temporally variable, driving forces such as rainfall and *PET*.

With advancement in RS techniques, various satellite rainfall products at different spatial and temporal resolutions are now readily available. However, these products typically need to be validated against in situ data to select optimal one and eventually to remove the bias (Lekula et al., 2018b; Rahmawati & Lubczynski, 2017). Also satellite derived *PET* data is available as RS product, although not as widely as rainfall and at much coarser spatial and temporal resolution. However, even with that limitation, the RS-based *PET* estimates, are still useful because *PET* is much less spatio-temporally variable than rainfall. Besides, if necessary (e.g. in local scale assessments), with some efforts, *PET* can be also defined at much better spatio-temporal resolution from raw multispectral RS data as for example by Kim and Hogue (2008).

The remotely sensed earth observation from space, cannot contribute to subsurface hydrostratigraphy of a model, except of the upper model boundary, i.e. the topographic surface. The topographic surface, is nowadays derived by RS techniques, applying for example interferometry (e.g. Noferini et al., 2007; Wegmüller et al., 2009), lidar (e.g. Liu et al., 2005; Ma, 2005) or analysis of stereoscopic images (e.g. Haala & Rothermel, 2012; Xu et al., 2010). These methods provide digital elevation models (DEMs) already at pretty fine spatial resolution - in this study the SRTM 90 m DEM was downloaded from CGIAR-CSI database (http://srtm.csi.cgiar.org).

The UZF1 package of MODFLOW, which links surface input with groundwater, requires soil physical parameters and evapotranspiration extinction depth. The soil physical parameters can be estimated based on field sampling and literature sources but the challenge is how to spatially distribute them in the IHMs. In that task, remotely sensed soil maps with pretty detailed spatial distribution of different soil types is a solution. In this study, the spatial distribution of the soil physical parameters was defined using Soil Atlas of Africa (Jones et al., 2013) largely based on remote sensing soil assessment, while parametric values were extracted from literature sources. The spatial distribution of the evapotranspiration extinction depth can be defined spatially based on vegetation maps, provided the rooting depths of individual species can be realistically estimated. In this study evapotranspiration extinction depth was defined based on the Land Use Land Cover (LULC) map of CKB (Loveland et al., 2000) while the rooting depth of plant species, based on Obakeng et al. (2007), Kleidon (2004) and Canadell et al. (1996).

Spatial and temporal resolution of the RS products can be an issue limiting their applicability as IHM input. If temporal resolution of most of the RS products is already sufficient for typical, daily input data requirements of most of the IHMs, the spatial resolution, particularly of RS rainfall, is still a limiting factor of IHMs' applicability to local scale applications, except maybe of some DEM products available at <100 m resolution. Because of that limitation, the RS products are still mainly used in regional scale models, particularly those over areas with lack or scarce monitoring networks such as the CKB However, the RS products continuously improve their spatial and temporal resolution, therefore it is expected that shortly, they will be also more frequently applied in IHMs at local scale applications.

Considering scarcity of fine spatial resolution RS products, at the local scale IHMs, only a tailor-made, quantitative RS applications based on high or very high spatial resolution images, can be utilized, such as for example: i) evapotranspiration mapping using Moderate Resolution Imaging Spectroradiometer (MODIS) with spatial resolution ranging from 0.5 to 1 km (Bastiaanssen et al., 1998a; Bastiaanssen et al., 1998b; Su, 2002); ii) tree transpiration mapping using QuickBird and WorldView at 60-40 cm per pixel

(Lubczynski et al., 2017; Reyes-Acosta & Lubczynski, 2013); iii) tree interception using QuickBird and WorldView at 60-40 cm per pixel (Hassan et al., 2017). In such RS applications, very convenient and efficient are already unmanned aerial systems (drones) that can provide required spatial resolution, can carry on-board multispectral cameras and are cost effective (Colomina & Molina, 2014), so very promising, although their data processing is still cumbersome and requires specialized knowledge.

The reliability of models depends not only on driving forces and parameters, but also on state variables that represent model calibration reference. The RS techniques of earth observation, cannot detect the most commonly calibrated state variable, i.e. the water table, even at shallow water table condition. In that respect promising was the launch of the Gravity Recovery and Climate Experiment (GRACE) satellite, a joint mission by National Aeronautics Space Administration (NASA) and German Aerospace Center (DLR), which throughout the analysis of gravity change, detects change of subsurface water storage so also a change of aquifer water level (e.g. Leblanc et al., 2009; Rodell & Famiglietti, 2001; Seoane et al., 2013; Yeh et al., 2006) although only at very coarse resolution (Sutanudjaja et al., 2014; Tapley et al., 2004), restricting its applicability to regional, or even continental scale basins. Another popular state variable applied in IHMs is river discharge. In contrast to water levels, a river discharge can be estimated in ungauged catchments applying RS techniques (e.g Brakenridge et al., 2007; De Groeve, 2010; Hirpa et al., 2013). With advancement in IHMs and with improvement of accuracy of RS solutions of spatio-temporal soil moisture and actual evapotranspiration, these two, can also be used as state variables in model calibration (e.g. Li et al., 2009; Lopez et al., 2017), although the currently available RS solutions of soil moisture and actual evapotranspiration still involve substantial error particularly in dry land applications where the RS quantification error can be comparable or larger than the size of recorded water fluxes. Besides, the web-based products of soil moisture and actual evapotranspiration are still available at the coarse resolution, which restricts IHMs to large scale, regional assessments or force researchers for self-processing based on raw data, which considering typically applied daily IHM data processing stress period, is cumbersome and time consuming.

5.5 Conclusions

Advancement in the numerical groundwater modelling resulted in the continuous increase of use of integrated hydrological models (IHMs). IHMs need spatio-temporally distributed, surface input data such as *P-I* and *PET* (driving forces), unsaturated zone parameters, i.e. soil physical properties and evapotranspiration extinction depths, hydrogeological parameters, also required by standalone groundwater models and state variables such as for example hydraulic heads. Typically such data at the ground basis, are scarce

or unavailable, particularly in remote areas of developing countries such as the CKB region. The alternative source of such data is from RS, although not with respect to all data types. The objective of this study was to showcase the use of RS data in the IHM of a multi-layered aquifer system (CKB) characterised by a thick unsaturated zone. The key findings of this study are listed below:

1. The presented multi-layered, CKB hydrogeological system has three aquifers, Lebung, Ecca and Ghanzi; each receives diffused recharge from rainfall through the top Kalahari Sand layer (either partially saturated or entirely unsaturated) while the Lebung and Ecca aquifers, receive also small lateral inflows. The flow patterns in all the aquifers are similar, with piezometric surfaces radially converging towards central part of the basin from where all three aquifers discharge groundwater towards Makgadikgadi Pans. Considerable amount of groundwater is also discharged by groundwater evapotranspiration.

2. In semi-arid aquifer systems with thick unsaturated zone, such as the CKB, the subsurface evapotranspiration is the dominant discharging flux, comparable with rainfall, while groundwater exfiltration is negligible because of deep water table. As a consequence of the latter, gross recharge and groundwater evapotranspiration are comparable, so their yearly balance represented by the net recharge, is typically low, close to zero and whether positive or negative, depends primarily on the annual rainfall amount and distribution, and secondarily on the current water table depth.

3. The groundwater resources in semi-arid aquifer systems with thick unsaturated zone, such as the CKB, are sustained through recharge events of exceptionally wet years; within the 13-year of the simulation period, from 2002 to 2014 there was no such a year while, the wettest year was 2006 with annual rainfall 664 mm, gross recharge 6.2 mm and net recharge 3.0 mm; in majority of other simulated years, with lower rainfall, gross recharge was less than groundwater evapotranspiration, resulting in typically negative net recharge, the lowest, -3.5 mm, in 2002. The generally negative net recharge within the simulation period, is the main reason of the observed declining trends of water table and groundwater storage.

4. Amount and temporal distribution of rain, thickness of an unsaturated zone (so WTD) and vegetation type/density, are primary determinants of the R_n strength and distribution in the CKB. The porosity, specific yield and vertical hydraulic conductivity of the unsaturated zone material are also important.

5. Advancement in integrated hydrological models (IHM) coupling surface and groundwater flows, created great opportunities of using remote sensing (RS) techniques in hydrogeology. The RS can nowadays provide input data for IHMs, at reasonable spatial and pretty good temporal resolutions, which is particularly important in data scarce areas with insufficient density of monitoring networks and/or inaccessible areas such as the CKB. In this CKB IHM study, the main RS contributions addressed: rainfall, potential evapotranspiration, land cover and land use types, and terrain elevation.

Chapter 6 : Synthesis

In arid and semi-arid regions, such as the Central Kalahari Basin (CKB), ground-based data are scarce, so typically insufficient to build reliable conceptual and numerical models for evaluation and management of groundwater resources. Reliability of such models largely depends on the availability of data with good spatio-temporal coverage, particularly in developing world such as the African Continent, where ground-based data are scarce. The recent introduction of integrated hydrological models (IHMs) created opportunity of using as input not only ground-based data, but also remote sensing (RS) data. In the IHMs, the external driving forces, such as for example rainfall and potential evapotranspiration, are directly measurable, in contrast to standard, standalone groundwater models, where recharge and groundwater evapotranspiration cannot be directly measured, so are typically defined arbitrarily. This study presents integration of various types of RS data (RS products) with ground-based data in the IHM of the regional (~200 Mm^2), Central Kalahari Basin (CKB) hydrogeological structure, hosting the most productive and exploitable transboundary Karoo Aquifer System of Botswana and Namibia.

In the development of the IHM of the CKB, three aspects were of particular importance. Firstly, the hydrogeological conceptual model (HCM) developed based on the available, fragmented geological, hydrogeological and RS data as presented in Chapter 3 and published in Lekula et al. (2018a). Secondly, assessment of RS data for the HCM and IHM, with the most important RS-rainfall assessment presented in Chapter 4 and in Lekula et al. (2018b) and with other RS-based input data described in Chapters 3 and 5. Thirdly, development, calibration and analysis of the IHM of the CKB, including evaluation of sustainability of groundwater resources in the CKB, but also reflection on the use of the RS data in the development of regional IHMs such as the IHM of the CKB as presented in Chapter 5 and also in Lekula and Lubczynski (2018, in review).

Hydrogeological conceptual model

In the multi-layered systems, an important part of HCM is a hydrostratigraphic model. In the CKB, the hydrostratigraphic model was developed based on a 3-D geological modelling applying RockWorks standalone code, which allowed to integrate all existing geological and hydrogeological data. That code, because of its simplicity of operation, in conjunctive, iterative use with other codes (such as ArcGIS and MODFLOW-NWT), was highly efficient in subsurface data processing of a large and complex multi-layered aquifer systems, as the CKB.

The CKB hydrostratigraphic units were defined, using available, archive, geological and hydrogeological data. The classification of the

hydrostratigraphic units was challenging, because of unclear regional transition between Groups and Formations, their inter-dependencies and hydrogeological importance. That classification resulted in presentation of the novel, tabulated stratigraphy and hydrostratigraphy of the CKB (Table 2-1) and in 3D hydrostratigraphic model consisting of six hydrostratigraphic units (model layers): Kalahari Sand Unit (KSU), Stormberg Basalt Aquitard (SBA), Lebung Aquifer (LA), Inter-Karoo Aquitard (IKA), Ecca Aquifer (EA) and Ghanzi Aquifer (GA).

The first KSU, is the only spatially continuous, thick, sandy layer (typically >60 m), only locally saturated and unconfined at the bottom. Other five layers are spatially discontinuous with variable thickness and characteristic layer pinch out, challenging not only the hydrostratigraphic model setup but also the numerical model setup. The three aquifers, are unconfined if directly overlain by KSU, otherwise confined by one of the two aquitards.

Any hydrostratigraphic unit of HCM, must be associated with parameters. The CKB system parameterization was done based on pumping tests and borehole lithology. In areas lacking such data, the HCM-assigned parameterization, was left to be adjusted in the numerical model calibration.

In the CKB, there are three aquifer flow systems, Lebung, Ecca and Ghanzi. It is remarkable that all the three, have nearly the same, radially-concentric, regional groundwater flow patterns, all directed towards Makgadikgadi Pans' discharge area (Figure 2-4). That similarity is likely due to various hydraulic interconnections, direct or through aquitard leakages, and also due to the hydraulic function of the KSU, redistributing recharge into all of them.

Based on the available head distribution inside and outside of the CKB, and based on the study by de Vries et al. (2000), the CKB groundwater flow system was hypothesized to be of the closed-basin type, i.e. with no surface or groundwater inflow, where the only water input was by diffused rainfall-recharge while discharge (output) by groundwater evapotranspiration, lateral groundwater outflow towards Makgadikgadi Pans and by water-well abstractions. However, the hypothesized model boundaries were to be validated and eventually adjusted within the IHM calibration.

Considering the CKB water balance and particularly the CKB groundwater replenishment, the following were considered as critically important CKB characteristics, restricting recharge to erratic, approximately decadal episodes: i) generally low and highly spatio-temporally variable rainfall; ii) large and spatially variable thickness of the KSU; and iii) 'thirsty' and pretty dense, as for the desert, vegetation.

Based on the developed HCM, a fully 3-D, six-layer numerical model, with shallow, variably-saturated saturated and first layer unconfined, was finally

recommended to be developed (chapter 5) and calibrated in transient state, on daily basis, using 13,5-year of daily driving forces (rainfall, *PET* and well-abstractions) derived using coupled, RS and ground-based data, and available state variable data (hydraulic heads).

Remote sensing contribution to IHM

The contribution of remote sensing (RS) to the IHM in this study, included spatio-temporal, daily estimates of driving forces, i.e. of rainfall and potential evapotranspiration, as well as other ancillary data, mainly used for parameterization of the unsaturated zone.

Rainfall, is the most important data input of an IHM. A rainfall is typically measured by rain gauges and then interpolated from gauge estimates. However, such estimates, particularly in arid and semi-arid areas, are representative only for small areas adjacent to the gauges (Rahmawati & Lubczynski, 2017), so with limited amount of them and large spatio-temporal rainfall variability, as in the CKB, there are large areas without any rainfall data, so highly uncertain. The web-downloadable RS-rainfall products provide good spatial and temporal data coverage, so can well cover these areas, improving spatio-temporal rainfall estimates.

Various RS-rainfall products are available in nearly every place of the world. However, in different places, different RS products provide different accuracy of rainfall estimates. Therefore, in every study area, evaluation of the number of different RS-rainfall products is needed, in order to choose the optimal one. In this study, the CKB rain gauge network was insufficient for adequate, spatio-temporally variable rainfall interpolation. Therefore, four, web-downloadable, daily, satellite rainfall estimates (SREs), known to perform well in Southern Africa, were selected to be further investigated in order to define one, best performing in daily rainfall detection over the CKB. The four pre-selected products included: RFE, TRMM, $CMOPRH_{27}$ and $CMORPH_{8}$. All the four, were evaluated against nine, daily rain gauge records, over a five-year period, using descriptive and categorical statistics. In that assessment, the most reliable performance indicator was the frequency of the "*miss*" rainfall events and the "*miss-bias*", i.e. the quantity of rainfall missed by the SRE, as the two directly indicate sensitivity and bias of rainfall detection, respectively. Result of that evaluation showed, that the RFE performed best, mainly because of its inherent bias correction, although all SREs underestimated rainfall through the simulation period.

As RS-products, typically exhibit systematic (bias) and random errors, a selected product, should be investigated for possible, bias-correction before using it in a hydrologic model (Habib et al., 2014; Nicholson et al., 2003). This study attempted to perform the Time Varying and Space Fixed bias-correction scheme on all the four SREs, however, because of the limited number of

gauges, this bias-correction turned to be inconclusive, as also indicated by the spatial correlation function, turned not to be conclusive analysis. Finally, the RS RFE, daily rainfall product with 0.1^0 spatial resolution, after resampling, was integrated in the IHM.

The results of this study indicated that SREs can be used as complementary rainfall data sources, especially in areas where rain gauges are scarce, such as the CKB, because they provide valuable rainfall data with reasonable spatial and good temporal coverage. It also showed that the daily rainfall in the CKB was highly spatio-temporally variable, as also observed by Bhalotra (1987) and Obakeng et al. (2007).

The *PET* driving force of an IHM, was less spatially variable than rainfall, so did not require as high spatial resolution as the rainfall. Besides, the IHMs are much less sensitive to changes in *PET* than to rainfall. As such, the RS, daily *PET* product with 1^0 spatial resolution, after resampling and validation with ground-based data, was considered as reliable input and therefore directly integrated in the IHM.

Next to rainfall and *PET*, other RS data types were used to setup HCM and IHM. These were: 1) digital terrain model, used to define top of the first layer; 2) RS-based land use and land cover maps, to define vegetation type, density, and evapotranspiration extinction depths; 3) soil maps to parameterize the unsaturated zone. All these data were very helpful, eliminating arbitrary assumption in assigning various gridded data.

Integrated hydrological model

A six-layer, transient IHM of the CKB was developed and calibrated on daily basis, throughout 13-year period (2002-2014), using MOD-UZF platform (Chapter 5) and various RS products coupled with long term, in-situ monitoring data as input. The model boundary conditions, followed the HCM (Chapter 3). The RS-based, daily rainfall and *PET* data, as well as borehole abstractions, were assigned as the driving forces of the IHM. The unsaturated zone was parameterised by coupling RS and ground-based data. The saturated zone parameterization (Table 5-1) relied on pretty dense network of borehole data, including pumping tests as well as regional and local geological and hydrogeological studies, all integrated in the HCM (Chapter 3). That system parameterization, was further optimised during model calibration.

The model calibration itself, showed a good match between the simulated and measured temporal head patterns and also low *MAE*, ranging from 0.02 to 2.70 m and low *RMSE* ranging from 0.02 to 3.13 m, with the head differences attributed mainly to the unrepresented heterogeneity and head averaging within the 25 km^2 model cells.

The calibrated model indicated general water table decline within the 13 simulated years, with steep declines in the major wellfield abstraction areas. In the other areas, outside wellfields' influences, the declines were gentler but consistent over the CKB. This was because, within the 13 simulated years, gross recharge (R_g) was generally lower than groundwater discharge. The low Kalahari R_g, typically in order of only few mm y^{-1}, is mainly because of relatively low rainfall, large *PET* and thick unsaturated zone with pretty dense and thirsty plants, both enhancing Kalahari ET_{uz} (~96% of rainfall). Larger R_g, can occur only in response to exceptionally wet year, which however was not present within the 13-year of the simulation period. The relatively large CKB groundwater discharge is mainly due to the substantial groundwater evapotranspiration (ET_g) and rather small lateral groundwater outflow while groundwater exfiltration was negligible. The relatively large ET_g is due to groundwater uptake by deep-rooted and 'thirsty' acacia trees (Obakeng et al., 2007) and possibly also due to direct groundwater evaporation from water table and/or its capillary fringe (Balugani et al., 2016). Out of the 13 simulated years, only twice $R_g > ET_g$, in 2006 and in 2014, when rainfall was 664 and 606 mm yr^{-1} resulting in R_n of 3.4 and 1.0 mm yr^{-1}, respectively. In the other 12 simulated years, the R_n was negative, which explains the observed in this study area, declining trend of the water table.

It is remarkable that the model calibration rejected the hypothesis that the CKB is a closed basin as the selected external model boundaries, assigned as GHB model boundaries, indicated small lateral inflows, into the Lebung Aquifer (0.18 mm yr^{-1}) and Ecca Aquifer (0.21 mm yr^{-1}) (Figure 5-2 and Figure 5-4). These inflows, however, are located near the wellfields, so might be enforced by the well abstractions, resulting in the dynamic, outward movement of the hydraulic boundary condition of the groundwater divide (El-Zehairy et al., 2018).

The IHM results indicated large spatio-temporal variability of the CKB groundwater fluxes, R_g, ET_g and R_n. That variability was mainly determined by the high spatio-temporal rainfall variability (Bhalotra, 1987; Lekula et al., 2018b; Obakeng & Lubczynski, 2004), spatial variability of the thickness of unsaturated zone and by vegetation type and spatial density distribution, implying spatial extinction depth variability. It is observed that the groundwater fluxes are enhanced in fossil river channels and depressions, in consequence of shallowing of a water table and increase of soil moisture. However, even in these locations, the positive R_n occurred during the wettest years only.

The MOD-UZF code used in this study, turned to be optimal IHM for the CKB modelling challenge, because the study area is pretty flat with poor drainage network active only shortly after long heavy rains, so negligible surface runoff, which justifies the use of MOD-UZF rather than more sophisticated IHM.

Chapter 7 : Recommendations

Ground data

1. Increase number of rain gauges, particularly within the Central Kalahari Game Reserve, to provide additional point data of rainfall estimates to be used in validation of the satellite rainfall estimates.
2. Use geophysical data to validate and eventually improve the developed hydrogeological conceptual model, especially to evaluate the Ecca Aquifer thickness in the central and northern CKB.
3. Install more automated, piezometric observations.
4. Carry on detailed hydrogeological investigations at the local scale in the: a) southern part of the CKB, where the KSU is in hydraulic connection with the Ecca Aquifer, to define hydraulic regime of surface-groundwater interactions; b) northern part of the CKB, to investigate the CKB groundwater outflow dynamics; c) western part of the CKB, to assess and quantify aquifer recharge dynamics.

The IHM and its data

1. Increase spatial resolution of the developed IHM (also with appropriate increase of the resolution of reliable input data), from 5x5 to 1x1 km grid.
2. Increase spatial resolution of rainfall and *PET* driving forces;
3. Investigate extinction depth of the Kalahari plants and integrate it in the classified vegetation map of the CKB;
4. Assess model uncertainty;
5. Attempt to use RS actual evapotranspiration and/or soil moisture as state variables of the IHM, to improve confidence of the calibrated IHM.
6. Use the developed IHM to assess impact of climate change on sustainability of CKB groundwater resources.

Bibliography

Adeyewa, Z. D., & Nakamura, K. (2003). Validation of TRMM radar rainfall data over major climatic regions in Africa. *Journal of Applied Meteorology, 42*(2), 331-347. doi:10.1175/1520-0450(2003)042<0331:votrrd>2.0.co;2

AghaKouchak, A., Mehran, A., Norouzi, H., & Behrangi, A. (2012). Systematic and random error components in satellite precipitation data sets. *Geophysical Research Letters, 39*(9), n/a-n/a. doi:10.1029/2012GL051592

AghaKouchak, A., Nasrollahi, N., & Habib, E. (2009). Accounting for Uncertainties of the TRMM Satellite Estimates. *Remote Sensing, 1*(3), 606-619. doi:10.3390/rs1030606

Allen, D. M., Schuurman, N., Deshpande, A., & Scibek, J. (2008). Data integration and standardization in cross-border hydrogeological studies: a novel approach to hydrostratigraphic model development. *Environmental Geology, 53*(7), 1441-1453. doi:10.1007/s00254-007-0753-3

Anderson, M. P., Woessner, W. W., & Hunt, R. J. (2015). *Applied Groundwater Modeling : Simulation of Flow and Advective Transport*

Arias-Hidalgo, M., Bhattacharya, B., Mynett, A. E., & Griensven, A. v. (2013). Experiences in using the TMPA-3B42R satellite data to complement rain gauge measurements in the Ecuadorian coastal foothills. *Hydrology and Earth System Sciences, 17*(7), 2905-2915. doi:10.5194/hess-17-2905-2013

Artan, G., Gadain, H., Smith, J., Asante, K., Bandaragoda, C., & Verdin, J. (2007). Adequacy of satellite derived rainfall data for stream flow modeling. *Natural Hazards, 43*(2), 167-185. doi:10.1007/s11069-007-9121-6

Awan, U. K., Tischbein, B., & Martius, C. (2013). Combining hydrological modeling and GIS approaches to determine the spatial distribution of groundwater recharge in an arid irrigation scheme. *Irrigation Science, 31*(4), 793-806. doi:10.1007/s00271-012-0362-0

Bailey, R. T., Morway, E. D., Niswonger, R. G., & Gates, T. K. (2013). Modeling Variably Saturated Multispecies Reactive Groundwater Solute Transport with MODFLOW-UZF and RT3D. *Ground Water, 51*(5), 752-761. doi:10.1111/j.1745-6584.2012.01009.x

Balugani, E., Lubczynski, M. W., & Metselaar, K. (2016). A framework for sourcing of evaporation between saturated and unsaturated zone in bare soil condition. *Hydrological Sciences Journal-Journal Des Sciences Hydrologiques, 61*(11), 1981-1995. doi:10.1080/02626667.2014.966718

Bastiaanssen, W. G. M., Menenti, M., Feddes, R. A., & Holtslag, A. A. M. (1998a). A remote sensing surface energy balance algorithm for land

(SEBAL) - 1. Formulation. *Journal of Hydrology, 212*(1-4), 198-212. doi:10.1016/s0022-1694(98)00253-4

Bastiaanssen, W. G. M., Pelgrum, H., Wang, J., Ma, Y., Moreno, J. F., Roerink, G. J., & van der Wal, T. (1998b). A remote sensing surface energy balance algorithm for land (SEBAL) - 2. Validation. *Journal of Hydrology, 212*(1-4), 213-229. doi:10.1016/s0022-1694(98)00254-6

Batisani, N., & Yarnal, B. (2010). Rainfall variability and trends in semi-arid Botswana: Implications for climate change adaptation policy. *Applied Geography, 30*(4), 483-489. doi:http://dx.doi.org/10.1016/j.apgeog.2009.10.007

Bauer, P., Gumbricht, T., & Kinzelbach, W. (2006). A regional coupled surface water/groundwater model of the Okavango Delta, Botswana. *Water Resources Research, 42*(4), W04403. doi:10.1029/2005WR004234

Bhalotra, Y. P. R. (1987). *Climate of Botswana Part II : Elements of climate*. Retrieved from

Bordy, E. M., Segwabe, T., & Makuke, B. (2010). Sedimentology of the Upper Triassic-Lower Jurassic (?) Mosolotsane Formation (Karoo Supergroup), Kalahari Karoo Basin, Botswana. *Journal of African Earth Sciences, 58*(1), 127-140. doi:10.1016/j.jafrearsci.2010.02.006

Brakenridge, G. R., Nghiem, S. V., Anderson, E., & Mic, R. (2007). Orbital microwave measurement of river discharge and ice status. *Water Resources Research, 43*(4). doi:doi:10.1029/2006WR005238

Brassington, F. C., & Younger, P. L. (2010). A proposed framework for hydrogeological conceptual modelling. *Water and Environment Journal, 24*(4), 261-273. doi:10.1111/j.1747-6593.2009.00173.x

Brassington, R. (1998). *Field hydrogeology* (Second edition ed.). Chichester etc.: Wiley & Sons.

Bredehoeft, J. D. (2002). The water budget myth revisited: Why hydrogeologists model. *Ground Water, 40*(4), 340-345. doi:10.1111/j.1745-6584.2002.tb02511.x

Brooks, R. H., & Corey, A. T. (1966). Properties of porous media affecting fluid flow. *Journal of the Irrigation and Drainage Division, 92*(2), 61-90.

Brown, M. E. (2008). *Famine early warning systems and remote sensing data*: Springer Science & Business Media.

Brunner, P., Bauer, P., Eugster, M., & Kinzelbach, W. (2004). Using remote sensing to regionalize local precipitation recharge rates obtained from the Chloride Method. *Journal of Hydrology, 294*(4), 241-250. doi:http://dx.doi.org/10.1016/j.jhydrol.2004.02.023

Brunner, P., Hendricks Franssen, H. J., Kgotlhang, L., Bauer-Gottwein, P., & Kinzelbach, W. (2007). How can remote sensing contribute in groundwater modeling? *Hydrogeology Journal, 15*(1), 5-18. doi:10.1007/s10040-006-0127-z

Brunner, P., & Simmons, C. T. (2012). HydroGeoSphere: A Fully Integrated, Physically Based Hydrological Model. *Ground Water, 50*(2), 170-176. doi:10.1111/j.1745-6584.2011.00882.x

Bureau de Recherches Géologiques et Minières (BRGM). (1991). *Letlhakeng Botlhapatlou groundwater project TB 10/2/16/88-89*. (Final report). Department of Geological Survey, Botswana: Unpublished report.

Canadell, J., Jackson, R. B., Ehleringer, J. R., Mooney, H. A., Sala, O. E., & Schulze, E. D. (1996). Maximum rooting depth of vegetation types at the global scale. *Oecologia, 108*(4), 583-595. doi:10.1007/bf00329030

Carney, J., Aldiss, D., & Lock, N. P. (1994). *The geology of Botswana*. (Bulletin 37). Department of Geological Survey.

Carsel, R. F., & Parrish, R. S. (1988). Developing joint probability-distributions of soil-water retention characteristics. *Water Resources Research, 24*(5), 755-769. doi:10.1029/WR024i005p00755

Catuneanu, O., Wopfner, H., Eriksson, P. G., Cairncross, B., Rubidge, B. S., Smith, R. M. H., & Hancox, P. J. (2005). The Karoo basins of south-central Africa. *Journal of African Earth Sciences, 43*(1-3), 211-253. doi:10.1016/j.jafrearsci.2005.07.007

Chandler, R. E., & Wheater, H. S. (2002). Analysis of rainfall variability using generalized linear models: A case study from the west of Ireland. *Water Resources Research, 38*(10), 10-11-10-11. doi:10.1029/2001WR000906

Choudhury, B. J. (1997). Global pattern of potential evaporation calculated from the Penman-Monteith equation using satellite and assimilated data. *Remote Sensing of Environment, 61*(1), 64-81. doi:https://doi.org/10.1016/S0034-4257(96)00241-6

Coelho, V. H. R., Montenegro, S., Almeida, C. N., Silva, B. B., Oliveira, L. M., Gusmao, A. C. V., Freitas,. E.S., Montenegro, A. A. A. (2017). Alluvial groundwater recharge estimation in semi-arid environment using remotely sensed data. *Journal of Hydrology, 548*, 1-15. doi:10.1016/j.jhydrol.2017.02.054

Colomina, I., & Molina, P. (2014). Unmanned aerial systems for photogrammetry and remote sensing: A review. *ISPRS Journal of Photogrammetry and Remote Sensing, 92*, 79-97. doi:https://doi.org/10.1016/j.isprsjprs.2014.02.013

Cox, M. E., James, A., Hawke, A., & Raiber, M. (2013). Groundwater Visualisation System (GVS): A software framework for integrated display and interrogation of conceptual hydrogeological models, data and time-series animation. *Journal of Hydrology, 491*, 56-72. doi:http://doi.org/10.1016/j.jhydrol.2013.03.023

Danish Hydraulic Institute. (1998). MIKE SHE water movement—User's guide and technical reference manual.

De Groeve, T. (2010). Flood monitoring and mapping using passive microwave remote sensing in Namibia. *Geomatics, Natural Hazards and Risk, 1*(1), 19-35.

de Vries, J. J. (1984). Holocene depletion and active recharge of the Kalahari groundwaters - a review and an indicative model. *Journal of Hydrology, 70*(1-4), 221-232. doi:10.1016/0022-1694(84)90123-9

de Vries, J. J., Selaolo, E. T., & Beekman, H. E. (2000). Groundwater recharge in the Kalahari, with reference to paleo-hydrologic conditions. *Journal of Hydrology, 238*(1-2), 110-123. doi:10.1016/s0022-1694(00)00325-5

de Vries, J. J., & Simmers, I. (2002). Groundwater recharge: an overview of processes and challenges. *Hydrogeology Journal, 10*(1), 5-17. doi:10.1007/s10040-001-0171-7

Dembele, M., & Zwart, S. J. (2016). Evaluation and comparison of satellite-based rainfall products in Burkina Faso, West Africa. *International Journal of Remote Sensing, 37*(17), 3995-4014. doi:10.1080/01431161.2016.1207258

Dietvorst, E. J. L., De Vries, J. J., & Gieske, A. (1991). Coincidence of Well Fields and Tectonic Basins in the Precambrian Shield Area of Southeast Botswana. *Ground Water, 29*(6), 869-877. doi:10.1111/j.1745-6584.1991.tb00574.x

Dinku, T., Ceccato, P., & Connor, S. J. (2011). Challenges of satellite rainfall estimation over mountainous and arid parts of east Africa. *International Journal of Remote Sensing, 32*(21), 5965-5979. doi:10.1080/01431161.2010.499381

Dinku, T., Chidzambwa, S., Ceccato, P., Connor, S. J., & Ropelewski, C. F. (2008). Validation of high-resolution satellite rainfall products over complex terrain. *International Journal of Remote Sensing, 29*(14), 4097-4110. doi:10.1080/01431160701772526

Dinku, T., Connor, S., & Ceccato, P. (2010). Comparison of CMORPH and TRMM-3B42 over Mountainous Regions of Africa and South America. In M. Gebremichael & F. Hossain (Eds.), *Satellite Rainfall Applications for Surface Hydrology* (pp. 193-204): Springer Netherlands.

Doherty, J. E., & Hunt, R. J. (2010). *Approaches to highly parameterized inversion-A guide to using PEST for groundwater-model calibration* (2328-0328). Retrieved from

Domenico, P. A., & Schwartz, F. W. (1998). *Physical and chemical hydrogeology* (Second edition ed.). New York etc.: Wiley & Sons.

Downer, C. W., & Ogden, F. L. (2004). Appropriate vertical discretization of Richards' equation for two-dimensional watershed-scale modelling. *Hydrological Processes, 18*(1), 1-22. doi:10.1002/hyp.1306

El-Zehairy, A. A., Lubczynski, M. W., & Gurwin, J. (2018). Interactions of artificial lakes with groundwater applying an integrated MODFLOW

solution. *Hydrogeology Journal, 26*(1), 109-132. doi:10.1007/s10040-017-1641-x

Environmental Modeling Research Laboratory. (1999). *Groundwater Modeling System (GMS)*.

Farr, J., Cheney, C., Baron, J., & Peart, R. (1981). *GS10 Project: Evaluation of Underground Water Resources* (Final report). Retrieved from

Frances, A. P., Lubczynski, M. W., Roy, J., Santos, F. A. M., & Ardekani, M. R. M. (2014). Hydrogeophysics and remote sensing for the design of hydrogeological conceptual models in hard rocks - Sardon catchment (Spain). *Journal of Applied Geophysics, 110*, 63-81. doi:10.1016/j.jappgeo.2014.08.015

Francés, A. P., Su, Z., & Lubczynski, M. W. (2015). *Integration of hydrogeophysics and remote sensing with coupled hydrological models.* (PhD), University of Twente Faculty of Geo-Information and Earth Observation (ITC), Enschede. Retrieved from http://www.itc.nl/library/papers_2015/phd/frances.pdf

Freeze, R. A., & Cherry, J. A. (1979). *Groundwater*. Englewood Cliffs: Prentice-Hall.

Gebremichael, M., & Krajewski, W. F. (2004). Characterization of the temporal sampling error in space-time-averaged rainfall estimates from satellites. *Journal of Geophysical Research-Atmospheres, 109*(D11). doi:10.1029/2004jd004509

Geotechnical Consulting Services (Pty) Ltd. (2000). *Review of monitoring performed by DWA and DGS, Assessment of Water Resources and Suggestion for Improvements. TB 10/3/4/96-97*. (Volume 20: Serowe wellfield final report). Department of Water Affairs, Botswana: Unpublished report.

Geotechnical Consulting Services (Pty) Ltd. (2014). *Post-Auditing of the Serowe groundwater model (Wellfields 1 and 2). MTC/MMEWWR/DWA/1/10/12-13*. (Final report). Department of Water Affairs, Botswana: Unpublished report.

Gieske, A. (1992). *Dynamics of groundwater recharge; a case study in the arid eastern Botswana.* (PhD), Vrije Universiteit Amsterdam.

Gill, B., Cherry, D., Adelana, M., Cheng, X., & Reid, M. (2011). Using three-dimensional geological mapping methods to inform sustainable groundwater development in a volcanic landscape, Victoria, Australia. *Hydrogeology Journal, 19*(7), 1349-1365. doi:10.1007/s10040-011-0757-7

Gong, H., Pan, Y., & Xu, Y. (2012). Spatio-temporal variation of groundwater recharge in response to variability in precipitation, land use and soil in Yanqing Basin, Beijing, China. *Hydrogeology Journal, 20*(7), 1331-1340. doi:10.1007/s10040-012-0883-x

Gurwin, J., & Lubczynski, M. (2005). Modeling of complex multi-aquifer systems for groundwater resources evaluation - Swidnica study case

(Poland). *Hydrogeology Journal, 13*(4), 627-639. doi:10.1007/s10040-004-0382-9

Haala, N., & Rothermel, M. (2012). Dense Multi-Stereo Matching for High Quality Digital Elevation Models. *Photogrammetrie Fernerkundung Geoinformation*(4), 331-343. doi:10.1127/1432-8364/2012/0121

Habib, E., Haile, A. T., Sazib, N., Zhang, Y., & Rientjes, T. (2014). Effect of Bias Correction of Satellite-Rainfall Estimates on Runoff Simulations at the Source of the Upper Blue Nile. *Remote Sensing, 6*(7), 6688-6708. doi:10.3390/rs6076688

Habib, E., Larson, B. F., & Graschel, J. (2009). Validation of NEXRAD multisensor precipitation estimates using an experimental dense rain gauge network in south Louisiana. *Journal of Hydrology, 373*(3–4), 463-478. doi:http://dx.doi.org/10.1016/j.jhydrol.2009.05.010

Haddon, I. G. (2005). *The Sub-Kalahari geology and tectronic evolution of the Kalahari basin, Southern Africa.* (PhD), University of the Witwatersrand.

Haile, A. T., Habib, E., & Rientjes, T. (2013). Evaluation of the climate prediction center (CPC) morphing technique (CMORPH) rainfall product on hourly time scales over the source of the Blue Nile River. *Hydrological Processes, 27*(12), 1829-1839. doi:10.1002/hyp.9330

Haile, A. T., Rientjes, T., Gieske, A., & Gebremichael, M. (2009). Rainfall Variability over Mountainous and Adjacent Lake Areas: The Case of Lake Tana Basin at the Source of the Blue Nile River. *Journal of Applied Meteorology and Climatology, 48*(8), 1696-1717. doi:10.1175/2009jamc2092.1

Harbaugh, A. W. (1990). *A computer program for calculating subregional water budgets using results from the US Geological Survey modular three-dimensional finite-difference ground-water flow model*: US Geological Survey.

Harter, T., & Hopmans, J. W. (2004). Role of vadose zone flow processes in regional scale hydrology: Review, opportunities and challenges. In R. Feddes, G. H. De Rooij, & J. C. Van Dam (Eds.), *Unsaturated Zone Modeling-Progress, Challenges and Applications* (Vol. Wageningen Frontis Series, pp. 179 - 208). Dordrecht, The Netherlands: Kluwer Academic Publisher.

Hassan, S. M. T., Ghimire, C. P., & Lubczynski, M. W. (2017). Remote sensing upscaling of interception loss from isolated oaks: Sardon catchment case study, Spain. *Journal of Hydrology, 555*, 489-505. doi:10.1016/j.jhydrol.2017.08.016

Hassan, S. M. T., Lubczynski, M. W., Niswonger, R. G., & Su, Z. (2014). Surface–groundwater interactions in hard rocks in Sardon Catchment of western Spain: An integrated modeling approach. *Journal of Hydrology, 517*(0), 390-410. doi:http://dx.doi.org/10.1016/j.jhydrol.2014.05.026

Hassen, I., Gibson, H., Hamzaoui-Azaza, F., Negro, F., Rachid, K., & Bouhlila, R. (2016). 3D geological modeling of the Kasserine Aquifer System, Central Tunisia: New insights into aquifer-geometry and interconnections for a better assessment of groundwater resources. *Journal of Hydrology, 539*, 223-236. doi:http://dx.doi.org/10.1016/j.jhydrol.2016.05.034

Hay, L. E., Markstrom, S. L., & Ward-Garrison, C. (2010). Watershed-Scale Response to Climate Change through the Twenty-First Century for Selected Basins across the United States. *Earth Interactions, 15*(17), 1-37. doi:10.1175/2010EI370.1

Henry, C. M., Allen, D. M., & Huang, J. (2011). Groundwater storage variability and annual recharge using well-hydrograph and GRACE satellite data. *Hydrogeology Journal, 19*(4), 741-755. doi:10.1007/s10040-011-0724-3

Herman, A., Kumar, V. B., Arkin, P. A., & Kousky, J. V. (1997). Objectively determined 10-day African rainfall estimates created for famine early warning systems. *International Journal of Remote Sensing, 18*(10), 2147-2159. doi:10.1080/014311697217800

Hill, M. C., & Tiedeman, C. R. (2006). *Effective groundwater model calibration: with analysis of data, sensitivities, predictions, and uncertainty*: John Wiley & Sons.

Hirpa, F. A., Hopson, T. M., De Groeve, T., Brakenridge, G. R., Gebremichael, M., & Restrepo, P. J. (2013). Upstream satellite remote sensing for river discharge forecasting: Application to major rivers in South Asia. *Remote Sensing of Environment, 131*, 140-151. doi:https://doi.org/10.1016/j.rse.2012.11.013

Hossain, F., & Huffman, G. J. (2008). Investigating Error Metrics for Satellite Rainfall Data at Hydrologically Relevant Scales. *Journal of Hydrometeorology, 9*(3), 563-575. doi:10.1175/2007jhm925.1

Hsieh, P. A., & Freckleton, J. R. (1993). *Documentation of a computer program to simulate horizontal-flow barriers using the US Geological Survey's modular three-dimensional finite-difference ground-water flow model*: US Department of the Interior, US Geological Survey.

Huntington, J. L., & Niswonger, R. G. (2012). Role of surface-water and groundwater interactions on projected summertime streamflow in snow dominated regions: An integrated modeling approach. *Water Resources Research, 48*(11), W11524. doi:10.1029/2012WR012319

Hutchins, D. G., & Reeves, C. V. (1980). Regional geophysical exploration of the Kalahari in Botswana. *Tectonophysics, 69*(3), 201-220. doi:https://doi.org/10.1016/0040-1951(80)90211-5

Jarvis, A., Reuter, H. I., Nelson, A., & Guevara, E. (2008). Hole-filled SRTM for the globe Version 4. *available from the CGIAR-CSI SRTM 90m Database (http://srtm.csi.cgiar.org)*.

Jasrotia, A. S., Kumar, R., & Saraf, A. K. (2007). Delineation of groundwater recharge sites using integrated remote sensing and GIS in Jammu district, India. *International Journal of Remote Sensing, 28*(22), 5019-5036. doi:10.1080/01431160701264276

Johnson, M. R., VanVuuren, C. J., Hegenberger, W. F., Key, R., & Shoko, U. (1996). Stratigraphy of the Karoo Supergroup in southern Africa: An overview. *Journal of African Earth Sciences, 23*(1), 3-15. doi:10.1016/s0899-5362(96)00048-6

Jones, A., Breuning-Madsen, H., Brossard, M., Dampha, A., Deckers, J., Dewitte, O., . . . Kilasara, M. (2013). *Soil Atlas of Africa. European Commission, Publications Office of the European Union, Luxembourg. 176 pp*. Retrieved from

Joshua, W. D. (1991). *Physical properties of the soils of Botswana*. (Field document 33).

Joyce, R. J., Janowiak, J. E., Arkin, P. A., & Xie, P. (2004). CMORPH: A Method that Produces Global Precipitation Estimates from Passive Microwave and Infrared Data at High Spatial and Temporal Resolution. *Journal of Hydrometeorology, 5*(3), 487-503. doi:10.1175/1525-7541(2004)005<0487:CAMTPG>2.0.CO;2

Kenabatho, P. K., Parida, B. P., & Moalafhi, D. B. (2017). Evaluation of satellite and simulated rainfall products for hydrological applications in the Notwane catchment, Botswana. *Physics and Chemistry of the Earth, Parts A/B/C, 100*, 19-30. doi:https://doi.org/10.1016/j.pce.2017.02.009

Key, R. M., & Ayres, N. (2000). The 1998 edition of the National Geological Map of Botswana. *Journal of African Earth Sciences, 30*(3), 427-451. doi:10.1016/s0899-5362(00)00030-0

Khalaf, A., & Donoghue, D. (2012). Estimating recharge distribution using remote sensing: A case study from the West Bank. *Journal of Hydrology, 414-415*(Supplement C), 354-363. doi:https://doi.org/10.1016/j.jhydrol.2011.11.006

Kim, J., & Hogue, T. S. (2008). Evaluation of a MODIS-Based Potential Evapotranspiration Product at the Point Scale. *Journal of Hydrometeorology, 9*(3), 444-460. doi:10.1175/2007jhm902.1

Kleidon, A. (2004). Global datasets of rooting zone depth inferred from inverse methods. *Journal of Climate, 17*(13), 2714-2722. doi:10.1175/1520-0442(2004)017<2714:gdorzd>2.0.co;2

Kummerow, C., Barnes, W., Kozu, T., Shiue, J., & Simpson, J. (1998). The Tropical Rainfall Measuring Mission (TRMM) Sensor Package. *Journal of Atmospheric and Oceanic Technology, 15*(3), 809-817. doi:10.1175/1520-0426(1998)015<0809:TTRMMT>2.0.CO;2

Kummerow, C., Poyner, P., Berg, W., & Thomas-Stahle, J. (2004). The Effects of Rainfall Inhomogeneity on Climate Variability of Rainfall Estimated from Passive Microwave Sensors. *Journal of Atmospheric and Oceanic*

Technology, 21(4), 624-638. doi:10.1175/1520-0426(2004)021<0624:TEORIO>2.0.CO;2

Le Maitre, D. C., Scott, D. F., & Colvin, C. (1999). A review of information on interactions between vegetation and groundwater. *Water Sa, 25*(2), 137-152.

Leblanc, M., Favreau, G., Tweed, S., Leduc, C., Razack, M., & Mofor, L. (2007). Remote sensing for groundwater modelling in large semiarid areas: Lake Chad Basin, Africa. *Hydrogeology Journal, 15*(1), 97-100. doi:10.1007/s10040-006-0126-0

Leblanc, M. J., Tregoning, P., Ramillien, G., Tweed, S. O., & Fakes, A. (2009). Basin-scale, integrated observations of the early 21st century multiyear drought in southeast Australia. *Water Resources Research, 45*(4). doi:doi:10.1029/2008WR007333

Lekula, M., Lubczynski, M. W., & Shemang, E. M. (2018a). Hydrogeological conceptual model of large and complex sedimentary aquifer systems – Central Kalahari Basin (Botswana). *Physics and Chemistry of the Earth, Parts A/B/C*. doi:https://doi.org/10.1016/j.pce.2018.05.006

Lekula, M., Lubczynski, M. W., Shemang, E. M., & Verhoef, W. (2018b). Validation of satellite-based rainfall in Kalahari. *Physics and Chemistry of the Earth, Parts A/B/C, 105*, 85-97. doi:https://doi.org/10.1016/j.pce.2018.02.010

Li, H. T., Brunner, P., Kinzelbach, W., Li, W. P., & Dong, X. G. (2009). Calibration of a groundwater model using pattern information from remote sensing data. *Journal of Hydrology, 377*(1-2), 120-130. doi:10.1016/j.jhydrol.2009.08.012

Liechti, T. C., Matos, J. P., Boillat, J. L., & Schleiss, A. J. (2012). Comparison and evaluation of satellite derived precipitation products for hydrological modeling of the Zambezi River Basin. *Hydrology and Earth System Sciences, 16*(2), 489-500. doi:10.5194/hess-16-489-2012

Lindenmaier, F., Miller, R., Fenner, J., Christelis, G., Dill, H. G., Himmelsbach, T., . . . van Wyk, B. (2014). Structure and genesis of the Cubango Megafan in northern Namibia: implications for its hydrogeology. *Hydrogeology Journal, 22*(6), 1307-1328. doi:10.1007/s10040-014-1141-1

Liu, X., Peterson, J., & Zhang, Z. (2005). High-Resolution DEM Generated from LiDAR Data for Water Resource Management. In A. Zerger & R. M. Argent (Eds.), *Modsim 2005: International Congress on Modelling and Simulation: Advances and Applications for Management and Decision Making: Advances and Applications for Management and Decision Making* (pp. 1402-1408). Nedlands: Univ Western Australia.

Lopez, P. L., Sutanudjaja, E. H., Schellekens, J., Sterk, G., & Bierkens, M. F. P. (2017). Calibration of a large-scale hydrological model using satellite-based soil moisture and evapotranspiration products.

Hydrology and Earth System Sciences, 21(6), 3125-3144. doi:10.5194/hess-21-3125-2017

Loveland, T. R., Reed, B. C., Brown, J. F., Ohlen, D. O., Zhu, Z., Yang, L., & Merchant, J. W. (2000). Development of a global land cover characteristics database and IGBP DISCover from 1 km AVHRR data. *International Journal of Remote Sensing, 21*(6-7), 1303-1330. doi:10.1080/014311600210191

Lubczynski, M. W. (2000). *Groundwater evapotranspiration - Underestimated component of the groundwater balance in a semi-arid environment - Serowe case, Botswana*.

Lubczynski, M. W. (2006). Groundwater fluxes in arid and semi-arid environments. In A. Baba, K. W. F. Howard, & O. Gunduz (Eds.), *Groundwater and Ecosystems* (Vol. 70, pp. 225-236).

Lubczynski, M. W. (2009). The hydrogeological role of trees in water-limited environments. *Hydrogeology Journal, 17*(1), 247-259. doi:10.1007/s10040-008-0357-3

Lubczynski, M. W. (2011). Groundwater Evapotranspiration - Underestimated Role of Tree Transpiration and Bare Soil Evaporation in Groundwater Balances of Dry Lands. In A. Baba, O. Gunduz, M. J. Friedel, G. Tayfur, K. W. F. Howard, & A. Chambel (Eds.), *Climate Change and Its Effects on Water Resources: Issues of National and Global Security* (pp. 183-190).

Lubczynski, M. W., Chavarro-Rincon, D. C., & Rossiter, D. G. (2017). Conductive sapwood area prediction from stem and canopy areas—allometric equations of Kalahari trees, Botswana. *Ecohydrology, 10*(6), e1856-n/a. doi:10.1002/eco.1856

Ma, L., He, C., Bian, H., & Sheng, L. (2016). MIKE SHE modeling of ecohydrological processes: Merits, applications, and challenges. *Ecological Engineering, 96*, 137-149. doi:https://doi.org/10.1016/j.ecoleng.2016.01.008

Ma, R. (2005). DEM Generation and Building Detection from Lidar Data. *Photogrammetric Engineering & Remote Sensing, 71*(7), 847-854. doi:10.14358/PERS.71.7.847

Markstrom, S. L., Niswonger, R. G., Regan, R. S., Prudic, D. E., & Barlow, P. M. (2008). *GSFLOW-Coupled Ground-water and Surface-water FLOW model based on the integration of the Precipitation-Runoff Modeling System (PRMS) and the Modular Ground-Water Flow Model (MODFLOW-2005)* (2328-7055). Retrieved from

Masterson, J. P., Pope, J. P., Fienen, M. N., Monti Jr, J., Nardi, M. R., & Finkelstein, J. S. (2016). *Documentation of a groundwater flow model developed to assess groundwater availability in the northern Atlantic coastal plain aquifer system from Long Island, New York, to North Carolina* (2328-0328). Retrieved from United States, Reston, VA:

Mazor, E. (1982). Rain recharge in the Kalahari — A note on some approaches to the problem. *Journal of Hydrology, 55*(1–4), 137-144. doi:http://dx.doi.org/10.1016/0022-1694(82)90124-X

McDonald, M. G., & Harbaugh, A. W. (1988). A modular three-dimensional finite-difference ground-water flow model.

Meijerink, A. M., Bannert, D., Batelaan, O., Lubczynski, M., & Pointet, T. (2007). *Remote sensing applications to groundwater*: United Nations Educational, Scientific and Cultural Organization (UNESCO).

Milzow, C., Kgotlhang, L., Kinzelbach, W., Meier, P., & Bauer-Gottwein, P. (2009). The role of remote sensing in hydrological modelling of the Okavango Delta, Botswana. *Journal of Environmental Management, 90*(7), 2252-2260. doi:10.1016/j.jenvman.2007.06.032

Milzow, C., Krogh, P. E., & Bauer-Gottwein, P. (2011). Combining satellite radar altimetry, SAR surface soil moisture and GRACE total storage changes for hydrological model calibration in a large poorly gauged catchment. *Hydrol. Earth Syst. Sci., 15*(6), 1729-1743. doi:10.5194/hess-15-1729-2011

Miralles, D. G., Gash, J. H., Holmes, T. R. H., de Jeu, R. A. M., & Dolman, A. J. (2010). Global canopy interception from satellite observations. *Journal of Geophysical Research: Atmospheres, 115*(D16), n/a-n/a. doi:10.1029/2009JD013530

Moazami, S., Golian, S., Kavianpour, M. R., & Hong, Y. (2013). Comparison of PERSIANN and V7 TRMM Multi-satellite Precipitation Analysis (TMPA) products with rain gauge data over Iran. *International Journal of Remote Sensing, 34*(22), 8156-8171. doi:10.1080/01431161.2013.833360

Morway, E. D., Niswonger, R. G., Langevin, C. D., Bailey, R. T., & Healy, R. W. (2013). Modeling Variably Saturated Subsurface Solute Transport with MODFLOW-UZF and MT3DMS. *Ground Water, 51*(2), 237-251. doi:10.1111/j.1745-6584.2012.00971.x

Nicholson, S. E., Some, B., McCollum, J., Nelkin, E., Klotter, D., Berte, Y., . . . Traore, A. K. (2003). Validation of TRMM and other rainfall estimates with a high-density gauge dataset for West Africa. Part I: Validation of GPCC rainfall product and pre-TRMM satellite and blended products. *Journal of Applied Meteorology, 42*(10), 1337-1354. doi:10.1175/1520-0450(2003)042<1337:votaor>2.0.co;2

Niswonger, R. G., Panday, S., & Ibaraki, M. (2011). *MODFLOW-NWT, a Newton formulation for MODFLOW-2005* (2328-7055). Retrieved from

Niswonger, R. G., & Prudic, D. E. (2004). Modeling Variably Saturated Flow Using Kinematic Waves in MODFLOW. In J. F. Hogan, F. M. Phillips, & B. R. Scanlon (Eds.), *Groundwater Recharge in a Desert Environment: The Southwestern United States. Water Science and Application. American Geophysical Union* (pp. 101 - 112).

Niswonger, R. G., Prudic, D. E., & Regan, R. S. (2006). *Documentation of the unsaturated-zone flow (UZF1) package for modeling unsaturated flow between the land surface and the water table with MODFLOW-2005* (2328-7055). Retrieved from

Noferini, L., Pieraccini, M., Mecatti, D., Macaluso, G., Luzi, G., & Atzeni, C. (2007). DEM by Ground-Based SAR Interferometry. *IEEE Geoscience and Remote Sensing Letters, 4*(4), 659-663. doi:10.1109/LGRS.2007.905118

Obakeng, O., & Lubczynski, M. W. (2004). Monitoring and modeling of fluxes on Kalahari ? setup and strategy of the Kalahari Monitoring project. Serowe study case, Botswana *Water Resources of Arid Areas* (pp. 271-278): Taylor & Francis.

Obakeng, O. T., de Vries, J. J., & Lubczynski, M. W. (2007). *Soil moisture dynamics and evapotranspiration at the fringe of the Botswana Kalahari, with emphasis on deep rooting vegetation.* (PhD), Vrije Universiteit Amsterdam, Amsterdam. Retrieved from http://www.itc.nl/library/papers_2007/phd/obakeng.pdf

Pacific Consultants International, & SANYU Consultants INC. (2002a). *The study on the groundwater potential evaluation and management plan in the southeast Kalahari (Stampriet) Artesian Basin in Namibia*. (Final report: Data book). Tokyo/Japan: Japan International Cooperation Agency.

Pacific Consultants International, & SANYU Consultants INC. (2002b). *The study on the groundwater potential evaluation and management plan in the southeast Kalahari (Stampriet) Artesian Basin in Namibia*. (Final report: Main report). Tokyo/Japan: Japan International Cooperation Agency.

Porporato, A., Laio, F., Ridolfi, L., Caylor, K. K., & Rodriguez-Iturbe, I. (2003). Soil moisture and plant stress dynamics along the Kalahari precipitation gradient. *Journal of Geophysical Research-Atmospheres, 108*(D3). doi:10.1029/2002jd002448

Post, D., Vaze, J., Teng, J., Crosbie, R., Marvanek, S., Wang, B., . . . Renzullo, L. (2012). *Impacts of climate change on water availability in Botswana*: CSIRO.

Pouliquen, G., Key, R., & Walker, A. (2008). The internal structure and geotectonic setting of the Xade and Tsetseng complexes in the western most part of the Kaapvaal Craton. *South African Journal of Geology, 111*(4), 345-356.

Qin, Y. X., Chen, Z. Q., Shen, Y., Zhang, S. P., & Shi, R. H. (2014). Evaluation of Satellite Rainfall Estimates over the Chinese Mainland. *Remote Sensing, 6*(11), 11649-11672. doi:10.3390/rs61111649

Rahmawati, N., & Lubczynski, M. W. (2017). Validation of satellite daily rainfall estimates in complex terrain of Bali Island, Indonesia. *Theoretical and Applied Climatology*. doi:10.1007/s00704-017-2290-7

Raiber, M., White, P. A., Daughney, C. J., Tschritter, C., Davidson, P., & Bainbridge, S. E. (2012). Three-dimensional geological modelling and multivariate statistical analysis of water chemistry data to analyse and visualise aquifer structure and groundwater composition in the Wairau Plain, Marlborough District, New Zealand. *Journal of Hydrology, 436–437*, 13-34. doi:http://dx.doi.org/10.1016/j.jhydrol.2012.01.045

Ramokate, L. V., Mapeo, R. M. M., Corfu, F., & Kampunzu, A. B. (2000). Proterozoic geology and regional correlation of the Ghanzi-Makunda area, western Botswana. *Journal of African Earth Sciences, 30*(3), 453-466. doi:http://dx.doi.org/10.1016/S0899-5362(00)00031-2

Refsgaard, J. C. J. J. C. (2010). Système Hydrologique Européen (SHE): Review and perspectives after 30 years development in distributed physically-based hydrological modelling. *Hydrology Research, 41*(5), 355-377.

Reyes-Acosta, J. L., & Lubczynski, M. W. (2013). Mapping dry-season tree transpiration of an oak woodland at the catchment scale, using object-attributes derived from satellite imagery and sap flow measurements. *Agricultural and Forest Meteorology, 174*, 184-201. doi:10.1016/j.agrformet.2013.02.012

Ringard, J., Becker, M., Seyler, F., & Linguet, L. (2015). Temporal and Spatial Assessment of Four Satellite Rainfall Estimates over French Guiana and North Brazil. *Remote Sensing, 7*(12), 16441-16459. doi:10.3390/rs71215831

Robins, N. S., Rutter, H. K., Dumpleton, S., & Peach, D. W. (2005). The role of 3D visualisation as an analytical tool preparatory to numerical modelling. *Journal of Hydrology, 301*(1-4), 287-295. doi:10.1016/j.jhydrol.2004.05.004

RockWare. (2017). Earth science & GIS Software: Available at https://www.rockware.com/.

Rodell, M., Chen, J. L., Kato, H., Famiglietti, J. S., Nigro, J., & Wilson, C. R. (2007). Estimating groundwater storage changes in the Mississippi River basin (USA) using GRACE. *Hydrogeology Journal, 15*(1), 159-166. doi:10.1007/s10040-006-0103-7

Rodell, M., & Famiglietti, J. S. (2001). An analysis of terrestrial water storage variations in Illinois with implications for the Gravity Recovery and Climate Experiment (GRACE). *Water Resources Research, 37*(5), 1327-1339. doi:10.1029/2000wr900306

Rodell, M., & Famiglietti, J. S. (2002). The potential for satellite-based monitoring of groundwater storage changes using GRACE: the High Plains aquifer, Central US. *Journal of Hydrology, 263*(1–4), 245-256. doi:http://dx.doi.org/10.1016/S0022-1694(02)00060-4

Romilly, T. G., & Gebremichael, M. (2011). Evaluation of satellite rainfall estimates over Ethiopian river basins. *Hydrol. Earth Syst. Sci., 15*(5), 1505-1514. doi:10.5194/hess-15-1505-2011

Royse, K. R. (2010). Combining numerical and cognitive 3D modelling approaches in order to determine the structure of the Chalk in the London Basin. *Computers & Geosciences, 36*(4), 500-511. doi:10.1016/j.cageo.2009.10.001

Sarma, D., & Xu, Y. (2017). The recharge process in alluvial strip aquifers in arid Namibia and implication for artificial recharge. *Hydrogeology Journal, 25*(1), 123-134. doi:10.1007/s10040-016-1474-z

Schmugge, T. J., Kustas, W. P., Ritchie, J. C., Jackson, T. J., & Rango, A. (2002). Remote sensing in hydrology. *Advances in Water Resources, 25*(8-12), 1367-1385. doi:10.1016/s0309-1708(02)00065-9

Selaolo, E. T. (1998). *Tracer studies and groundwater recharge assessment in the eastern fringe of the Botswana Kalahari, The Letlhakeng-Bothapatlou Area.* (PhD), Vrije Universiteit Amsterdam.

Seoane, L., Ramillien, G., Frappart, F., & Leblanc, M. (2013). Regional GRACE-based estimates of water mass variations over Australia: validation and interpretation. *Hydrology and Earth System Sciences, 17*(12), 4925-4939. doi:10.5194/hess-17-4925-2013

Sheikh, V., Visser, S., & Stroosnijder, L. (2009). A simple model to predict soil moisture: Bridging Event and Continuous Hydrological (BEACH) modelling. *Environmental Modelling & Software, 24*(4), 542-556. doi:https://doi.org/10.1016/j.envsoft.2008.10.005

Šimůnek, J., Van Genuchten, M. T., & Šejna, M. (2012). *The HYDRUS software package for simulating two-and three-dimensional movement of water, heat, and multiple solutes in variably-saturated media*. Retrieved from Praque, Czech Republic:

SMEC, & EHES. (2006). *Botswana National Water Master Plan Review*. (Volume 4: Groundwater Resources). Department of Water Affairs: Unpublished report of Snowy Mountains Engineering Corporation (SMEC) and EHES Consulting Engineers.

Smith, R. A. (1984). *The Lithostratigraphy of the Karoo Supergroup in Botswana*. (Bulletin 26). Department of Geological Survey.

Smith, R. E., & Hebbert, R. H. B. (1983). Mathematical simulation of interdependent surface and subsurface hydrologic processes. *Water Resources Research, 19*(4), 987-1001. doi:10.1029/WR019i004p00987

Sorooshian, S., Hsu, K.-L., Gao, X., Gupta, H. V., Imam, B., & Braithwaite, D. (2000). Evaluation of PERSIANN System Satellite–Based Estimates of Tropical Rainfall. *Bulletin of the American Meteorological Society, 81*(9), 2035-2046. doi:10.1175/1520-0477(2000)081<2035:EOPSSE>2.3.CO;2

Stadler, S., Osenbrück, K., Suckow, A. O., Himmelsbach, T., & Hötzl, H. (2010). Groundwater flow regime, recharge and regional-scale solute transport in the semi-arid Kalahari of Botswana derived from isotope

hydrology and hydrochemistry. *Journal of Hydrology, 388*(3–4), 291-303. doi:http://dx.doi.org/10.1016/j.jhydrol.2010.05.008

Su, Z. (2002). The Surface Energy Balance System (SEBS) for estimation of turbulent heat fluxes. *Hydrology and Earth System Sciences, 6*(1), 85-99. doi:10.5194/hess-6-85-2002

Surfleet, C. G., & Tullos, D. (2013). Uncertainty in hydrologic modelling for estimating hydrologic response due to climate change (Santiam River, Oregon). *Hydrological Processes, 27*(25), 3560-3576. doi:10.1002/hyp.9485

Surfleet, C. G., Tullos, D., Chang, H., & Jung, I. W. (2012). Selection of hydrologic modeling approaches for climate change assessment: A comparison of model scale and structures. *Journal of Hydrology, 464*, 233-248. doi:10.1016/j.jhydrol.2012.07.012

Sutanudjaja, E. H., van Beek, L. P. H., de Jong, S. M., van Geer, F. C., & Bierkens, M. F. P. (2014). Calibrating a large-extent high-resolution coupled groundwater-land surface model using soil moisture and discharge data. *Water Resources Research, 50*(1), 687-705. doi:doi:10.1002/2013WR013807

Tam, V. T., Batelaan, O., Le, T. T., & Nhan, P. Q. (2014). Three-dimensional hydrostratigraphical modelling to support evaluation of recharge and saltwater intrusion in a coastal groundwater system in Vietnam. *Hydrogeology Journal, 22*(8), 1749-1762. doi:10.1007/s10040-014-1185-2

Taniguchi, M., Yamamoto, K., & Sarukkalige, P. R. (2011). Groundwater resources assessment based on satellite GRACE and hydrogeology in Western Australia. In M. Hafeez, N. VanDeGiesen, E. Bardsley, F. Seyler, R. Pail, & M. Taniguchi (Eds.), *Grace, Remote Sensing and Ground-Based Methods in Multi-Scale Hydrology* (Vol. 343, pp. 3-8).

Tapley, B. D., Bettadpur, S., Watkins, M., & Reigber, C. (2004). The gravity recovery and climate experiment: Mission overview and early results. *Geophysical Research Letters, 31*(9). doi:doi:10.1029/2004GL019920

Therrien, R. (1992). *Three-dimensional analysis of variably-saturated flow and solute transport in discretely-fractured porous media.* (PhD), University of Waterloo, Waterloo, ON.

Tian, Y. D., Peters-Lidard, C. D., Eylander, J. B., Joyce, R. J., Huffman, G. J., Adler, R. F., . . . Zeng, J. (2009). Component analysis of errors in satellite-based precipitation estimates. *Journal of Geophysical Research-Atmospheres, 114*. doi:10.1029/2009jd011949

Tote, C., Patricio, D., Boogaard, H., van der Wijngaart, R., Tarnavsky, E., & Funk, C. (2015). Evaluation of Satellite Rainfall Estimates for Drought and Flood Monitoring in Mozambique. *Remote Sensing, 7*(2), 1758-1776. doi:10.3390/rs70201758

Toth, J. (1963). A THEORETICAL ANALYSIS OF GROUNDWATER FLOW IN SMALL DRAINAGE BASINS. *Journal of Geophysical Research, 68*(16), 4795-4812. doi:10.1029/JZ068i008p02354

Trabelsi, F., Tarhouni, J., Ben Mammou, A., & Ranieri, G. (2013). GIS-based subsurface databases and 3-D geological modeling as a tool for the set up of hydrogeological framework: Nabeul-Hammamet coastal aquifer case study (Northeast Tunisia). *Environmental Earth Sciences, 70*(5), 2087-2105. doi:10.1007/s12665-011-1416-y

Verweij, J. M. (1993). *Hydrocarbon migration systems analysis* (Vol. 35): Elsevier.

Voss, C. I. (2011). Editor's message: Groundwater modeling fantasies —part 1, adrift in the details. *Hydrogeology Journal, 19*(7), 1281-1284. doi:10.1007/s10040-011-0789-z

Wanke, H., Dunkeloh, A., & Udluft, P. (2008). Groundwater recharge assessment for the Kalahari catchment of north-eastern Namibia and north-western Botswana with a regional-scale water balance model. *Water Resources Management, 22*(9), 1143-1158. doi:10.1007/s11269-007-9217-5

Water Surveys Botswana (Pty) Ltd. (2008). *Central Kalahari Game Reserve and Khutse Game reserve artificial watering points construction and rehabilitation project.* (Inception Report). Department of wildlife and National Parks: Unpublished report.

Water Surveys Botswana (Pty) Ltd & Aqualogic (Pty) Ltd. (2007). *Groundwater resources investigation and development for the Morupule B Power station project.* . (Final Report). Botswana Power Corporation: Unpublished report.

Wegmüller, U., Santoro, M., Werner, C., Strozzi, T., Wiesmann, A., & Lengert, W. (2009). DEM generation using ERS–ENVISAT interferometry. *Journal of Applied Geophysics, 69*(1), 51-58. doi:https://doi.org/10.1016/j.jappgeo.2009.04.002

Wellfield Consulting Services (Pty) Ltd. (2001). *Hunhukwe-Lokalane groundwater survey project TB 10/2/1/98-99*. (Final Report). Department of Geological Survey, Botswana: Unpublished report.

Wellfield Consulting Services (Pty) Ltd. (2007). *Kang-Phuduhudu regional groundwater resources investigation and development project. TB 10/85/2001-2002*. (Final Report). Department of Water Affairs, Botswana: Unpublished report.

Wellfield Consulting Services (Pty) Ltd. (2009). *Botlhapatlou groundwater exploration and wellfield development PR 10/3/3/08-2*. (Inception report). Department of Water Affairs, Botswana: Unpublished report.

Wellfield Consulting Services (Pty) Ltd. (2012). *Botlhapatlou Groundwater exploration and wellfield development project PR 10/3/3/08-2*. (Final Report). Department of Water Affairs, Botswana: Unpublished report.

Werger, M. J., & van Bruggen, A. C. (1978). *Biogeography and ecology of southern Africa* (Vol. 31): Springer Science & Business Media.

Wilks, D. S. (2006). *Statistical methods in the atmospheric sciences* (Second ed. Vol. 100). Burlington, MA: Academic press.

Winston, R. (2009). ModelMuse-A graphical user interface for MODFLOW-2005 and PHAST: US Geological Survey techniques and methods 6-A29. *US Geological Survey. Available online at http://pubs. usgs. gov/tm/tm6A29*.

Xiaoyang, H., Wenzhao, L., & Wen, L. (2015). Spatiotemporal analysis of potential evapotranspiration in the Changwu tableland from 1957 to 2012. *Meteorological Applications, 22*(3), 586-591. doi:doi:10.1002/met.1490

Xu, C., Wei, M., Griffiths, S., Mercer, B., Abdoullaev, R., & Isprs. (2010). Hybrid dem generation and evaluation from spaceborne radargrammetric and optical stereoscopic dems *2010 Canadian Geomatics Conference and Symposium of Commission I, Isprs Convergence in Geomatics - Shaping Canada's Competitive Landscape* (Vol. 38). Gottingen: Copernicus Gesellschaft Mbh.

Yang, Y. F., & Luo, Y. (2014). Evaluating the performance of remote sensing precipitation products CMORPH, PERSIANN, and TMPA, in the arid region of northwest China. *Theoretical and Applied Climatology, 118*(3), 429-445. doi:10.1007/s00704-013-1072-0

Yeh, P. J. F., Swenson, S. C., Famiglietti, J. S., & Rodell, M. (2006). Remote sensing of groundwater storage changes in Illinois using the Gravity Recovery and Climate Experiment (GRACE). *Water Resources Research, 42*(12). doi:10.1029/2006wr005374

Zhang, W. M., Brandt, M., Guichard, F., Tian, Q. J., & Fensholt, R. (2017). Using long-term daily satellite based rainfall data (1983-2015) to analyze spatio-temporal changes in the sahelian rainfall regime. *Journal of Hydrology, 550*, 427-440. doi:10.1016/j.jhydrol.2017.05.033

Zhu, T. J., & Ringler, C. (2012). Climate Change Impacts on Water Availability and Use in the Limpopo River Basin. *Water, 4*(1), 63-84. doi:10.3390/w4010063

Summary

Groundwater resources in arid and semi-arid regions is often the only, but vulnerable source of potable water; therefore its reliable evaluation and management is critically important. As such, it is typically done through integrated hydrological models (IHM), considered nowadays as most reliable simulators because they dynamically integrate surface and groundwater fluxes. Once properly calibrated, they allow to predict aquifer behaviour in response to groundwater abstraction, climatic and/or land use changes etc. However, the reliability of the IHMs, as of any other models, is constrained by availability and quality of model input data, by realism of hydrogeological conceptual model and by adequate numerical model setup and calibration.

Data scarcity, particularly in arid to semi-arid Developing Countries, has always been hampering development of IHMs. Advancement in IHMs, made remote sensing (RS) data an alternative to the scarce, ground-based data sets. Integration of these RS-data, together with other available data sets in IHMs, is thus vital in water resource management in arid and semi-arid regions, hence, also in the Central Kalahari Basin (CKB), hosting the most productive and exploitable transboundary Karoo System Aquifer in Botswana and Namibia. As such, the CKB became an interesting and strategic study area considering its promising hydrogeological characteristics and importance of groundwater resources. The main objective of this PhD research was therefore the assessment of groundwater resources in the CKB using multiple data sources and integrated hydrological modelling.

The CKB study area, with its geological and hydrogeological characteristics were described in details in Chapter 2. These characteristics are particularly important because they were used as the basis to define hydrogeological conceptual model of the CKB.

The development of the hydrogeological conceptual model (HCM) is presented in Chapter 3. The HCM was developed with help of 3-D geological modelling code called Rockworks, operated in iterative combination with ArcGIS. As a result, a six-layer model was defined. A characteristic feature of the CKB and of the model, is its first, thick Kalahari Sand layer (~60 m), that restricts the erratic groundwater recharge to <1 mm yr^{-1} in the centre of CKB and to about 5-10 mm yr^{-1} in the eastern fringe. That layer is the only one in the system, which covers the entire study area. The other five layers are non-uniformly distributed, having variable thickness. Among them there are three aquifers (locally divided by semi-permeable layers), all having similar, radially-concentric regional groundwater flow patterns, all directed towards the same discharge area of Makgadikgadi Pans. That similarity is likely due to various layer-to-layer, hydraulic interconnections. The iterative use of RockWorks code with ArcGIS turned out to be relatively simple and efficient solution for

developing HCM of a large and complex multi-layered aquifer system such as the CKB and also for interfacing it with the numerical model. The developed HCM was the basis for the setup of the numerical model of the CKB.

Rainfall, addressed in Chapter 4, is the main driving force of IHMs. Most of IHMs require spatial data coverage of daily rainfall. It used to be defined by interpolation of rain gauge data, which usually have limited spatial coverage, especially in arid to semi-arid areas of developing countries such as the CKB area. An alternative source of rainfall data for IHMs, are satellite-based rainfall estimates (SREs). A complication is that different SREs, perform differently in different parts of the world, hence at each study area, various SREs need to be investigated to find the best performing one and optimize it to be used in hydrological studies. The Chapter 4 presents detailed evaluation of daily rainfall detection capabilities of four SREs in the CKB, i.e. FEWSNET RFE 2.0 with ~11 km spatial resolution, TRMM-3B42 v7 with ~27 km spatial resolution, CMORPH v1 with 8 km spatial resolution and CMORPH v1with ~27 km spatial resolution. The results showed that FEWSNET RFE 2.0 had best daily rainfall detection capability and therefore was further used as input of the IHM. The analysis of the four SREs highlighted also the high spatial and temporal variability of rainfall in the CKB. The overall rainfall assessment confirmed usefulness of using SREs in areas where rain gauges are scarce, such as the CKB.

A six-layer IHM of the CKB, calibrated in transient on daily basis, throughout a 13-year period (2002-2014) was developed and is presented in Chapter 5. For that purpose, MODFLOW-NWT code with active UZF1 package capable to simulate variably saturated flow, was used. In that model setup, various RS products coupled with long term, in-situ monitoring data were used as inputs. The calibrated model showed a good match between the simulated and measured temporal head patterns, with low *MAE* ranging from 0.02 to 2.70 m and low *RMSE* from 0.02 to 3.13 m. The 13-year model simulation confirmed steep water table declines in the major wellfields and gentler declines in the areas outside wellfields' influences. The declines outside wellfields' influences, were due to the generally lower gross recharge (R_g) than groundwater discharge, the latter consisting mainly of groundwater evapotranspiration (ET_g) and implying generally negative, yearly net recharge (R_n). The large ET_g was due to groundwater uptake by deep-rooted and 'thirsty' acacia trees and possibly also due to direct evaporation from the water table. The positive R_n occurred only twice in the 13 year simulation period, i.e. in 2006 and in 2014, when rainfall was 664 and 606 mm yr^{-1}, resulting in R_n of 3.4 and 1.0 mm yr^{-1}, respectively. The IHM results showed also large spatial variability of the R_g, ET_g and R_n, all attributed mainly to: i) large spatio-temporal variability of rainfall; ii) presence of local surface morphological features such as dry river channels or local pans; iii) variable thickness of the unsaturated zone; and iv) variable vegetation density and species diversity. The proposed MODFLOW-

NWT model solution with active UZF1 package and remote sensing data integrated with ground-based data as model input, showed to be optimal modelling solution for the study area such as the CKB.

Chapter 6 presents the synthesis of the PhD thesis while in chapter 7 recommendations are formulated.

Samenvatting

In droge en semi-aride gebieden vormt het grondwater vaak de enige, maar ook een kwetsbare bron van drinkwater; daarom zijn een betrouwbare evaluatie en een goed beheer ervan van cruciaal belang. Als zodanig wordt dit meestal gedaan met geïntegreerde hydrologische modellen (IHM's), die tegenwoordig worden beschouwd als de meest betrouwbare simulatiemiddelen, omdat deze de stromen van oppervlakte- en grondwater op dynamische wijze integreren. Eenmaal juist gekalibreerd, maken zij het mogelijk het gedrag van aquifers te voorspellen in reactie op grondwateronttrekking, klimaatverandering en/of veranderingen in landgebruik, enz. Echter, zoals bij veel andere modellen, wordt de betrouwbaarheid van de IHM's beperkt door de beschikbaarheid en de kwaliteit van de invoergegevens, door de mate van realisme in het hydrogeologische modelconcept, en door een adequate numerieke opzet en ijking van het model. Gebrek aan gegevens, met name in droge en semi-aride Ontwikkelingslanden, heeft het ontwikkelen van IHM's altijd in de weg gestaan. Vooruitgang in IHM's heeft ervoor gezorgd dat remote sensing (RS) gegevens als een alternatief voor de schaarse op de grond verzamelde gegevens konden worden gebruikt. Het integreren van deze RS-gegevens, tezamen met andere beschikbare datasets in IHM's, is dus essentieel bij het beheer van waterbronnen in droge en semi-aride gebieden, en daardoor ook in het Centrale Kalahari Bekken (CKB), dat de meest productieve en exploiteerbare grensoverschrijdende Karoo Systeem Aquifer, in Botswana en Namibië, herbergt. Het CKB werd een interessant en strategisch studiegebied gezien het veelbelovende hydrogeologische karakter ervan en het belang ervan als grondwaterbron. Het hoofddoel van dit promotieonderzoek was daarom het beoordelen van grondwaterbronnen in het CKB door het gebruik van diverse gegevens en geïntegreerde hydrogeologische modellering.

Het CKB studiegebied, met zijn geologische en hydrogeologische eigenschappen, wordt in detail beschreven in Hoofdstuk 3. Deze eigenschappen zijn vooral belangrijk omdat ze zijn gebruikt als basis voor het definiëren van het hydrogeologische modelconcept van het CKB. De ontwikkeling van het hydrogeologisch conceptueel model (HCM) wordt gepresenteerd in Hoofdstuk 3. Het HCM is ontwikkeld met behulp van het 3-D geologisch modeleerprogramma Rockworks, iteratief gebruikt in combinatie met ArcGIS. Als resultaat is een zes-laags model gedefinieerd. Een karakteristiek kenmerk van het CKB en van het model is de eerste, dikke Kalahari Zandlaag (~60m), die de onbedoelde aanvulling van het grondwater beperkt tot < 1 mm per jaar in het midden van het CKB en tot ongeveer 5 - 10 mm per jaar aan de oostelijke rand. Die laag is de enige in het systeem welke het gehele studiegebied beslaat. De andere vijf lagen zijn ongelijk verdeeld en hebben verschillende diktes. Daaronder zijn drie aquifers (lokaal

verdeeld door halfdoorlatende lagen), die alle soortgelijke radiaal-concentrische regionale grondwaterpatronen bezitten die allemaal lopen in de richting van het afvoergebied Makgadikgadi Pans. Die gelijksoortigheid komt waarschijnlijk door verscheidene hydraulische verbindingen tussen de lagen. Het iteratief gebruik van het RockWorks programma met ArcGIS bleek een betrekkelijk eenvoudige en efficiënte oplossing voor het ontwikkelen van een HCM van een uitgestrekt en complex multilaags aquifer systeem zoals het CKB en ook voor de koppeling met het numerieke model. Het ontwikkelde HCM vormde de basis voor het opzetten van het numerieke model van het KCB.

Regenval, behandeld in Hoofdstuk 4, vormt de voornaamste aandrijvende kracht van IHM's. De meeste IHM's verlangen ruimtelijk dekkende gegevens over de dagelijkse regenval. Vroeger werden deze verkregen door interpolatie van regenmetergegevens, die gewoonlijk een beperkte ruimtelijke dekking hebben, vooral in aride en semi-aride gebieden in ontwikkelingslanden zoals het CKB gebied. Een alternatieve bron van regenvalgegevens voor IHM's zijn op satellietwaarnemingen gebaseerde regenvalschattingen (SRE's). Een complicatie hierbij is dat verschillende SRE's verschillend presteren in verschillende delen van de wereld, dus in elk studiegebied moeten diverse SRE's worden onderzocht om de best presterende te vinden en deze te optimaliseren voor gebruik in hydrologische studies. Hoofdstuk 4 presenteert een gedetailleerde evaluatie van de regenvaldetectiecapaciteit van vier SRE's in het CKB, nl. FEWSNET RFE 2.0 met ~11 km spatiële resolutie, TRMM-3B42 v7 met ~27 km spatiële resolutie, CMORPH v1 met 8 km spatiële resolutie, en CMORPH v1 met ~27 km spatiële resolutie. De resultaten laten zien dat FEWSNET RFE 2.0 de beste dagelijkse regenvaldetectie opleverde en daarom werd deze verder gebruikt als input van het IHM. De analyse van de vier SRE's bracht ook de hoge ruimtelijke en temporele variabiliteit van de regenval in het KCB aan het licht. In het algemeen bevestigde de regenvalschatting het nut van het gebruik van SRE's in gebieden waar regenmeters schaars zijn, zoals in het KCB.

Een zes-laags IHM van het CKB, gekalibreerd op de dagelijkse gang over een periode van 13 jaar (2002 – 2014) is ontwikkeld en gepresenteerd in Hoofdstuk 5. Voor dat doel is het MODFLOW-NWT programma met een actief UZF1 pakket, dat de veranderlijke verzadigde stroom kan simuleren, gebruikt. In deze modelopzet zijn diverse RS producten, gekoppeld met op lange termijn in-situ geregistreerde gegevens, gebruikt als invoer. Het gekalibreerde model toonde een goede overeenkomst tussen de gesimuleerde en de gemeten temporele frontpatronen, met een lage gemiddelde absolute fout (MAE) van 0.02 tot 2.70 m and a lage root-mean-squared-error (RMSE) van 0.02 tot 3.13 m. De 13-jarige modelsimulatie bevestigde sterke dalingen in de grondwaterspiegel van de voornaamste brongebieden en gematigder afnames daarbuiten. De dalingen buiten de invloedsfeer van de brongebieden kwamen

door de in het algemeen lagere bruto aanvulling (R_g) dan de grondwateronttrekking, die voornamelijk bestond uit grondwaterverdamping (ET_g) en die een over het geheel negatieve jaarlijkse netto aanvulling (R_n) inhoudt. De omvangrijke ET_g wordt veroorzaakt door de opname van grondwater door diepwortelende en 'dorstige' acaciabomen en mogelijk ook door directe verdamping vanuit de grondwaterspiegel. Een positieve R_n trad maar tweemaal op in de 13-jarige simulatieperiode, nl. in 2006 en in 2014, toen de neerslag 664 en 606 mm / jaar bedroeg, resulterend in een R_n van respectievelijk 4.3 en 1.0 mm / jaar. De IHM resultaten laten ook een grote ruimtelijke variabiliteit zien van R_g, ET_g en R_n, die in alle gevallen te relateren is aan: i) de grote ruimtelijke / temporele variabiliteit van de regenval; ii) de aanwezigheid van lokale oppervlakte-morfologische kenmerken zoals droge rivierbeddingen en zoutpannen; iii) de variabele dikte van de onverzadigde zone; en iv) de variabele vegetatiedichtheid en soortenrijkdom. De voorgestelde MODFLOW-NWT modeloplossing met actief UZF1 pakket en met remote sensing gegevens geïntegreerd met grondmetingen als modelinvoer bleek een optimale modelbenadering voor een studiegebied zoals het KCB.

Hoofdstuk 6 presenteert de synthese van dit proefschrift, terwijl in Hoofdstuk 7 de aanbevelingen worden geformuleerd.